OUKA
Osaka University Knowledge Archive

Title	SCANNING TUNNELING MICROSCOPY OF SEMICONDUCTOR SURFACES
Author(s)	田中, 一郎
Citation	大阪大学, 1993, 博士論文
Version Type	VoR
URL	https://doi.org/10.11501/3072880
rights	
Note	

Osaka University Knowledge Archive : OUKA

https://ir.library.osaka-u.ac.jp/

Osaka University

SCANNING TUNNELING MICROSCOPY OF SEMICONDUCTOR SURFACES

by

Ichiro TANAKA

DISSERTATION IN PHYSICS

THE OSAKA UNIVERSITY

GRADUATE SCHOOL OF SCIENCE

TOYONAKA, OSAKA

Contents

Part 1: Semiconductor Surface Structures Observed by Scanning Tunneling Microscopy in Air

Abstract 1

1. Introduction 2

2. Microcrystalline Silicon Surfaces 4

3. Multiquantum Well Structures 13

4. Conclusions 27

References 28

Part 2: Investigation of Processed Semiconductor Surfaces by Ultrahigh Vacuum Scanning Tunneling Microscopy

Abstract 30

1. Introduction 32

2. Multi-chamber Ultrahigh Vacuum Scanning Tunneling Microscope System

2-1. Introduction 34

2-2. Outline of the System 34

2-3. MBE Growth Conditions of GaAs Layers 35

2-4. STM System
(2-4-1) STM Unit Designed for the System 37
(2-4-2) STM Control Electronics 39

2-5. Tip Preparation 41

2-6. Observation of MBE-Grown and Ar Ion-Bombarded Surfaces 42

2-7. Summary 44

3. Surface Reconstructed Structure of Molecular Beam Epitaxially Grown GaAs Layers

3-1. Introduction 61

3-2. Experiment 61

3-3. RHEED Observations 62

3-4. STM Observations 63

3-5. Conclusions 66

4. Step Structures of Molecular Beam Epitaxially Grown GaAs (001) Vicinal Surfaces

4-1. Introduction 76

4-2. Experiment 77

4-3. Step Structures of GaAs (001) Vicinal Surfaces 78

4-4. Step Structure Changes with MBE Growth 80

4-5. Summary 82

5. Heteroepitaxy of GaAs on InP (001) Substrates

5-1. Introduction 89

5-2. Observation of InP (001) Surfaces Thermally Cleaned in an Arsenic Flux 90

5-3. GaAs Heteroepitaxial Growth on InP (001) Substrates 94

5-4. Conclusions 98

6. Conclusions 108

References 110

Acknowledgements 113

PART 1

Semiconductor Surface Structures Observed by Scanning Tunneling Microscopy in Air

Abstract

Microcrystalline silicon film surfaces and multiquantum well (MQW) structures of cleaved surfaces are investigated using a scanning tunneling microscope (STM) in air. Grain-like structures of 30-80 nm size which correspond to transmission electron microscope data are observed in the images of microcrystalline silicon surfaces. The film surface is found to be geometrically rather flat but the structure is imaged electrically, that is, the resistivity seems to be inhomogeneous due to preferential oxidation. As for the MQW structure, we have obtained clear images of GaInAs/InP and AlAs/GaAs MQWs with nanometer resolution. These corrugations come not from a topological difference but from the difference between the tunneling conductances of the well layers to the tip and that of the barrier layers to the tip. Also the STM images are affected by various factors such as contamination and humidity in air. Degradation of the STM images are observed for the both cases, which may be due to the surface oxidation accelerated by the tunneling current injection.

1. Introduction

Scanning tunneling microscopy is a technique based on the tunneling phenomenon which offers direct observation of surface structures of conducting or semiconducting materials in real-scale with atomic resolution, including non-periodic structures.[1,2] A sharp metal tip is brought to the surface close enough to measure a tunneling current between the tip and surface with a tip-to-sample bias voltage, and the tip scans the surface two-dimensionally, while its height is controlled to keep a constant tunneling current. The motion of the tip corresponds to a contour map of the surface. Since the tunneling conductance depends on the tip-height exponentially, very high resolution is achieved; typical resolution is 0.01 nm in z-direction and 0.1 nm in xy-plane.

One advantage of STM is that high resolution is obtained even under atmospheric conditions. In particular, atomic-scale resolution is obtained with layer-material such as graphite, whose surface is stable against oxidation and contamination.[3-5] For example, Binnig et al. reported on atomic-scale images of graphite surfaces in 1986, and Weimer et al. observed those of MoS_2 in 1988. This advantage makes it easy to apply STM for various materials. Though it is, in general, difficult to get atomic images on semiconductor surfaces in air, submicron to nanometer resolution images are easily obtained in real space; neither complicated sample preparation nor high-cost vacuum system is required. Therefore STM has been widely used as a high-resolution microscope.[6]

The first part of this thesis reports on observations of microcrystalline silicon film surfaces and multiquantum well (MQW) structures in air. The origin of the STM images and atmospheric factors

which affect images are discussed. In addition, image degradation accelerated by the tunneling current is described.

2. Microcrystalline Silicon Surfaces [7]

Microcrystalline silicon films are a promising material for applications in electronic devices with large areas, for example, solar cells and thin-film transistor arrays.[8,9] These devices are generally multilayered structures, so that their structural and electronic surface characteristics of morphology and degree of oxidation are important factors in their performance. Nevertheless, it was difficult to characterize nonperiodic or disordered surfaces such as that of microcrystalline silicon films with nanometer scale resolution in real space before the advent of STM.

The STM has made it possible to observe surfaces with submicron to atomic scale in real space under various environments. Its high resolution even in a laboratory atmosphere makes it potentially useful for investigation of various semiconductor processes like thin-film deposition, epitaxy, and etching. Gimzewski et al. first investigated the surface of nanocrystalline silicon film by STM under a vacuum of 10^{-6} Pa and observed 10 nm order structures which apparently granular.[10]

In this chapter, the in-air STM study of surface morphology of microcrystalline silicon films prepared by the glow discharge method is described.

N-type microcrystalline silicon films were prepared by rf(13.56 MHz) glow discharge decomposition of a monosilane (SiH_4), phosphine (PH_3), and hydrogen (H_2) mixture in a capacitively coupled diode system. The films were grown to 0.1-0.2 μm thickness on Corning 7059 glass substrates and had n-type conductivity of 1 /ohm/cm. The substrate temperature, chamber pressure, and rf power density were 230 °C, 80 Pa, and 0.4 W/cm^2, respectively.

One sample was cut into three pieces; one piece was observed by STM without further processing; a 4 nm thick gold film was evaporated on the second piece in order to eliminate electric information from STM data and to provide only geometric information; the last piece was HF etched to remove the native oxide from the microcrystalline silicon surface. The etching was made with 4.5% HF aqueous solution at room temperature for 30 second.

The STM we used was a commercially available one (Nanoscope1), which had a step-motor for coarse positioning of a tip and a piezo-electric tube scanner for topographic measurements. An electrochemically etched Pt-Ir alloy tip was used in this study. STM data were taken with the following conditions; constant tunneling current of I_t=2nA, bias voltage of V_b=2-4V(tip positive), and scanning rate of f=5Hz for as-deposited and HF-etched samples. It was impossible to obtain a stable STM image with V_b<1.5V. As for gold-evaporated samples, V_b=50 mV was used while other conditions remained the same.

Figure 2-1 shows a typical STM image of an as-deposited microcrystalline surface. Granular structures 30-80 nm wide and 5-10 nm high are clearly seen.

STM images generally contain both geometric and electric information. In order to obtain geometric information only, we examined the gold-evaporated sample, the surface of which showed a larger and smoother topographic pattern (Fig.2-2). Examination of the gold-evaporated surface revealed a geometric pattern size of microcrystalline silicon film which seemed larger than the characteristic size of the granular structure in Fig.2-1. Thus the structure in Fig.2-1 reflects electric information, that is, the electric resistance is not

uniform throughout the surface. Since STM images of the HF-etched surface show large topographic patterns similar to the gold evaporated surfaces (Fig.2-3), inhomogeneous oxidation seems the probable cause of the resistance variation on the surface.

Because a transmission electron microscope (TEM) image of a sample prepared by a similar process (Fig.2-4) shows grains of comparable size with our STM data in Fig.2-1, this inhomogeneity may reflect the micrograin structure. At the grain boundary, the resistance could be higher than that of the crystallized region because of preferential oxidation and the microcrystalline boundary may be observed not geometrically but electrically.

Gimzewski et al. investigated the surface of a nanocrystalline silicon film under a vacuum of 10^{-6} Pa and observed 10 nm order structures geometrically which they interpreted as individual grains because they had the same characteristic size as that of a TEM lattice image.[10]

It would be possible to observe the micrograin boundaries electrically when they are preferentially oxidized, although it seems difficult to observe them geometrically in atmosphere.

Another interesting fact is that the image of the HF-etched microcrystalline silicon surface became inferior during STM observation. Photographs in Fig.2-5 shows a gradual increase in the noise with scanning. This phenomenon is believed to be due to some surface reaction caused by tunneling current because when the tip was moved to another place a clear image was obtained, which was then again followed by rapid degradation. This demonstrates one possible STM application for nanometer-scale processing.

This degradation of images was not seen in HF-etched amorphous silicon which was grown by a similar glow discharge process. Thus, the

observed degradation of STM images is related to the microcrystalline boundary.

Microcrystalline silicon surfaces have been investigated by STM in air. A surface topographic pattern which has the same characteristic size as that of a TEM image was observed on the as-deposited film surface. Since gold-evaporated and HF-etched sample surfaces show larger topographic patterns, not only geometric but also electric properties contribute to STM images probably through oxidation at the grain boundary. Namely, the microcrystalline silicon film surface seems to be rather smooth but inhomogeneously oxidized.

Degradation of STM images of a HF-etched microcrystalline silicon film surface has been observed for the first time. This is an interesting phenomenon from the viewpoint of nanometer-scale processing.

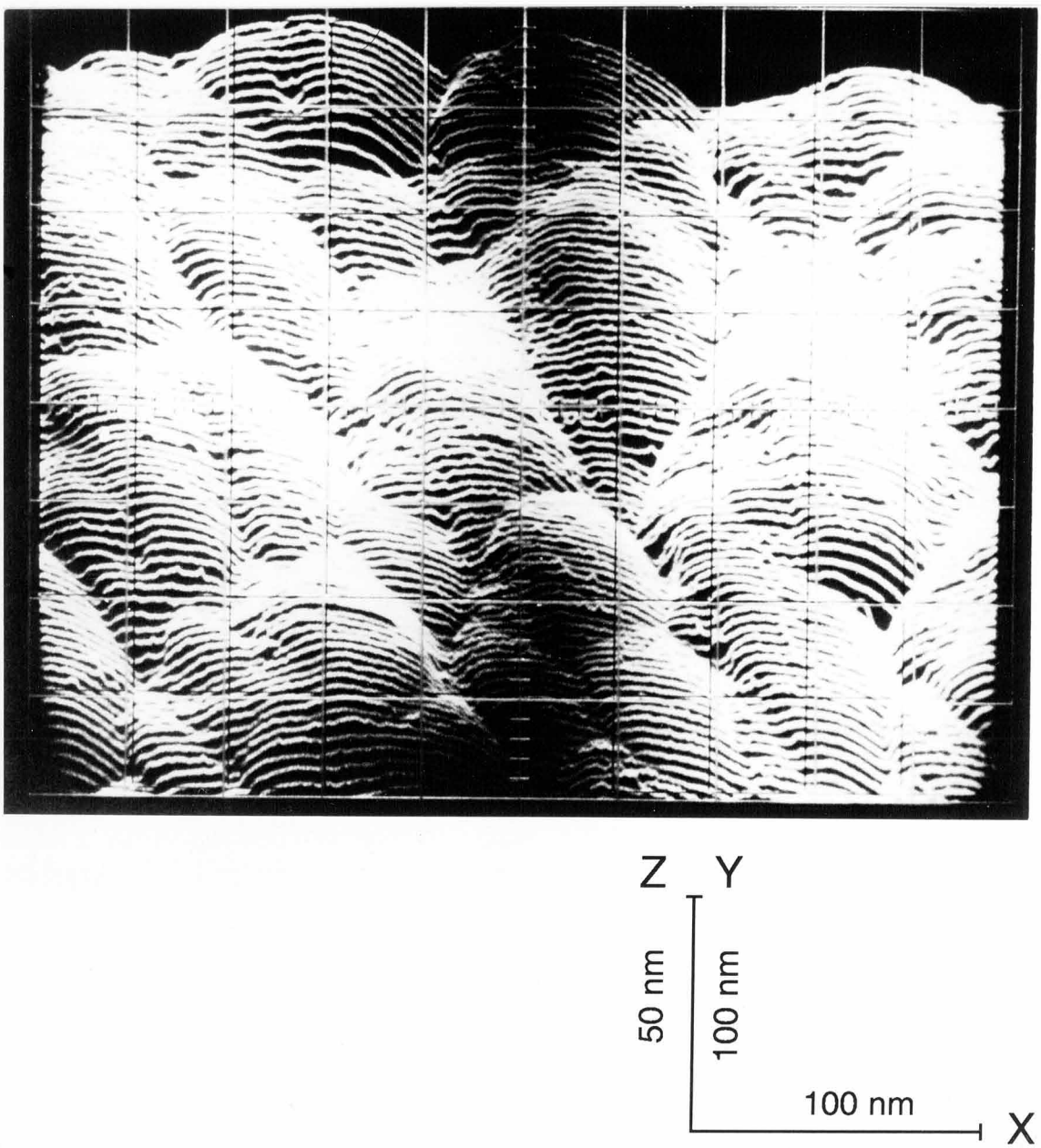

Fig. 2-1. STM image of as-deposited microcrystalline silicon surface

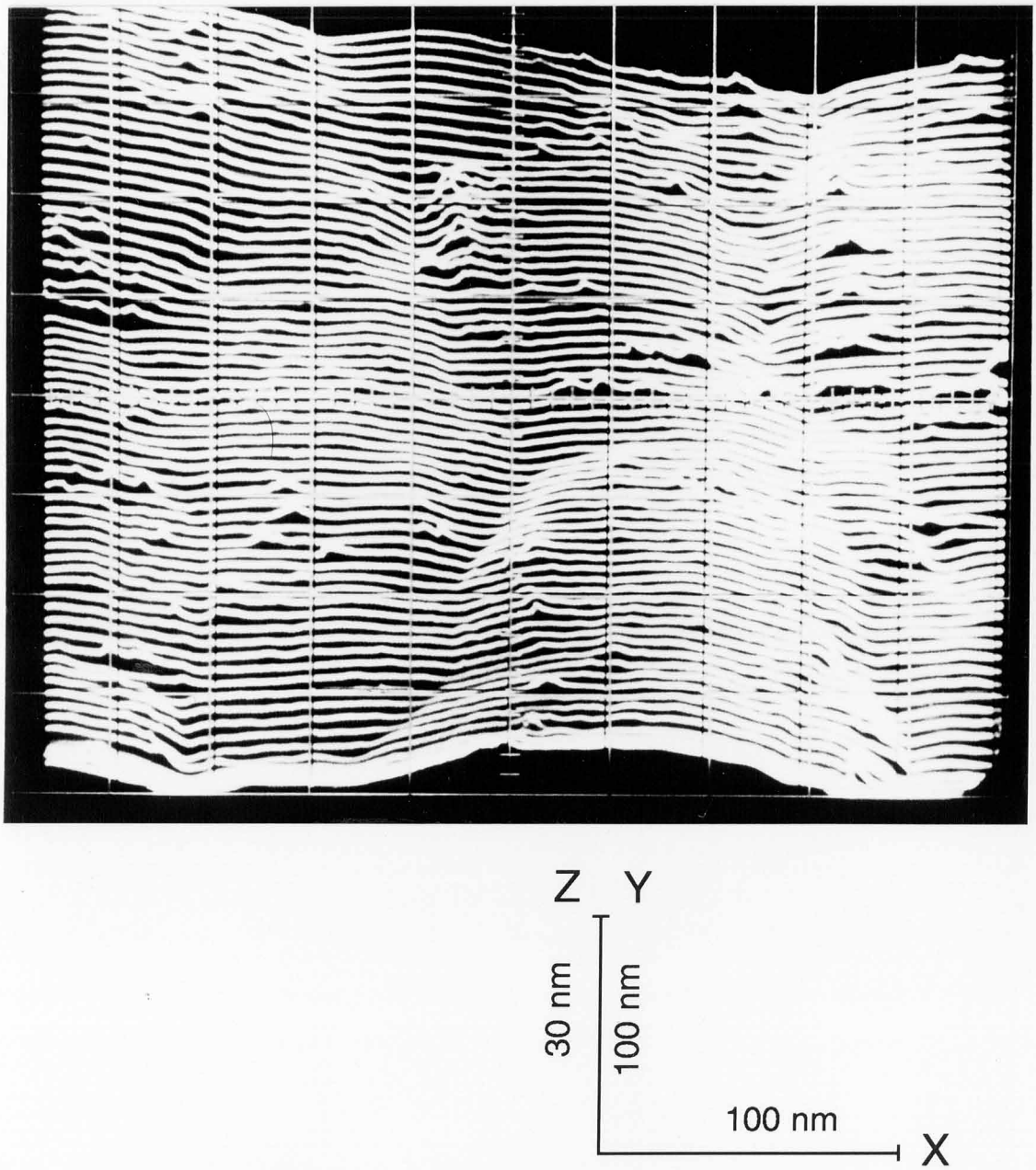

Fig. 2-2. STM image of gold-evaporated microcrystalline silicon surface

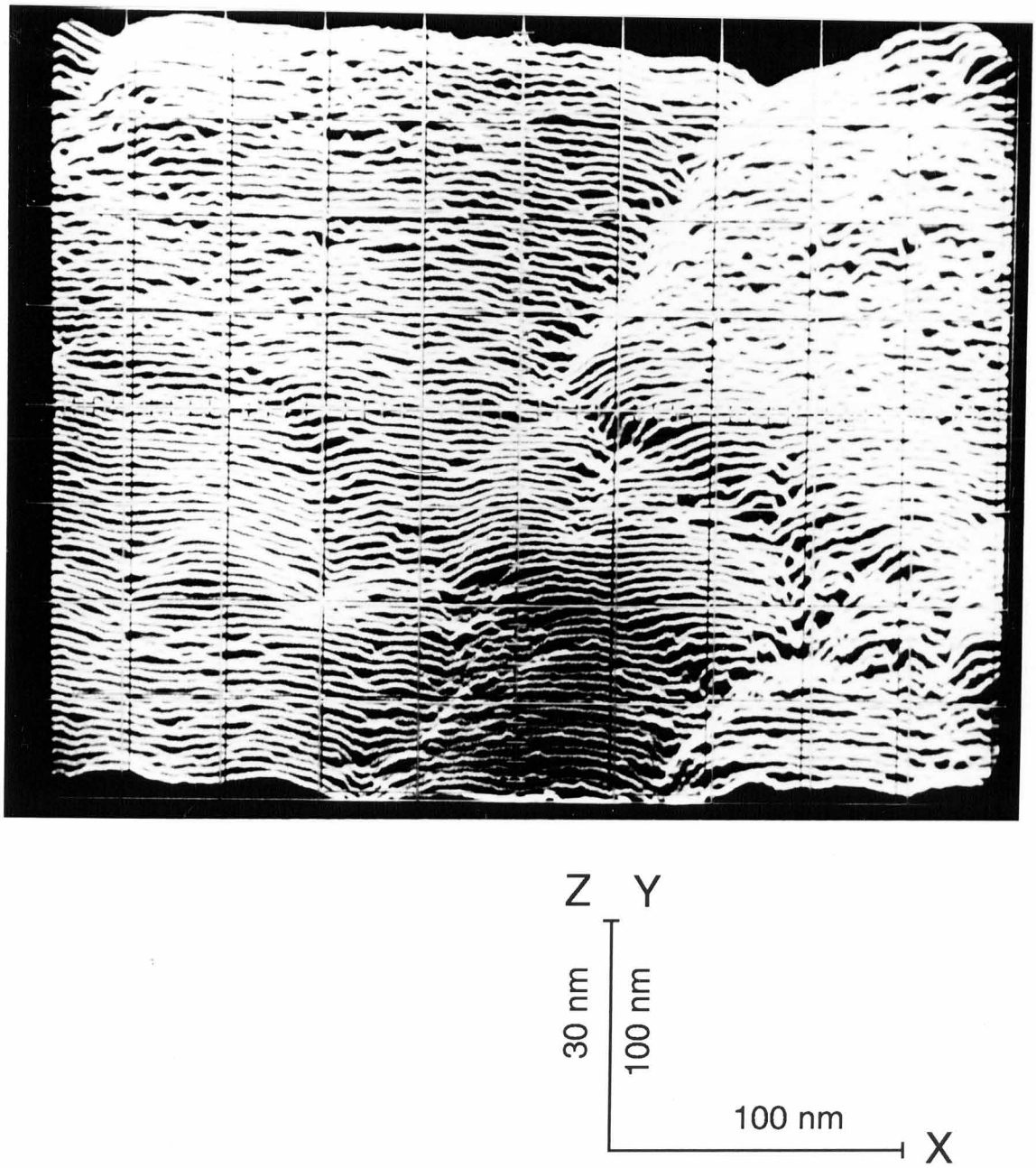

Fig. 2-3. STM image of HF-etched microcrystalline silicon surface

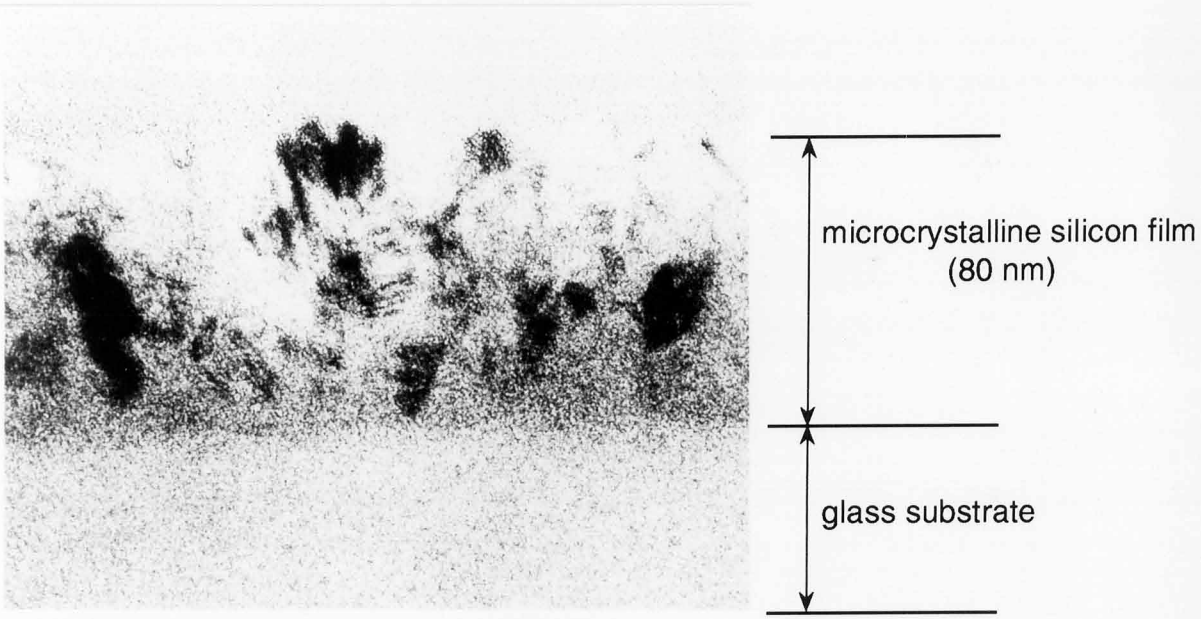

Fig. 2-4. Cross-sectional TEM image of microcrystalline silicon film.

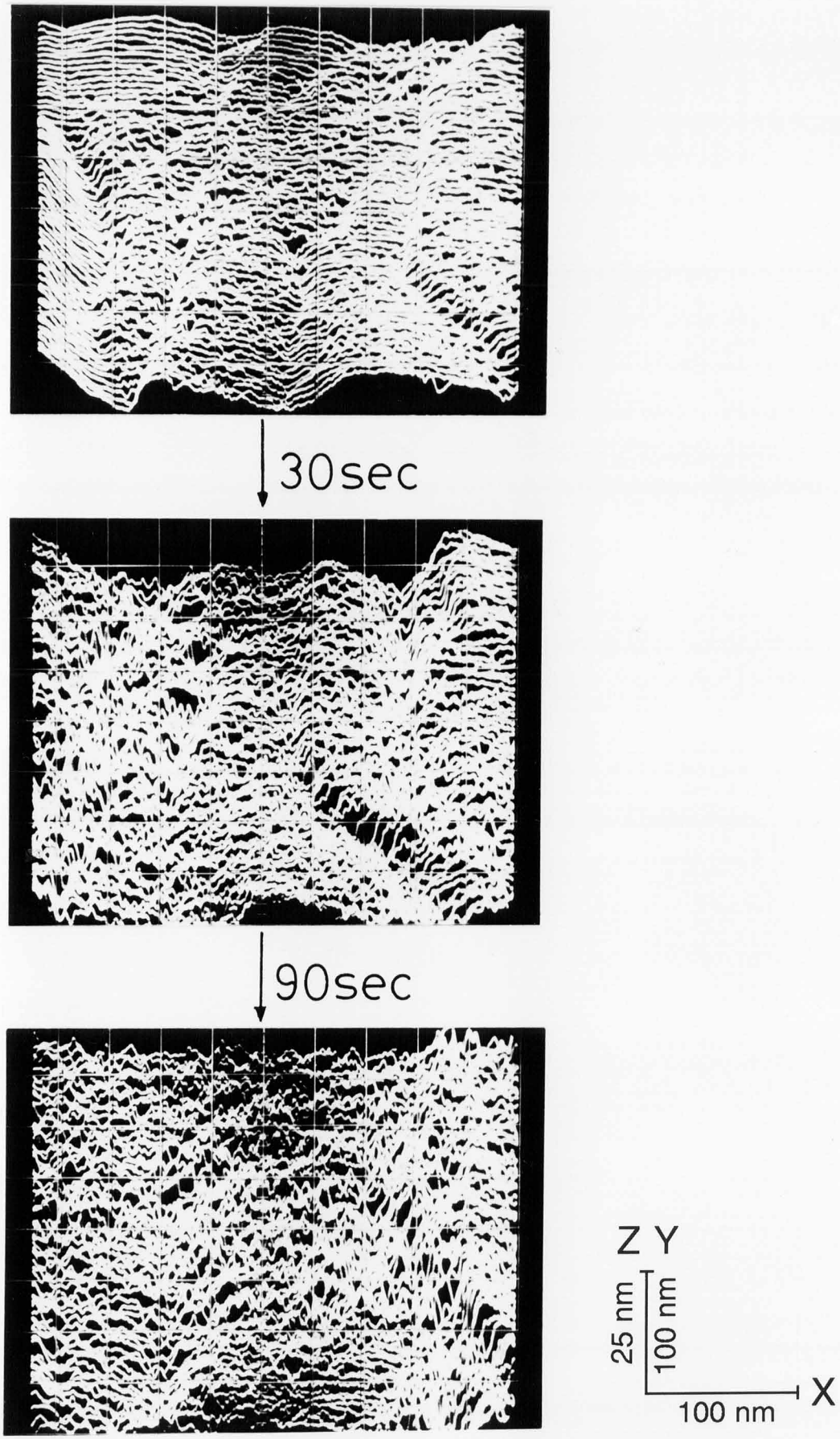

Fig. 2-5. Degradation of STM image by tunneling current.

3. Multiquantum Well Structures [11-13]

Multiquantum well (MQW) structures, which consists of alternately grown thin epitaxial layers of two semiconductor materials, have been attracting much attention because they are promising for applications in electronic and optoelectronic devices such as resonant hot electron transistors and low threshold lasers.[14] The device quality strongly depends on the MQW structures. The evaluation of MQW structures is therefore important for the development of the device technology. Though transmission electron microscopy and Auger electron spectroscopy have been used to measure the period and uniformity of MQW structures,[15] it is necessary to prepare samples in elaborate and complicated ways.

We observed cleaved surfaces of GaInAs/InP and GaAs/AlAs MQW structures in air using an STM and obtained clear corrugated images which corresponded to the MQW structures. The grooves and ridges of the corrugation show the well layers (InP or AlAs) and the barrier layers (GaInP or GaAs), respectively. These corrugations are not of topological nature but from the difference between the tunneling conductance of the tip to the well layers and that of the tip to the barrier layers, which may reflect the difference in the electronic structures of the two materials. The amplitude of the corrugation is found to be affected by contamination and humidity in air and scattered widely.

Also we found that the STM images degrades during observation and that the degradation is accelerated by the tunneling current. The stability of the images is different for different materials. The AlAs/GaAs MQW images degrades in a few minutes while the GaInAs/InP MQW images are stably observed for a few tens of minutes.

In this chapter the origin of the STM image of the MQWs, factors which affect the images and the possibility of new STM application for nanometer scale processing are discussed.

We used 20 nm period GaInAs/InP MQWs prepared by metalorganic chemical vapor deposition and 60 nm period AlAs/GaAs MQWs prepared by molecular beam epitaxy for the experiments. The GaInAs/InP MQWs contains unintentionally doped $10^{15}cm^{-3}$ donors, and the AlAs/GaAs MQWs were doped with $2\times10^{17}cm^{-3}$ donors. A schematic illustration of the sample and the experimental set up is shown in Fig.3-1.

After cleaving the sample in air, we observed the cleaved (110) surface by an STM (Nanoscope1) with a tube scanner which had scan area of 9 mm x 9 mm. The sample was set for the y-axis of the STM to be parallel to the MQW layers. An electrochemically etched Pt-Ir tip was moved into the tunneling region on the cleaved surface at an arbitrary position and scanned over 9 μm in the x-direction. The sample was moved 9 μm by 9 μm along the x-direction towards the MQW region until the MQW structure was found. STM images were taken under the following conditions; tip bias voltage was 1-2 V, tunneling current was 1-2 nA, scanning rates for horizontal and vertical directions were 5 and 0.04 Hz, respectively.

Figure 3-2(a) shows an STM image of the GaInAs/InP MQW structure. The left-hand part of the image shows a flat area which corresponds to the InP buffer layer and the right-hand part shows the corrugation corresponding to the MQWs. The period of the corrugation is estimated to be 20 nm which agrees with that of the MQWs. From this image we can see that the grooves of the corrugation correspond to the

InP barrier layers because the InP buffer layer and the grooves of the corrugation have almost same height in the STM image. The ridges of the corrugation therefore correspond to the GaInAs well layers.

Figure 3-2(b) shows an STM image of the AlAs/GaAs MQW structure. In this figure, the right-hand area shows the GaAs cap layer and the left-hand area shows the MQW region. The period of the corrugated image is about 60 nm which agrees with that of the MQWs again. Similarly to the GaInAs/InP MQWs, we can see that the grooves and ridges correspond to the AlAs barrier layers and GaAs well layers, respectively.

If the geometric corrugation is generated when the sample is cleaved, the STM images of the cleaved surfaces should be inverse to each other as shown schematically in Fig.3-3. The topographic STM image of the opposite cleaved surface of Fig.3-2(a) is shown in Fig.3-4. Since the relation of the elevations of the MQW layers and the buffer layer is the same as that in Fig.3-2(a), geometrical corrugation caused by cleavage cannot explain these observations. It is thus clear that the corrugated STM images of the MQW structures originate from the difference between the tunneling conductance of the tip to the well layers and that of the tip to the barrier layers, i.e., the the tunneling conductance between the tip and the well layers is larger than that between the tip and the barrier layers.

This can be understood qualitatively if the surface band structure of the well layers and the barrier layers closely resemble the bulk band structures. Figure 3-5 shows the band diagram at positive tip bias voltage electrons in the MQWs are supposed to tunnel from the occupied states in the valence bands to the empty states above the Fermi level of the metal tip. The occupied states are represented by regions of slashed lines in Fig.3-5. The numbers of electrons tunneling from the well layer

valence band is larger than that of electrons from the barrier layer valence band because the band gap energy is smaller in the well layers.

The corrugation amplitude in the STM images of the MQWs scattered widely in a range of 0.2 - 20 nm. We examined the factors which affect the corrugation amplitude to see the reason why the amplitude of the corrugation was scattered so much.

In the STM images of graphite surfaces in air, contamination on the surfaces has been reported to cause distortion of the STM images, enhancement of the corrugation amplitude and an anomalously low barrier height.[16,17]

These phenomena may also occur during STM observation of MQWs in air. First, we observed the distortion of the STM image of the MQW layers when the corrugation amplitude is as large as 20 nm. Second, the barrier height which was obtained from Z-piezo voltage vs tunneling current measurement was found to be of the order of a few meV, which is anomalously low when compared with electron affinities of the semiconductor samples. From these results, we suppose that the tip is in touch with contaminations on the sample surface and the actual change of the distance between the tip and the sample surface is smaller than the movement of the Z-piezo element, which will both increase the corrugation amplitude of the STM images and decrease the observed barrier height. Thus, the corrugation amplitude depends on the atmospheric environmental conditions which affect the contamination layer and scatters widely.

Another factor which influences the corrugation amplitude is the humidity. Figure 3-6 shows the increase in the corrugation amplitude with time when the sample was cleaved at about 50% relative humidity and maintained at about 80% relative humidity. The amplitude was 0.5 nm just after cleavage and became 10 times larger after 20 minute

humidification. It is therefore clear that different corrugation amplitude are obtained under various humidity conditions.

Also we found that the STM images of the MQWs deteriorated during the observation. The AlAs/GaAs MQW images degraded in a few minutes. In Fig.3-7 the changes of the AlAs/GaAs MQW image with time is shown. The corrugated image became noisier in a few minutes and disappeared in the noise after 8 minutes. We were able to observe the AlAs/GaAs MQW image for at most 15 minutes and sometimes only for 1-2 minutes. On the other hand, the GaInAs/InP MQW image changed much more slowly and could be observed for about an hour. Figure 8 shows the case for the GaInAs/InP MQWs. This difference suggests that the cleaved surface of the AlAs/GaAs MQWs is less stable than that of the GaInAs/InP MQWs in air against oxidation and/or contamination. Also this degradation was accelerated by the tunneling current because without prior observation we were able to measure the corrugation even more than 3 hours after cleaving.

The AlAs layers became noisy faster than the GaAs layers. Hence the reaction which caused the degradation of the images might be the oxidation at the surface because aluminum is very easily oxidized. It therefore will be possible to control the surface reaction on nanometer scale, if the environmental conditions are controlled properly. This shows a possibility of STM application for new nanometer fabrication technology.

We investigated the cleaved surface of MQWs using an STM in air. The corrugation images of the periodic MQW structure originate from not geometrical sources but the difference in the tunneling conductances which may reflect the bulk electronic structure of the well layers and the barrier layers. The large scattering range of the

corrugation amplitude seems to be due to atmospheric factors such as contamination and humidity. Also the degradation of MQW STM images was observed. The degradation rate of the AlAs/GaAs MQW image is much larger than that of the GaInAs/InP MQW image. This degradation might be due to the surface oxidation accelerated by the tunneling current and is interesting from the viewpoint of new nanolithography technology.

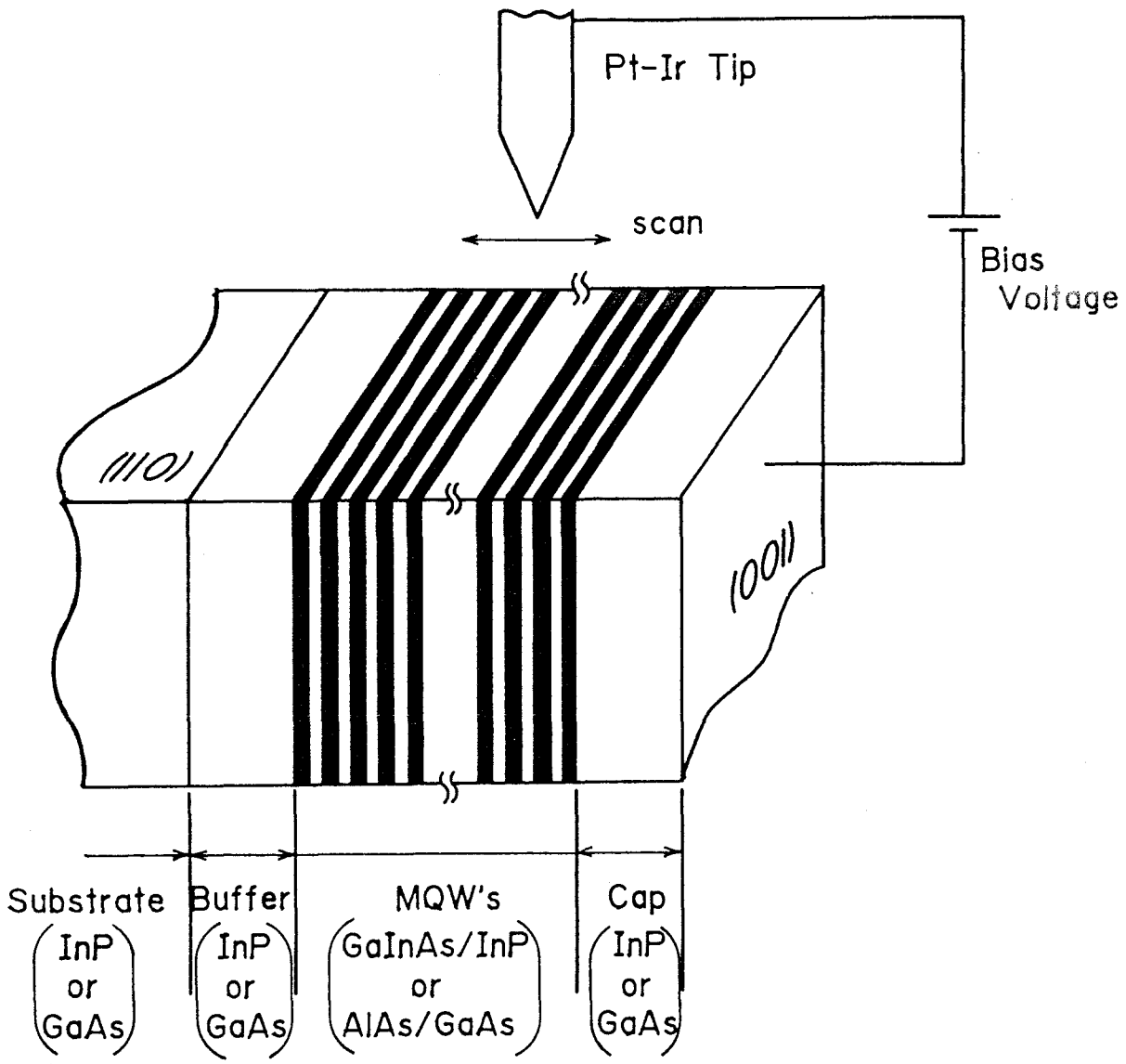

Fig. 3-1. Schematic diagram of the multiquantum well sample and the experimental setup for STM measurements.

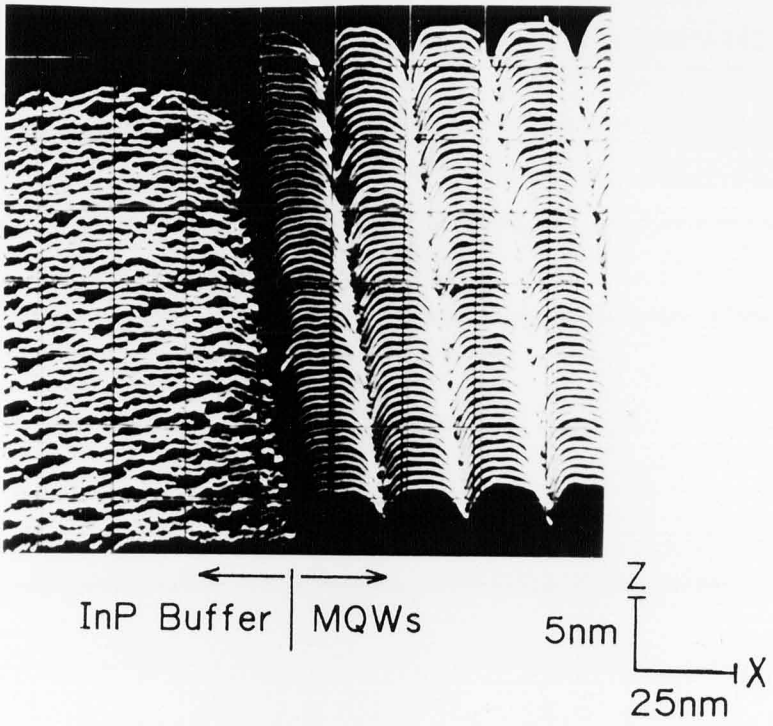

(a)

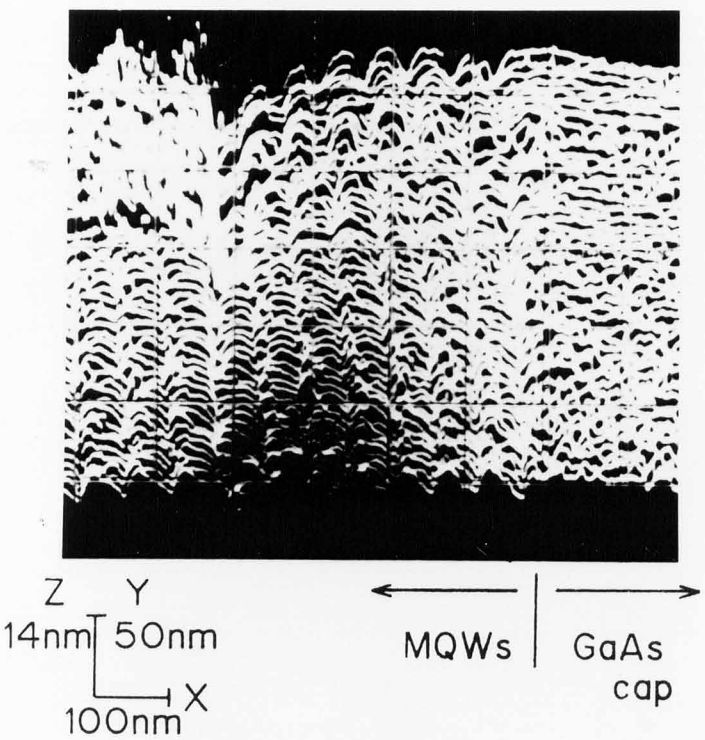

(b)

Fig. 3-2. (a) Topographic STM image of GaInAs/InP MQWs and InP buffer layer and
(b) Topographic STM image of AlAs/GaAs MQWs and GaAs cap layer.

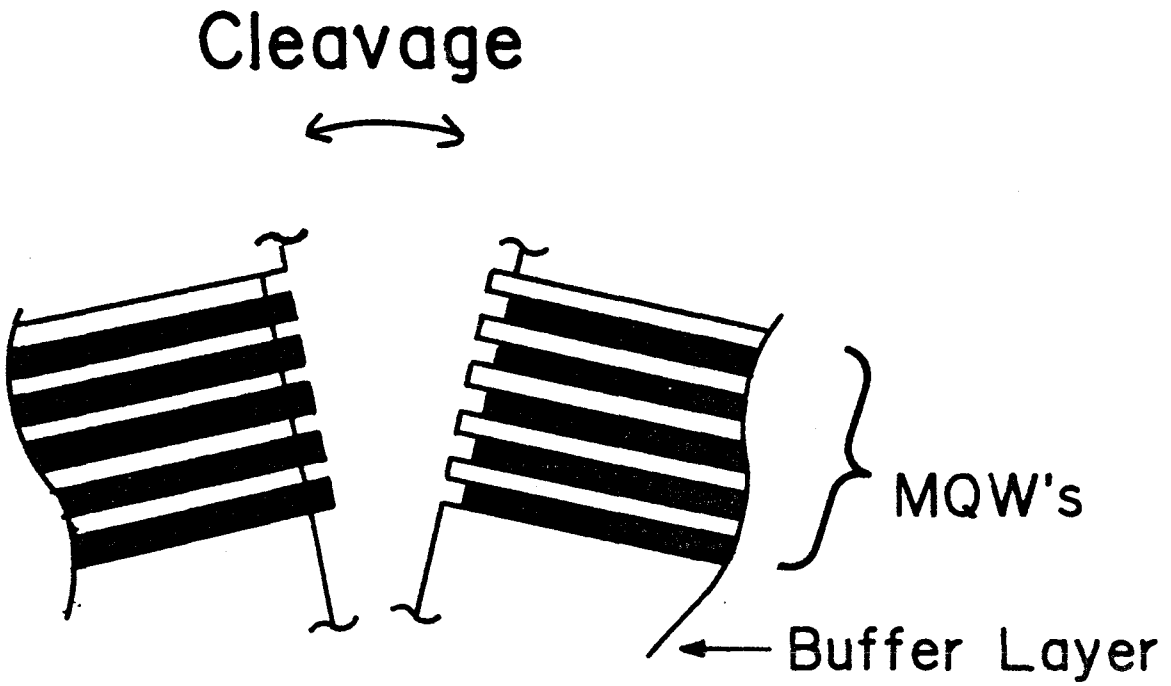

Fig. 3-3. Schematic illustration of the cleaved sample, if the geometric corrugation is assumed to be caused by cleavage.

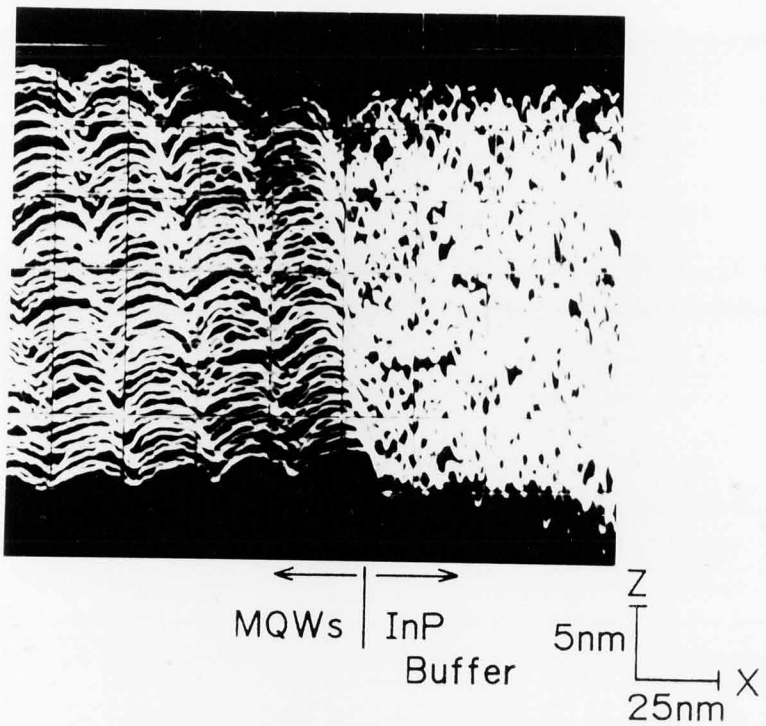

Fig. 3-4. Topographic STM image of the opposite cleaved surface of Fig. 3-2 (a).

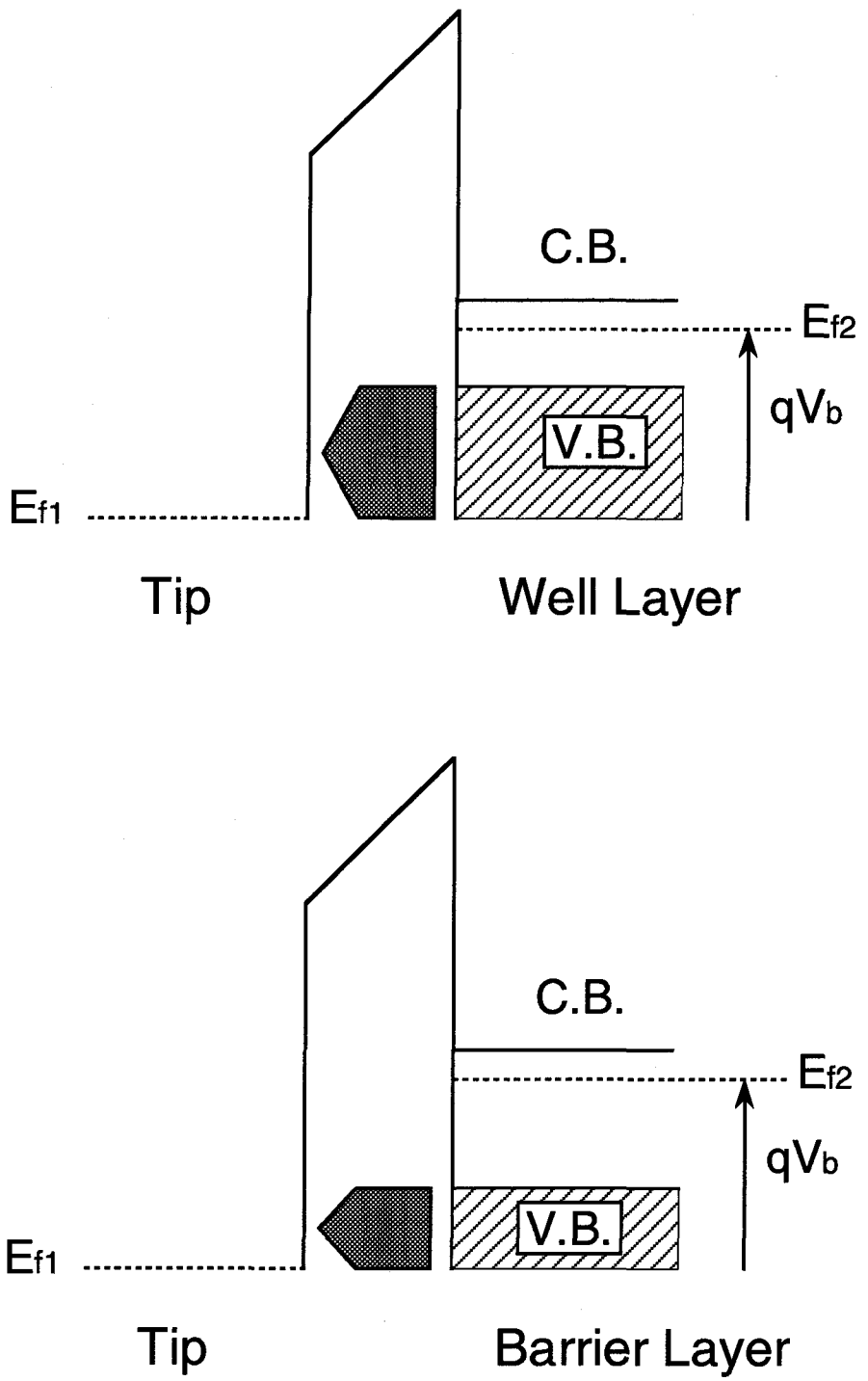

Fig. 3-5. Schematic illustration of the tunneling from well and barrier layers to the tip at positive tip-bias voltage. C.B. and V.B. denote conduction band and valence band, respectively. E_{f1} and E_{f2} denote Fermi levels of the tip and sample, respectively.

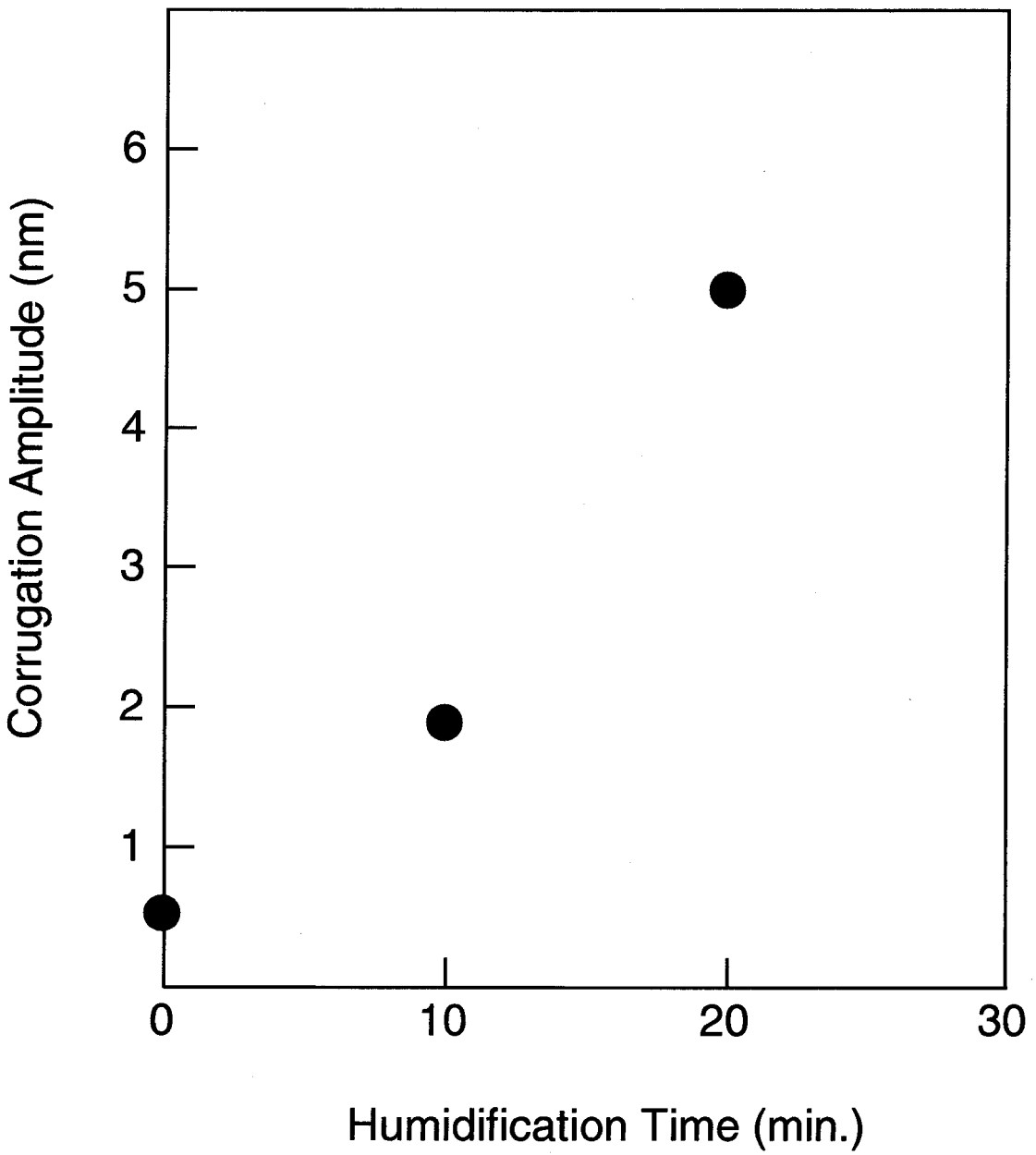

Fig. 3-6. Increase in the corrugation amplitude of the GaInAs/InP MQW STM image with time when the sample was cleaved in the atmosphere of 50% relative humidity and kept in the atmosphere of 80% relative humidity.

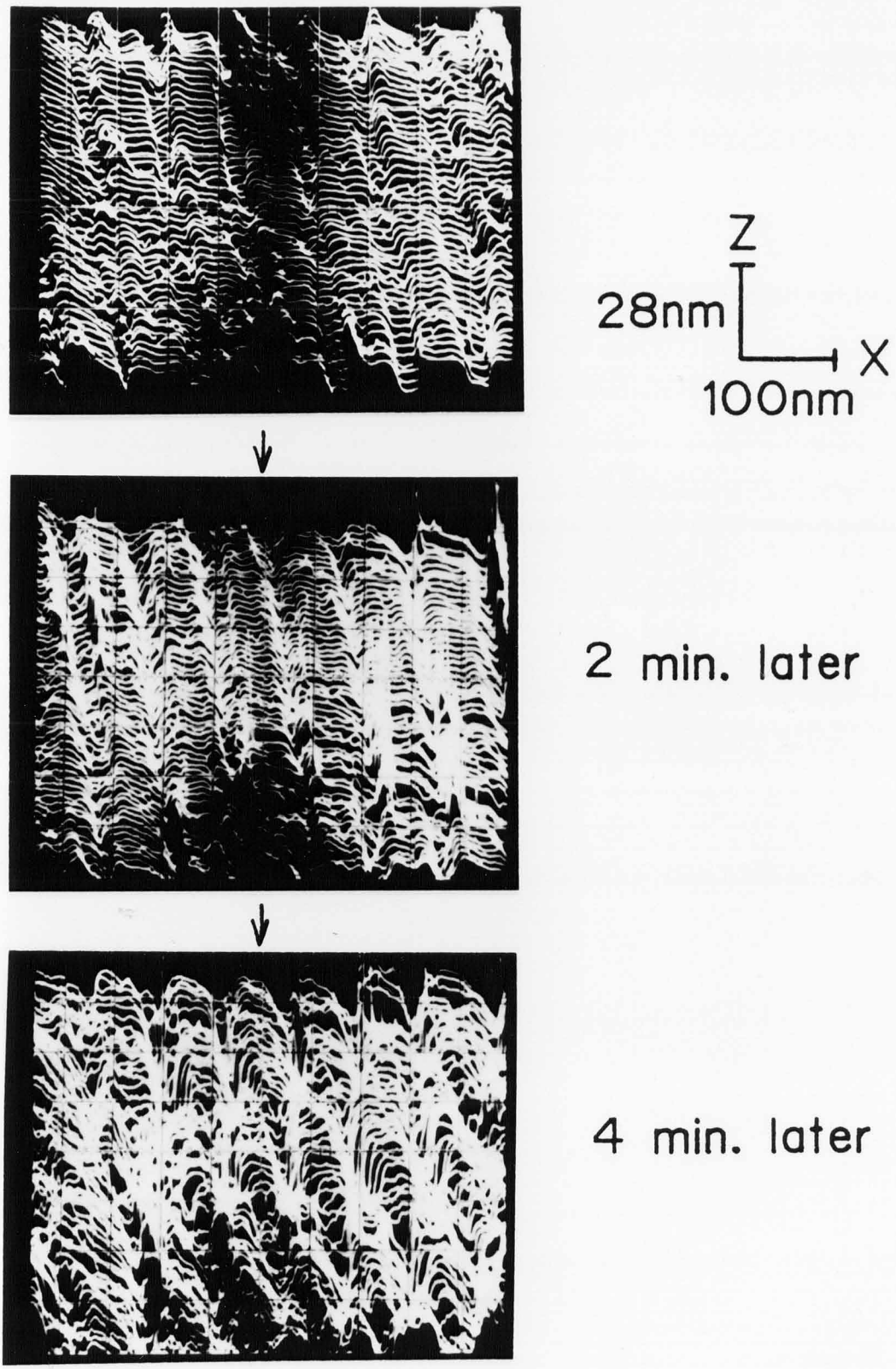

Fig. 3-7. Degradation of AlAs/GaAs MQW STM image with time.

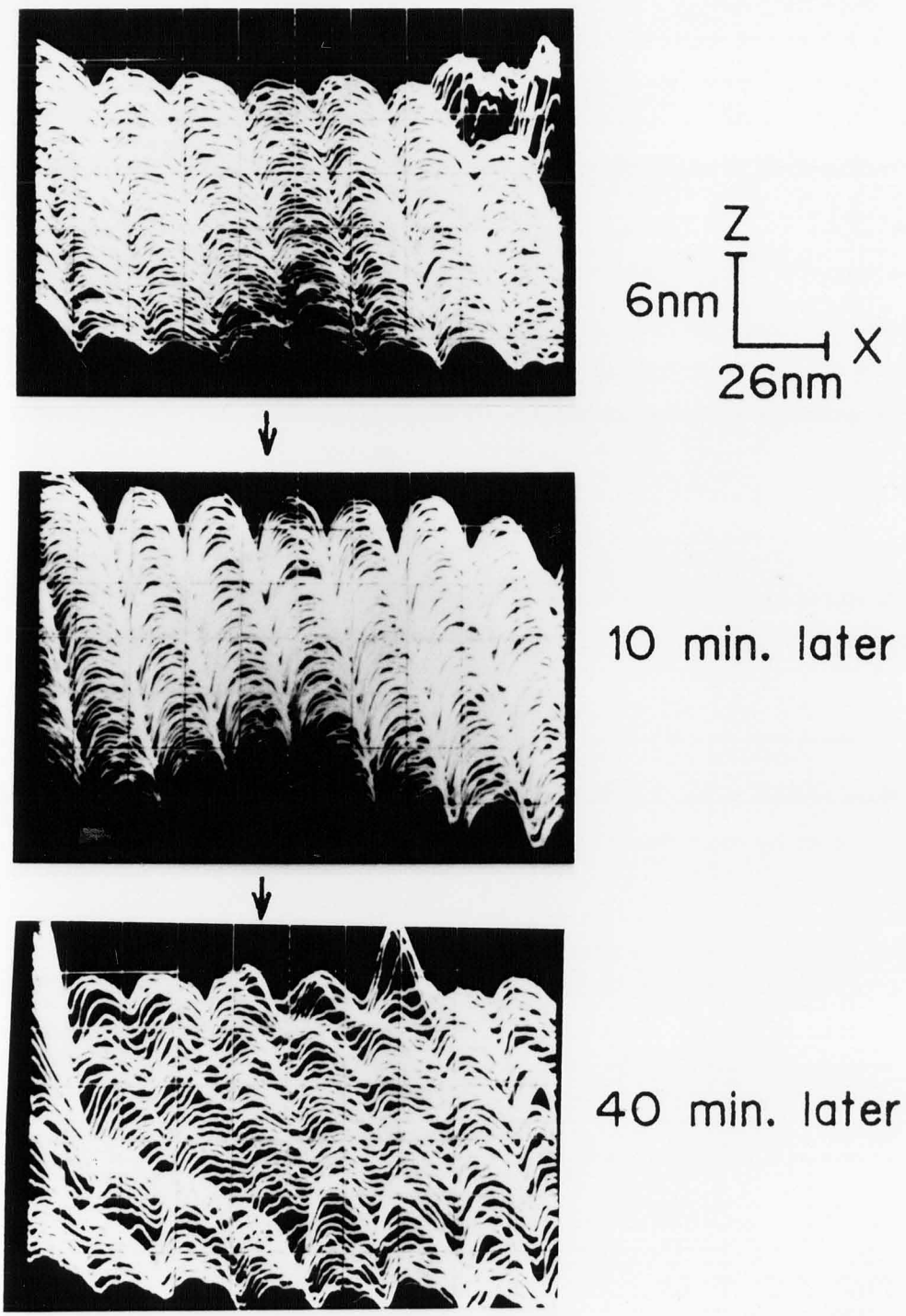

Fig. 3-8. Degradation of GaInAs/InP MQW STM image with time.

4. Conclusions

Surface structures of microcrystalline silicon film and MQW structures of GaInAs/InP and GaAs/AlAs cleaved surfaces are observed with an STM in air. The origin of the STM images are investigated; it has been found that the corrugation images are not from the geographic properties but from the differences in the tunneling conductances in both cases. Also it is discussed that atmospheric factors such as oxidation, humidity and contamination affects the STM images.

It has been found that the STM images degrade with time for the both cases; the tunneling current injection seems to accelerate oxidation at the surfaces. This phenomena is interesting from the view point of STM application for nanometer scale processing.

References

[1] G.Binning, H.Rohrer, Ch.Gerber, and E.Weibel, Phys. Rev. Lett., **49**, 57 (1982).

[2] J.Tersoff and D.R.Hamann, Phys. Rev., **B31**, 805 (1985).

[3] G.Binning, H.Fucks, Ch.Gerber, H.Rohrer, E.Stoll, and E.Tosatti, Europhys. Lett., **1**, 31 (1986).

[4] S.Park and C.F.Quate, Appl. Phys. Lett., **48**, 112 (1986).

[5] M.Weimer, J.Kramer, C.Bai, and J.D.Baldeschweiler, Phys. Rev., **B37**, 4292 (1988).

[6] C.F.Quate, Phys. Today, August, 26 (1986).
G.Binning and H.Rohrer, Review of Modern Phys., **59**, 615 (1987).

[7] I.Tanaka, F.Osaka, T.Kato, and Y.Katayama, Appl. Phys. Lett., **54**, 427 (1989).

[8] Y.Hamakawa, Japan Annual Review in Electries, Computers and Telecommunications, **Vol.16**, Amorphous Semiconductor Technologies and Devices (OHM and North-Holland, Tokyo, Amsterdom, 1984).

[9] J.I.Pankove, Semiconductor and Semimetals, Vol.21, Hydrogenerated Amorphous Silicon Part D, Device Applications (Academie, Orlando, 1984).

[10] J.K.Gimzewski, A.Humbert, D.W.Pohl, and S.Veprek, Surf. Sci., **168**, 795 (1986).

[11] F.Osaka, I.Tanaka, T.Kato, and Y.Katayama, Jpn. J. Appl. Phys., **27**, L1193 (1988).

[12] I.Tanaka, T.Kato, S.Ohkouchi, and F.Osaka, J. Vac. Sci. Technol., **A8**, 567 (1990).

[13] T.Kato, F.Osaka, and I.Tanaka, Jpn. J. Appl. Phys., **28**, 1050 (1989).

[14] L.Esaki, IEEE J. Quantum Electron., **QE-22**, 1611 (1986).

[15] H.Kakibayashi and F.Nagata, Jpn. J. Appl. Phys., **24**, L905 (1985).

[16] H.J.Mamin, E.Ganz, D.W.Abraham, R.E.Thompson, and J.Clarke, Phys. Rev., **B34**, 9015 (1986).

[17] J.H.Coombs and J.B.Pethica, IBM J. Res. Develop. **30**, 455 (1986).

PART 2

Investigation of Processed Semiconductor Surfaces by Ultrahigh Vacuum Scanning Tunneling Microscopy

Abstract

A multi-chamber ultrahigh vacuum scanning tunneling microscope (UHV-STM) system has been constructed for investigations of the processed semiconductor surfaces. This system comprises five UHV chambers connected by UHV tunnels. A specially designed STM unit, which can be used with a 23 mm diameter molybdenum blocks, is installed in an STM chamber for surface observations. A molecular beam epitaxy (MBE) chamber for epitaxial growth of GaAs layers and a process chamber for other processes, such as etching, are included in the five chambers. Therefore STM observation of MBE grown surfaces and other processed surfaces are performed keeping the surfaces free from contaminations with this system. Surface reconstructions of MBE grown GaAs layers in the arsenic stabilized region are observed; different arrangements of arsenic dimers including new ones are found corresponding to the different process conditions. Furthermore, step structures of MBE-grown GaAs layers on vicinal (001) substrates and their changes with growth are observed with atomic resolution. Finally heteroepitaxial growth mechanism of GaAs on InP (001) substrates is investigated with this system. Two dimensional growth and island formation are observed for GaAs deposition of less than 1.5 mono-layer (ML) and for that of more than 2.5 ML, respectively. It is suggested from the observations that the previously deposited GaAs are involved

in the island formation when critical thickness of the GaAs layer is exceeded.

1. Introduction

Nanostructures such as quantum wires and boxes have been proposed and attracting a growing attention because they are not only potentially promising for applications in future electronic and optoelectronic devices but also interesting from a view point of physics in nanometer-size structure.[1,2]

It is required to evaluate semiconductor structures with atomic resolution and control processes in atomic level in order to fabricate semiconductor nanostructures. For example, molecular beam epitaxy (MBE) and other semiconductor process technologies are based on various surface phenomena. It is thus important to investigate the mechanism of those phenomena for the development of technologies to control processes in atomic scale. Though it seems to be rather difficult with conventional technologies, the advent of STM has made it possible to investigate semiconductor nanostructures and processes with atomic resolution.

During the last decade scanning tunneling microscopy (STM) was widely applied to the study of semiconductor surface structures. In 1983, Binnig et al. observed 7×7 reconstruction of Si (111) surface in ultrahigh vacuum (UHV),[3] and obtained an STM image which coincides with dimer-adatom-stacking fault (DAS) model proposed by Takayanagi et al.[4] This work was so impressive that it was followed by a lot of studies concerning to various Si surfaces with an STM. Also Tromp et al. observed a Si(001) surface in 1985 and reported that the 2×1 structure consists of Si-Si dimers.[5]

As for compound semiconductors, Feenstra et al. pioneered observation of cleaved GaAs (110) surfaces with a UHV-STM in 1986. They reported that As atoms are observed with a negative sample-to-tip bias voltage and Ga atoms with a positive sample-to-tip bias

voltage.[6] Pashley et al. observed the 2×4 structure of an arsenic stabilized GaAs (001) surface for the first time in 1988, and found that 2×4 pattern of electron diffraction comes from missing dimers,[7] which had been theoretically proposed by Chadi.[8] They used MBE grown and arsenic passivated surface prepared in an MBE system. The sample was transferred to a separated UHV-STM through air and heated in UHV to remove arsenic cap layer. The symmetry of the reconstruction was confirmed by low energy electron diffraction (LEED) and the surface was observed by STM.

Biegelsen et al. built a UHV-STM connected with an MBE system for quasi in-situ observation of MBE grown GaAs surfaces. They reported on various reconstructions of MBE grown GaAs (001) and (111) surfaces in 1989.[9] Pashley et al. also added an MBE growth chamber to their UHV-STM system and observed step structures on GaAs vicinal (001) surfaces in 1991.[10] A multi-chamber UHV-STM system was constructed in 1989-1990 at Optoelectronics Technology Research Laboratory (OTL) for the purpose of investigating compound semiconductor processes such as epitaxy and etching in atomic level by the author and his colleagues. The second part of the present thesis describes the multi-chamber UHV-STM system which comprises an STM-, an MBE- and a process-chambers. Then investigation of surface reconstruction structures of compound semiconductors and that of such processes as epitaxy and etching in atomic level using the UHV-STM are reported.

2. Multi-chamber Ultrahigh Vacuum Scanning Tunneling Microscope System [11]

2-1. Introduction

STM is a technique which enables us to investigate metal or semiconductor surfaces with atomic resolution; it is widely used to study various types of surface. In particular, a UHV-STM combined with an MBE system has been developed and used for studying MBE-grown compound semiconductor surfaces.[12-14]

In this chapter we describe our multi-chamber UHV-STM system, which is designed for investigating processed semiconductor surfaces. This system comprises five UHV chambers, including an STM chamber, an MBE chamber and a process chamber. In order to carry out UHV-STM observations of processed semiconductor surfaces, we have developed an STM unit which can accept a molybdenum (Mo) block of 23 mm diameter as a sample holder used in MBE and other processes.

We obtained clear images of the 2×4 reconstructed surface structure of an MBE grown layer on a GaAs (001) wafer with this multi-chamber UHV-STM system. Argon ion bombardment was also preformed on an MBE grown GaAs (001) surface; many atomic-scale defects were found on the bombarded surface with the UHV-STM.

2-2. Outline of the System

Figure 2-1 is a schematic illustration of the multi-chamber UHV-STM. This system has five chambers for UHV-STM observations, MBE growth, such processing as etching, Auger electron spectroscopy (AES), sample exchange, and sample loading. Each chamber is connected to the sample exchange chamber by a vacuum tunnel and is separated by a gate-valve. The load-lock chamber is evacuated by a turbomolecular

pump (TMP) to a base pressure of 1.3×10^{-6} Pa; the others are evacuated by a titanium sublimation pump and a sputter ion pump (SIP) to a base pressures of less than 1.3×10^{-8} Pa.

A sample in the load-lock chamber is transferred to the sample exchange chamber and then preheated for several hours, before being transferred to the MBE chamber. The MBE system used here is a conventional type with four Knudsen cells used for the effusion of As, Ga, Al, and Si. This chamber is also equipped with a reflection high energy electron diffraction (RHEED) system. RHEED data show the symmetry of the surface structure over wide area in contrary to STM data, which show local surface structure. They are therefore complementary each other.

After growth, a sample is either transferred to the STM chamber for UHV-STM observations, or is transferred to the process chamber for additional processing. The sample transfer is carried out by magnetically-coupled transfer rods with a bionet coupler between the sample exchange chamber and other chambers, except for the STM chamber. A transfer rod with a screw is used for the transfer to/from the STM chamber, as shown in Fig. 2-8. It takes only several minutes to transfer a sample from the MBE chamber to the STM chamber. Since transfers are performed under a UHV in which the pressure is less than 1.3×10^{-8} Pa, it is possible to keep a sample surface clean during a transfer.

2-3. MBE Growth Conditions of GaAs Layers

The base pressure of the MBE chamber was lowered to 1.3×10^{-8} Pa after the cryo-shroud was cooled with liquid nitrogen. The beam flux of each Knudsen cell was measured with an ion gauge placed behind the

specimen location. Figures 2-2 (a) and (b) are measured beam flux data for Ga-, Al-, Si-, and As-cells, respectively.

A commercially available Si-doped n^+-GaAs (001) wafer was used for the growth experiments. A two-inch wafer was cleaved into 9 mm x 11 mm pieces. One piece of the sample was prepared by the following cleaning steps; it was etched for 1 minute in 5:1:1 H_2SO_4:H_2O_2:H_2O at 50 °C, rinsed in flowing de-ionized water for 5 minutes, and dried by nitrogen gas blowing. It was, then, soldered onto a molybdenum block of 23 mm diameter with indium.

After being put into the exchange chamber, the sample was prebaked at 370 °C for three hours. Then it was transferred to the MBE chamber, and heated slowly in order to sublime the surface oxides off in an arsenic flux of $4x10^{-3}$ Pa. The substrate temperature was raised gradually starting from about 400 °C until the desorption of oxide was confirmed by RHEED. The substrate temperature was measure with an infrared thermometer. A four-fold RHEED pattern appeared for an incident electron beam in the $[\bar{1}10]$ azimuth when the surface oxide desorbed at typically 590 °C. The shutters of the Ga- and Si-cells were then opened to begin the growth.

The growth rate was measured from the frequency of RHEED intensity oscillation. Figure 2-3 shows an example of the intensity oscillation of a specular spot of a RHEED pattern when the Ga-shutter was opened under an arsenic flux of $2.9x10^{-3}$ Pa at substrate temperature of 550 °C. The temperatures of the Ga- and As-cells were kept at 920 °C and 210 °C, respectively at this experiment. The one-cycle of the oscillation corresponds to the one mono-layer (ML) growth of GaAs. The growth rate is calculated to be 1 ML/sec from Fig. 2-3.

The dopant concentration was measured with a profiler for a sample which was MBE-grown under the following conditions; temperatures of Si- and Ga-cells were 1000 °C and 930 °C, respectively; the arsenic flux was 4.3×10^{-3} Pa; the substrate temperature was 572 °C. Figure 2-4 shows the measurement result. The dip corresponds to the interface between the substrate and the epitaxially grown layer; the right-hand region and the left-hand region to the substrate and the 0.3 μm thick epitaxy layer, respectively. The dopant concentrations of the substrate and the epitaxy layer are seen to be 5.8×10^{17} cm^{-3} and 1.1×10^{18} cm^{-3}, respectively.

In order to check the surface cleanliness of the grown layer, AES measurements were curried out in the exchange chamber. Fig. 2-5 shows an Auger electron energy spectrum of a GaAs surface before growth. The peaks at 1070 eV and at 1228 eV are from Ga atoms and Arsenic atoms, respectively. In addition, the Carbon peak at 272 eV and the Oxygen peak at 503 eV are observed. After an MBE-growth, the sample was transferred into the exchange chamber and an AES measurement was performed again. The result is shown in Fig. 2-6; the peaks correspond to only Ga atoms and As atoms are remained, and those resulting from carbon and oxygen are not observed any more. The experimental parameters for the AES measurements were as follows; the electron beam energy for excitation was 3 keV, the modulation energy was 2 eV and, the beam current was 20 μA.

2-4. STM System

(2-4-1) STM Unit Designed for the System

The STM unit is supported with a double spring anti-vibration suspension within the chamber as shown Fig.2-7. The designed resonance frequencies of the suspension are 1.2 Hz and 1.8 Hz, and

measured one is 3.7 Hz. The suspension system is assembled with a vacuum flange of 253 mm diameter, which is attached to the chamber vertically.

When a sample is transferred to/from the STM chamber, the STM unit is pressed against a stage under the unit using a linear-motion feedthrough.

We have designed and constructed a small-size STM unit in order to carry out observations with a 23 mm diameter Mo-block (Fig.2-8). It has a piezo-tube of 9 mm-diameter × 20 mm-length for scanning in the x, y, and z directions. A small inchworm-type positioner is used for coarse Z-positioning of the tip. It comprises two precise ceramic blocks and three stacked piezo-electric elements (Fig.2-9). The piezo-electric element (P3) which connects the two ceramic blocks expands 3 μm when 100 V is applied. The other piezo-electric elements (P1, P2) are glued to each ceramic block (C1, C2) and expand 15 μm when the same voltage is applied, thus cramping the ceramic blocks. A groove with a rectangular cross-section is formed in a stainless-steel base in order to move the inchworm-type positioner. The width of the groove is exactly same as the sum of the width of the ceramic block and the length of the PZT element, since the position of one wall can be adjusted. Figure 2-9 illustrates one step of the Z-positioner's movement. It consists of 6 stages corresponding to the extension and shrinkage of the three piezo-electric elements. At the 1st stage, P1 and P2 are extended to cramp C1 and C2 , respectively. P1, then, shrinks to unclamp C1 at the 2nd stage. From the 2nd stage to the 3rd stage, P3 extends in order to move C1 forward by a few microns. At the 4th stage P1 extends to cramp C1 again. Then, C2 is unclamped and P3 shrinks to move C2 forward (stage 6). Finally, P2 extends and one step movement is completed. Figure 2-10 shows the measured displacement of the positioner in air. The back-

rush was found to be about 0.5 μm, which is smaller than the maximum Z-extension of the tube scanner (1.6 μm).

When the tip approaches the sample surface, the coarse Z-positioner is controlled with a personal computer, and the feedback loop is active; the Z-displacement of the tube scanner is at its maximum. When the tip is brought into the tunneling region and a tunneling current of 1 nA is detected, the Z-displacement is reduced in order to avoid a collision; the positioner is automatically stopped at the same time.

The calculated resonance frequency of the base is approximately 20 kHz. It is therefore estimated that this STM unit has enough high resonant frequency to eliminate the effects of environmental vibrations. The Mo-block inserted into the sample holder of the STM unit is firmly fixed with a sheet-spring.

(2-4-2) STM Control Electronics [15]

Figure 2-11 shows the schematic block diagram of the STM control and data acquisition electronics system. This electronics is designed to perform measurements in three modes, that is, constant-current, constant-height, and scanning-tunneling-spectroscopy (STS) modes. The preamplifier magnifies the voltage across a resistor (1M ohm) generated by a tunneling current between the tip and sample. In the constant-current measurement mode, the feedback loop is closed, that is, the analog switch is on and the input and output voltages of the sample-and-hold (S/H) circuits are equal. The output signal of the preamplifier is transformed to its absolute value, then to its logarithm, and integrated with certain time-constant. The integrated feedback signal is applied to the Z-electrode of the tube scanner after high voltage (HV) amplification.

The data acquisition is performed by a personal computer (PC98) with a 80286 CPU and a 80287 math-coprocesser. The feedback signal is high-pass filtered in order to eliminate the effect of the sample tilt in topographic data, and also pass through a low-pass filter in order to reduce high frequency noises before they are converted to digital data by a 12-bit analog-to-digital converter (ADC) operating at a 200 kHz sampling rate. The converted data are stored in a 32-megabyte random access memory (RAM) which is increased in a expanded I/O slot.

The X-Y scanning signals and the sample bias voltage are generated by the personal computer; they are converted to analog signals by a 16-bit digital-to-analog converter (DAC) at the maximum convert speed of 140000 times per second; then, they are applied to the X-, Y-electrodes and samples, respectively.

The STS measurement is basically the same as the current-imaging-tunneling spectroscopy (CITS) technique.[16-18] Topographic data are obtained while the feedback loop is closed; at the same tip position the feedback loop is, then, opened and the bias voltage-tunneling current (Vs-It) spectroscopy is carried out. The feedback loop is switched by the two S/H circuits and the analog switch. The first S/H circuit is connected to the input of the logarithmic amplifier (LOG-AMP) in order to avoid a slow response of the LOG-AMP. Before and after switching the feedback loop, the input voltage of the LOG-AMP is kept constant by the first S/H circuit. The output voltage of the integrated circuit is maintained as follows; the current into the integrated circuit is shut by the analog switch in order to prevent the output voltage of the integrated circuit increasing with time and the second S/H circuit, which is connected after the integrated circuit, keeps the output voltage which would decrease with the time-constant of the integrated circuit without the second S/H circuit.

In order to perform a constant-height measurement, the time-constant of the feedback loop is set to be so large that the tip cannot follow surface corrugations, and data of tunneling current are acquired instead of the feedback voltage.

The data stored in the RAM are transferred to the 40-megabyte fixed disk connected with the personal computer or to the 300-megabyte fixed disk of the engineering work station (EWS, Hewlett-Packarde 340 SRX) at a rate of 10 Mbps through a local area network. Detailed analysis of the obtained data is performed on the EWS.

2-5. Tip Preparation

Tip preparation is the most important aspect of UHV-STM observation. We fabricate a tip from a polycrystalline (110) tungsten wire of 0.25 mm diameter by direct-current (DC) electrochemical etching in a NaOH 20 % aqueous solution as shown in Fig.2-12. An electric current flows through the Hg-layer in the bottom of the beaker, the tungsten wire, the NaOH solution layer, and the metal loop. The NaOH solution layer is electrically isolated from the Hg-layer by the Fluorinate layer.

The tungsten wire is etched with applied DC voltage of 5 V, and it takes several minutes to complete the etching. When it is finished, the lower part of the tungsten wire drops down into the Fluorinate layer, and the electric circuit is automatically shut down in order to avoid any further etching, which would make the tip dull. Figure 2-13 (a) shows a scanning electron microscope (SEM) image of a typical tip. The tip is so sharp that the resolution of the SEM is not sufficiently high to measure the radius of the tip curvature. We have estimated the radius of the tip curvature using a field ion microscope (FIM).[19] Figure 2-13 (b) shows an FIM image of a tungsten (110) tip made by this method. The radius

of the tip curvature is estimated to be a few tens of nm from the image. We choose a sharp tungsten tip of < 100 nm radius of curvature with an FIM, and use it for STM observations because tip sharpness is most critical for STM observations. Even though we replace tips in the atmosphere, we can obtain STM images with atomic resolution with a probability of more than 90 %.

2-6. Observation of MBE-Grown and Ar Ion-Bombarded Surfaces

GaAs MBE-grown surfaces and Ar ion-bombarded surfaces were observed using the multi-chamber UHV-STM in order to check the resolution of our STM and demonstrate the usefulness of the system.

A commercially available Si-doped GaAs (001) wafer of 11 mm × 9 mm size was soldered onto a Mo-block with indium and placed into the loading chamber. The loaded sample was transferred to the sample exchange chamber and preheated for several hours. After transferring the sample to the MBE chamber a surface oxide layer was sublimed off at 590 °C in an arsenic flux in which the beam equivalent pressure was 3.6×10^{-3} Pa. The sublimation of the oxide layer was confirmed with the appearance of the 2×4 RHEED pattern. The growth of 1 μm thick Si doped (10^{18} cm^{-3}) epitaxial layer was performed at the rate of 500 nm/h in the arsenic-stabilized region where the 2×4 RHEED pattern was observed. After growth, the sample was cooled to 550 °C in the arsenic flux and transferred to the STM chamber through the sample exchange chamber. An STM observation was performed in the constant current mode with a 200 pA current and a -2 V sample bias voltage relative to the tip.

The MBE-grown GaAs sample was transferred to the process chamber, which is equipped with an argon ion gun, after the STM

observation. The MBE-grown surface was, then, bombarded by argon ions of 500 eV at a dose of 8×10^{12} cm^{-2}, which was about one hundredth of the surface atom density of 6.25×10^{14} cm^{-2}. The ion dose was estimated from the ion current measured with a Faraday cup and the bombarded area. The sample was again transferred to the STM chamber after the ion-bombardment for further STM observation.

Figure 2-14 (a) shows an STM image of an MBE-grown GaAs surface. A clear image of the reconstruction has been obtained. For this surface, a 2×4 symmetry was observed by RHEED. Coinciding with the RHEED pattern, a 0.8 nm periodicity along the $[1\bar{1}0]$ direction and a 1.6 nm periodicity along the [110] direction are seen in the STM image. Chadi has proposed a model for this structure, in which model a cell consists of three arsenic dimers and a missing dimer; the cells are arranged so as to have 2×4 or c(2×8) symmetry.[8] The 0.8 nm periodicity is thus from arsenic dimers, and the 1.6 nm periodicity is form missing dimers. In Fig.2-14 (a), the model of a 2×4 unit cell and that of a c(2×8) unit cell are shown in the upper-right area; the arsenic dimer positions are indicated by closed circles and the missing-dimer sites are indicated by open circles.[7] In the STM image, several types of defects are also observed. For instance, one dimer seems to be missing at D_1; although the dimers do not line up, the center dimer seems to be shifted by 0.4 nm at D_2. A lower magnification image is shown in Fig.2-14 (b). The dark lines running in the $[1\bar{1}0]$ direction correspond to the missing dimer rows. The 0.8 nm periodicity in the [110] direction cannot be resolved with this low magnification. Planes, steps, large holes, and islands are seen in the image. Small dark defects, where the surface atoms are missing, are also observed.

Figure 2-15 (a) shows an STM image of an ion-bombarded GaAs surface of 140 nm × 80 nm size. Many small dark defects are observed all over the surface in the image. The number of defects is much larger than that in Fig.2-14 (b). Figure 2-15 (b) shows a larger magnification image of the ion-bombarded surface. The density of these defects was calculated to be 3×10^{12} cm^{-2} from the image. This density is not significantly different from the argon ion dose. Furthermore, it was observed that the density of the defect increased according to the increase in the argon ion dose for another sample.[20] It is therefore concluded that most of the defects were created by argon ion bombardment. The areas of the defects are scattered from a few nm^2 to a few tens of nm^2. The sum of the damaged area is calculated to be approximately 40 % of the surface, using the estimated ion dose of 8×10^{12} cm^{-2} and a defect area of 5 nm^2. If the ratio of the damaged area is much smaller than unity, most of the defects would have been created by a single ion. If it is close to unity, many of them created by two or more ions. Since our situation is between these two extreme cases, the smaller defects may correspond to single-ion bombardments, and the larger ones to those by two or more ions.

2-7. Summary

A multi-chamber UHV-STM system has been constructed for investigating processed compound semiconductor surfaces. It has five chambers, including MBE, process, and STM chambers. A sample is transferred to the MBE chamber for epitaxial growth. It is then transferred to either the STM chamber for an STM study using our specially designed STM or to the process chamber for further processing.

We observed an MBE grown GaAs (001) surface and a clear STM image of a 2×4 reconstructed structure was obtained. This sample was

transferred to the process chamber and bombarded with an argon ion beam. The ion beam bombarded surface was, then, observed with the STM. In the image, defects were found which seemed to be created by ion bombardment. It is thus demonstrated that our multi-chamber UHV-STM system is useful for investigating various surface processes with atomic resolution.

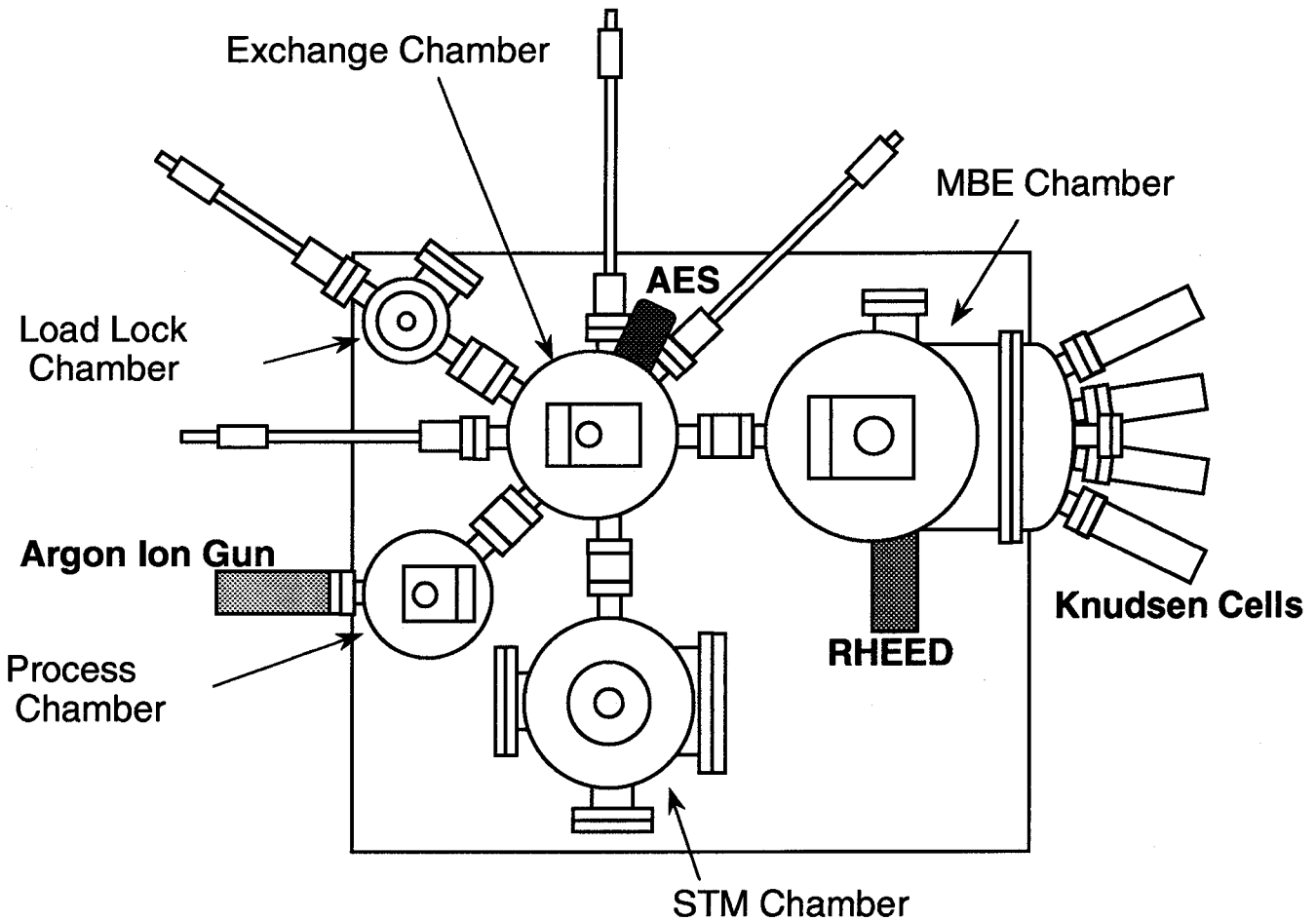

Fig. 2-1. Schematic illustration of the multi-chamber UHV-STM system (top-view).

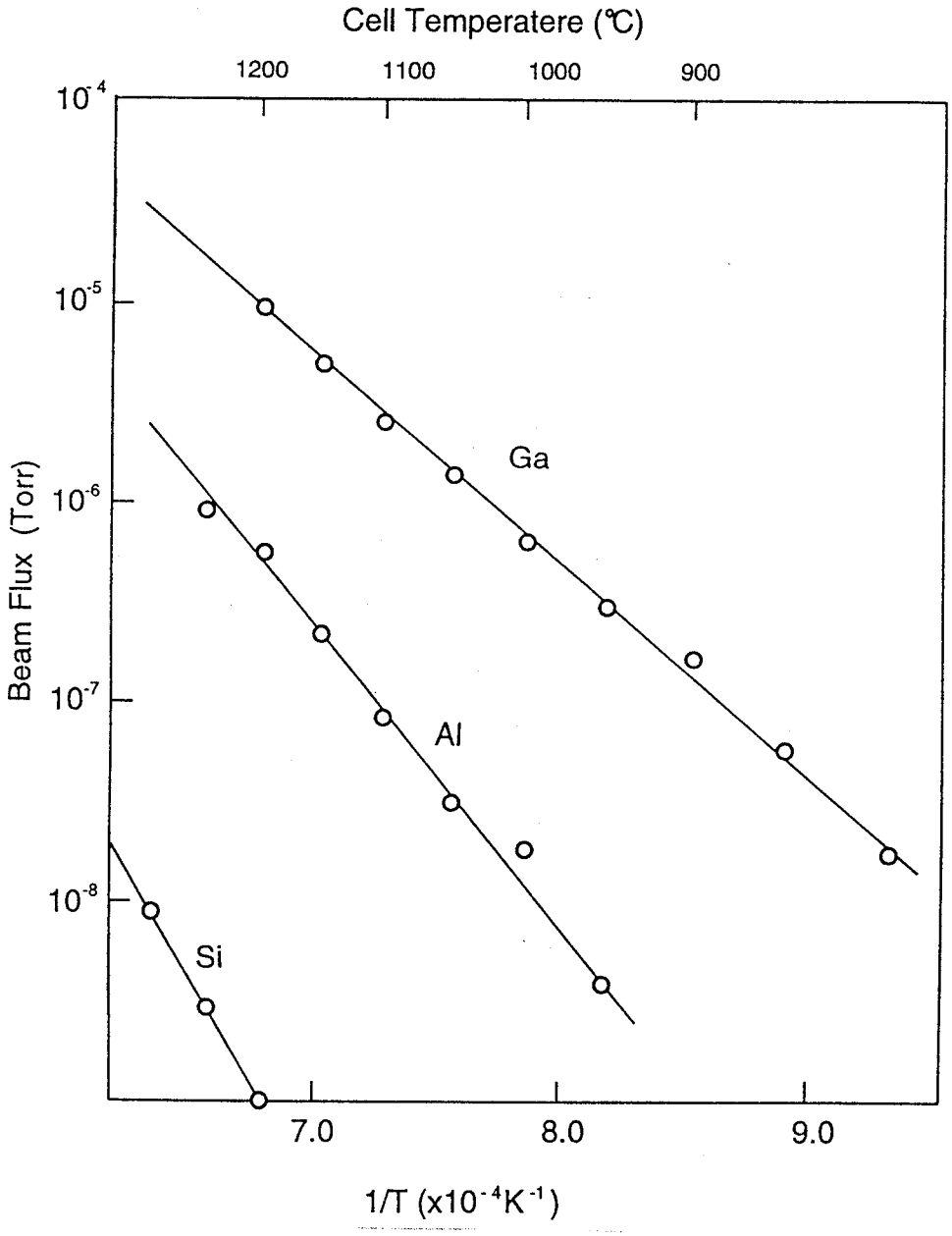

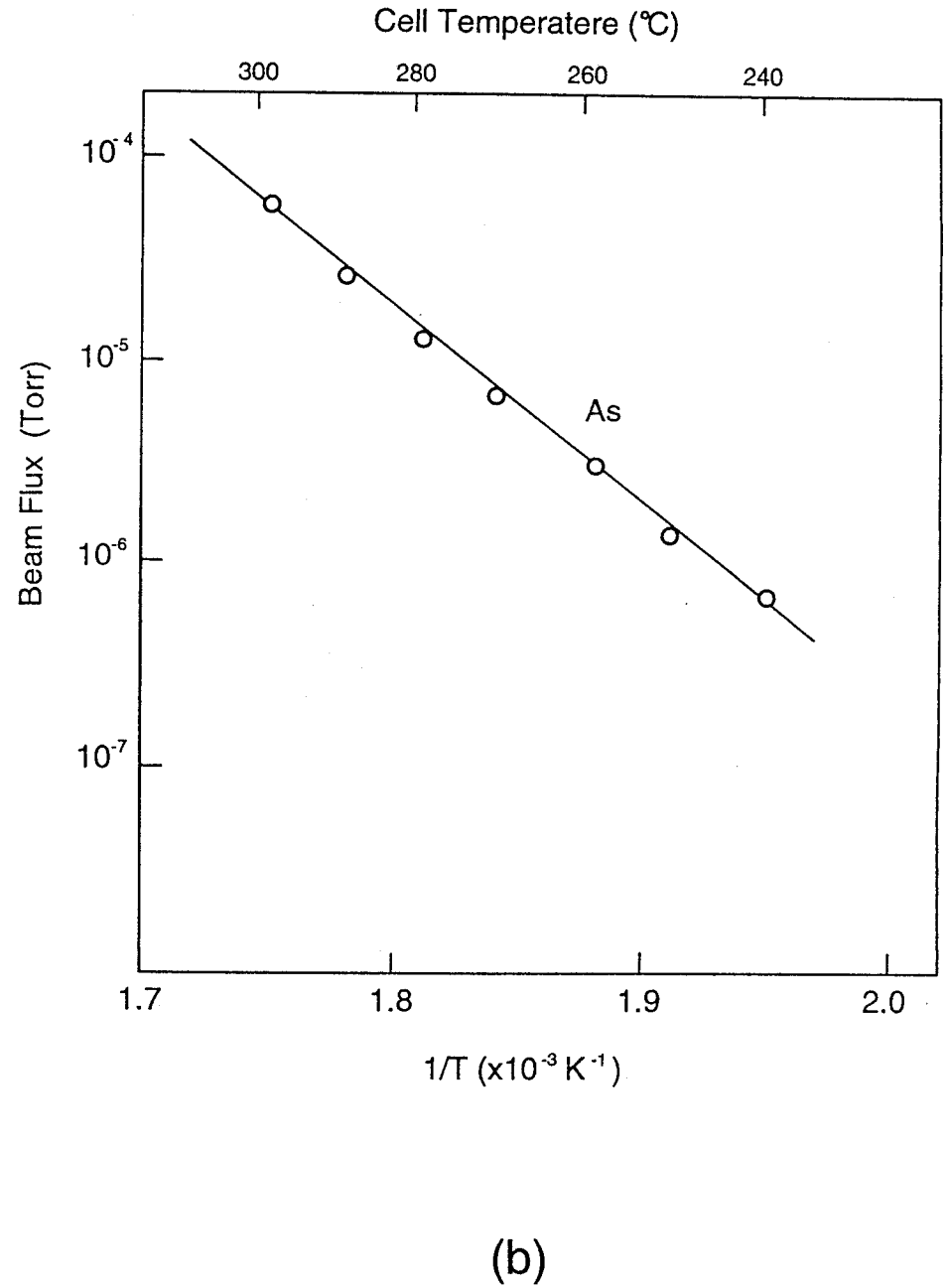

Fig. 2-2. Beam flux versus cell-temperature for (a) Ga, Al, Si and (b) As.

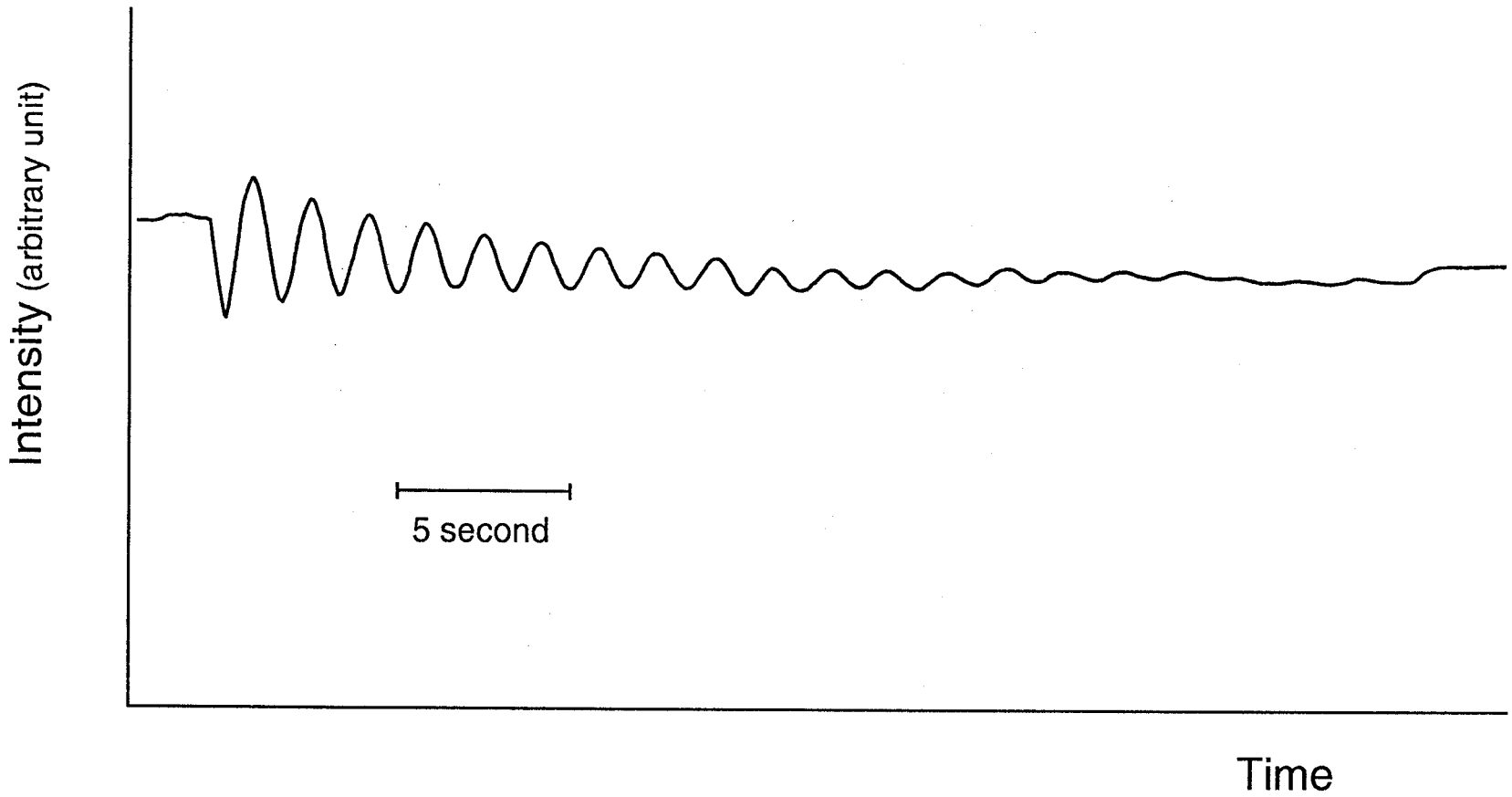

Fig. 2-3. An example of RHEED intensity oscillation during MBE-growth of GaAs.

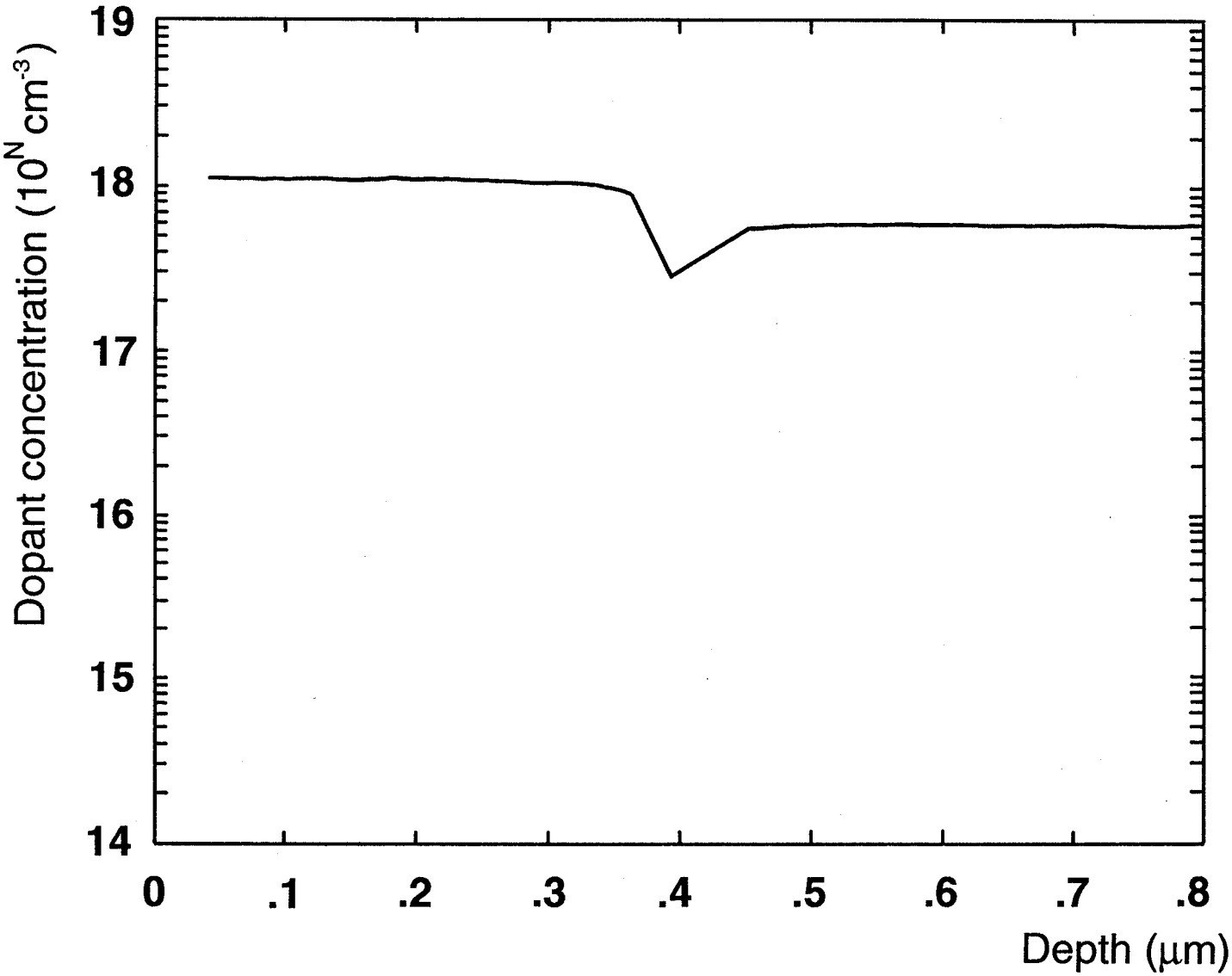

Fig. 2-4. Dopant concentration of an MBE-grown layer and a substrate.

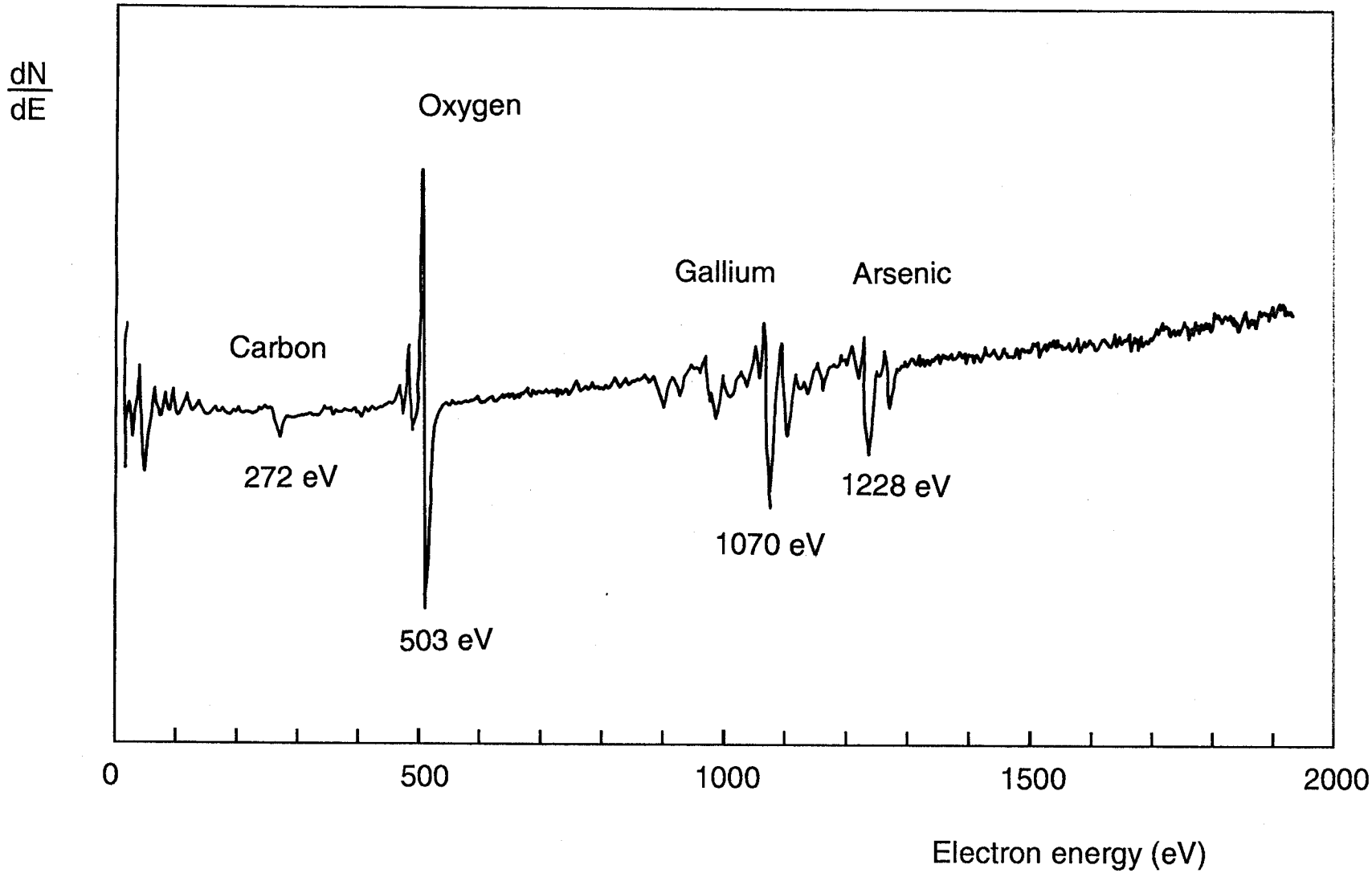

Fig. 2-5. Auger electron spectrum of a GaAs surface before MBE growth.

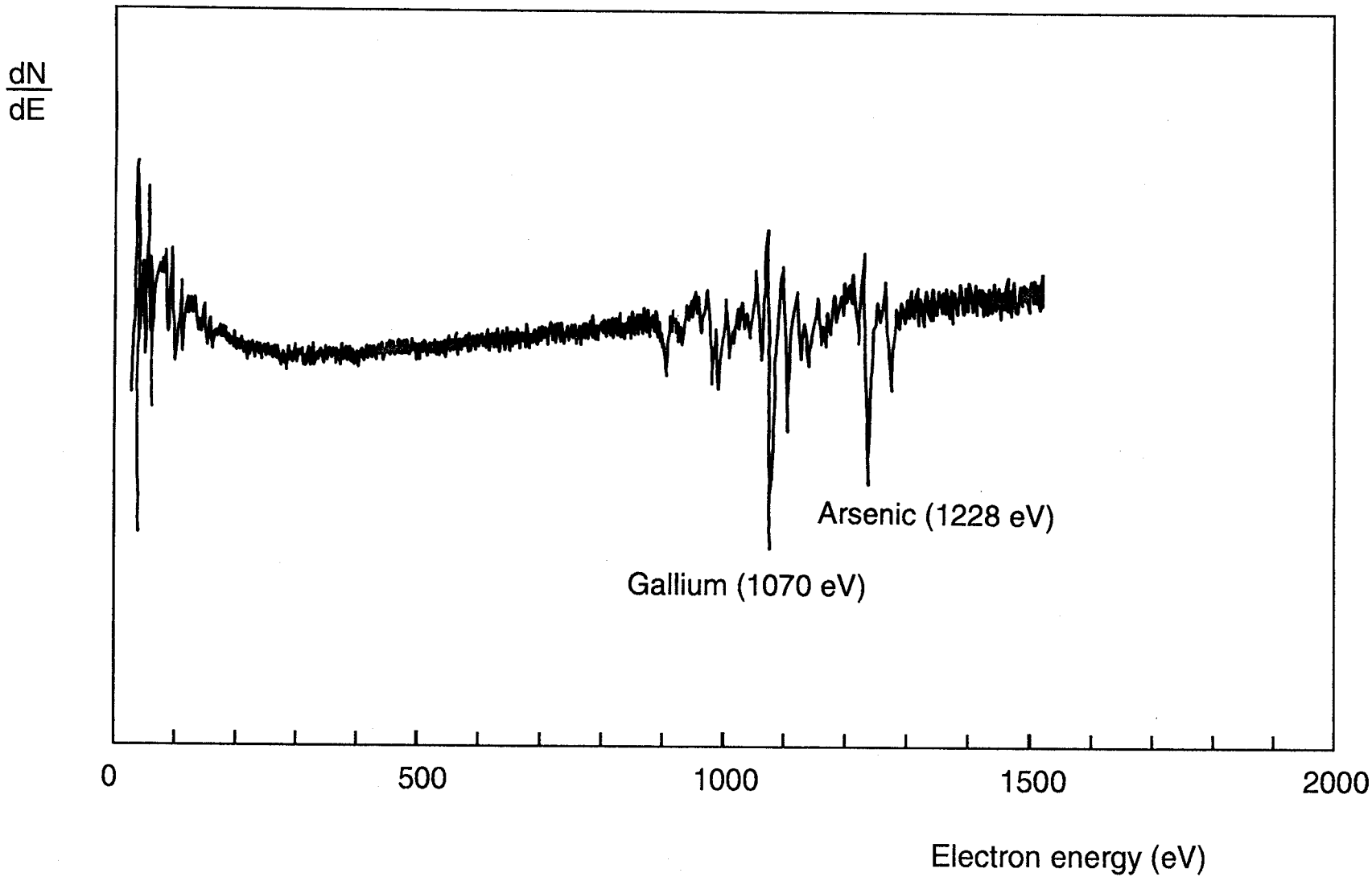

Fig. 2-6. Auger electron spectrum of an MBE-grown GaAs layer.

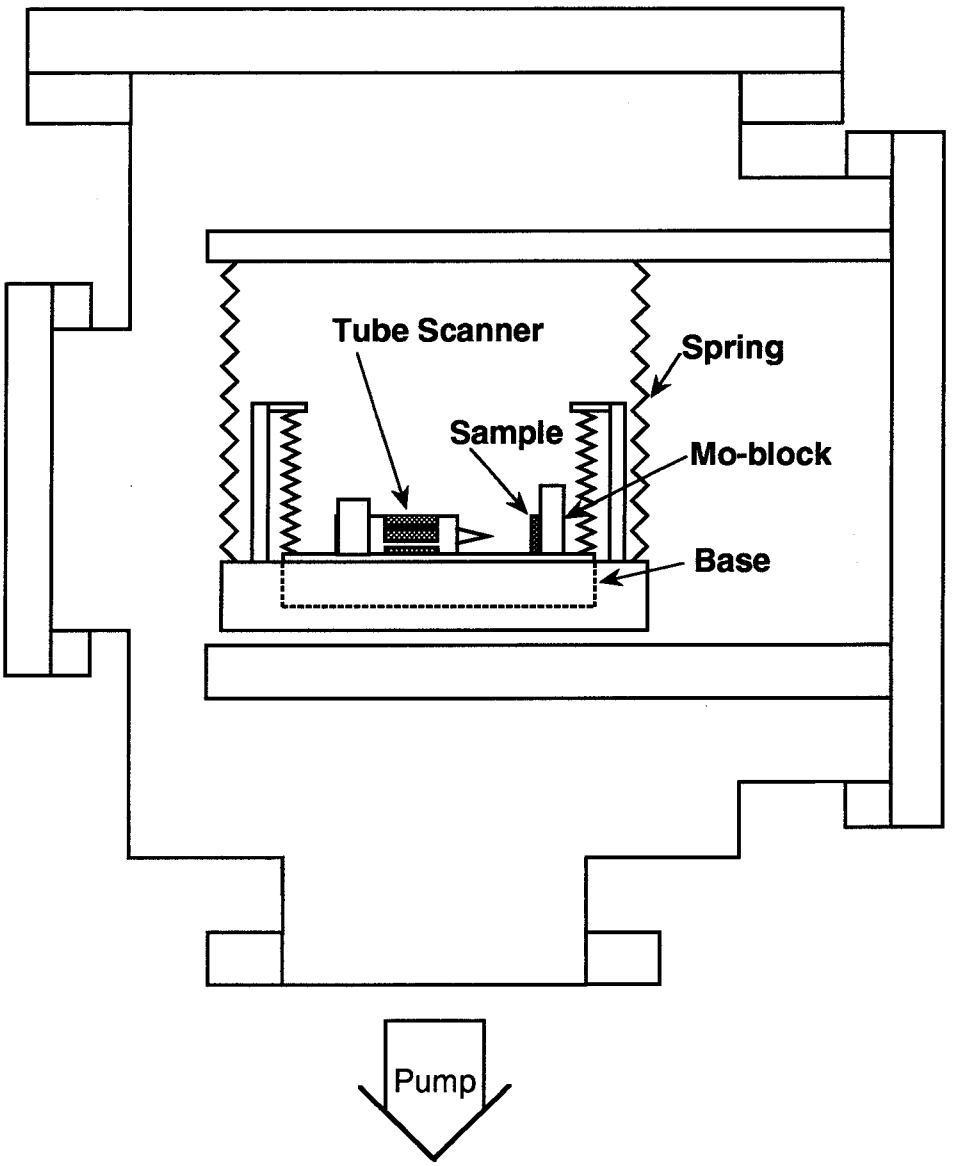

Fig. 2-7. The STM unit supported with a double-spring anti-vibration suspension in the STM chamber.

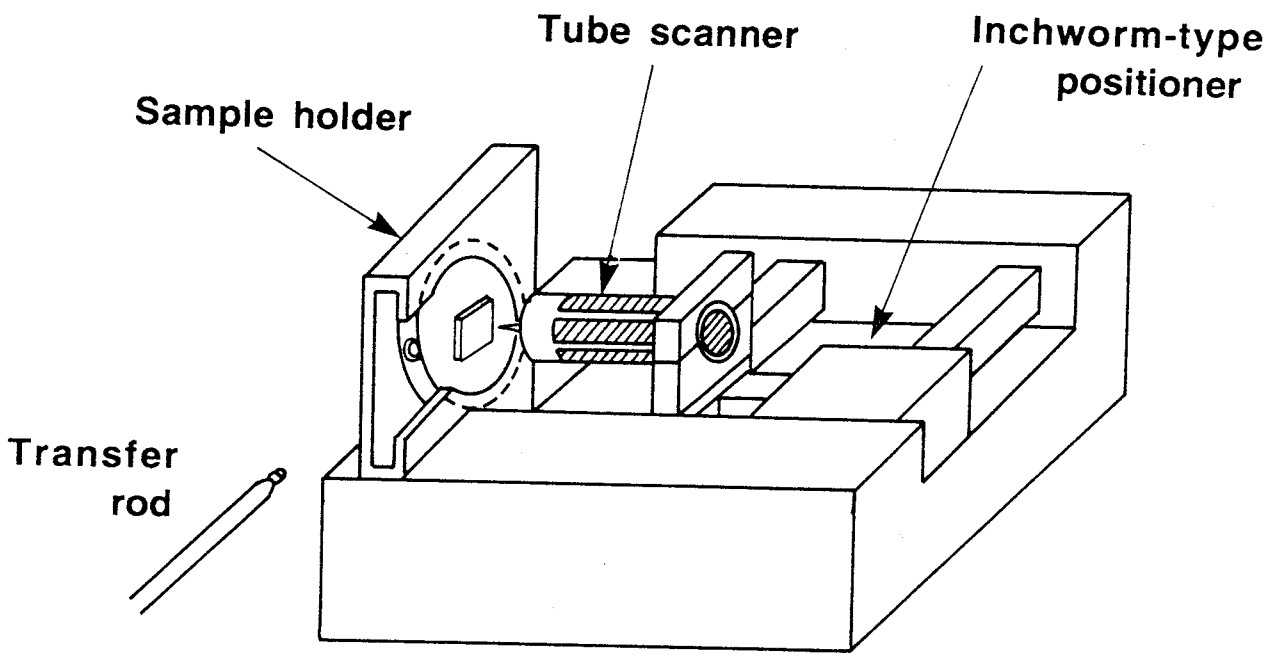

Fig. 2-8 STM unit developed for observing processed semiconductor surfaces. A 23 mm-diameter Mo-block can be used.

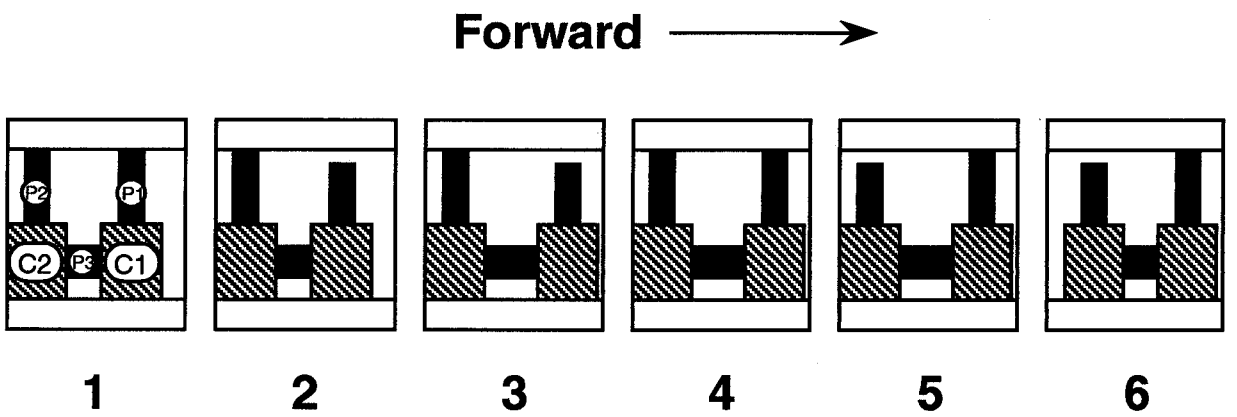

Fig. 2-9. Illustration of the one-step movement of the coarse Z-positioner.

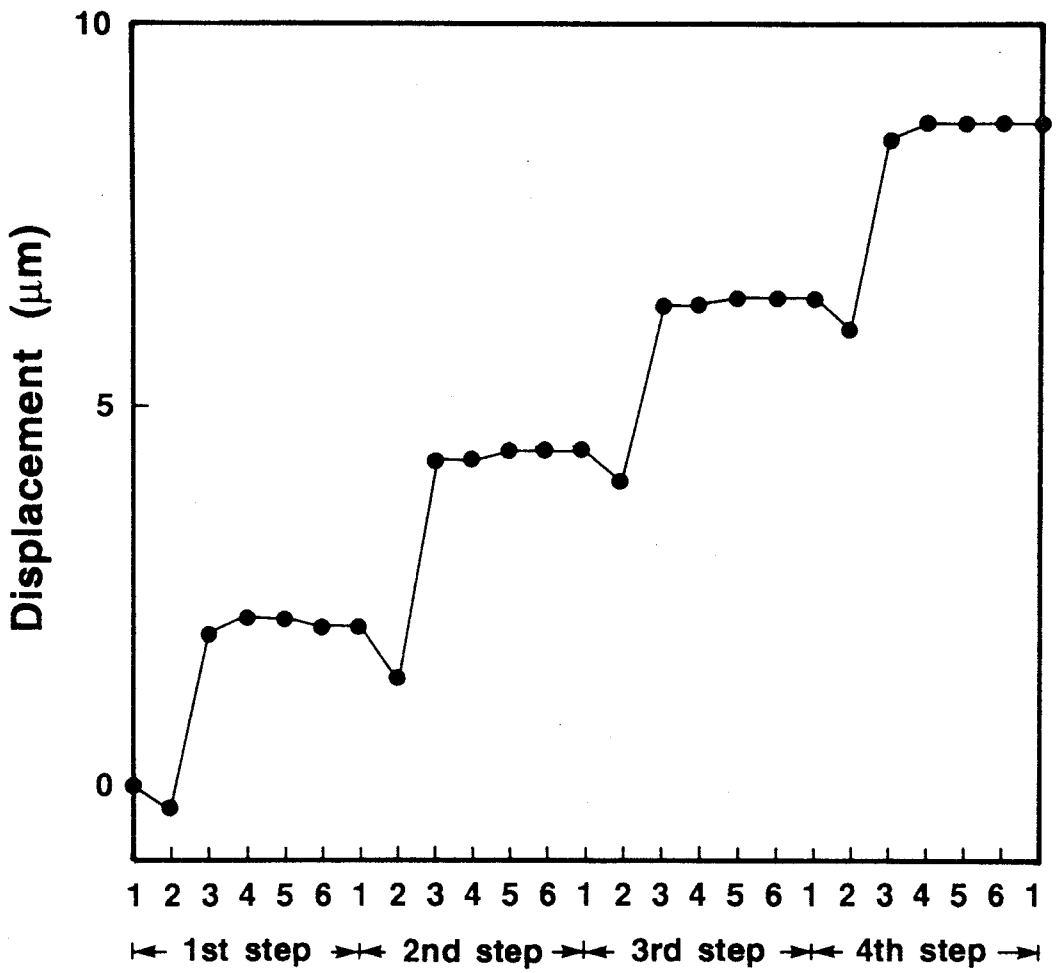

Fig. 2-10. Measured displacement of the coarse Z-positioner.

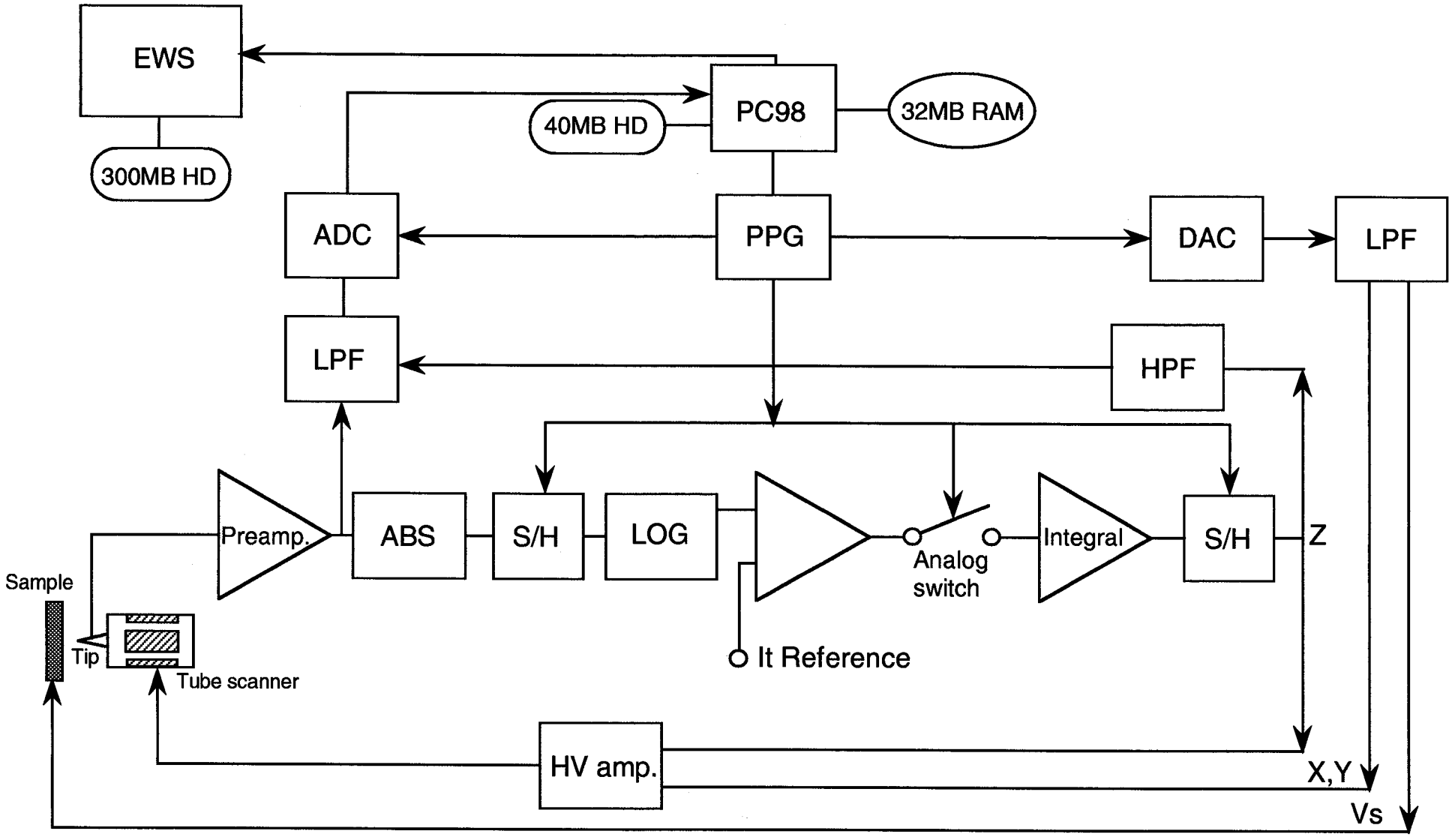

Fig. 2-11. Block diagram of the STM control and data acquisition electronics.
(Preamp.=preamplifier, ABS=absolute circuit, S/H=sample-and-hold circuit, LOG=logarithmic amplifier, HPF=high-pass filter, LPF=low-pass filter, ADC=analog-to-digital converter, DAC=digital-to-analog converter, PPG=programmable pulse generator, HD=hard disc, EWS=engineering work station, RAM=random access memory, HV amp.=high voltage amplifier.)

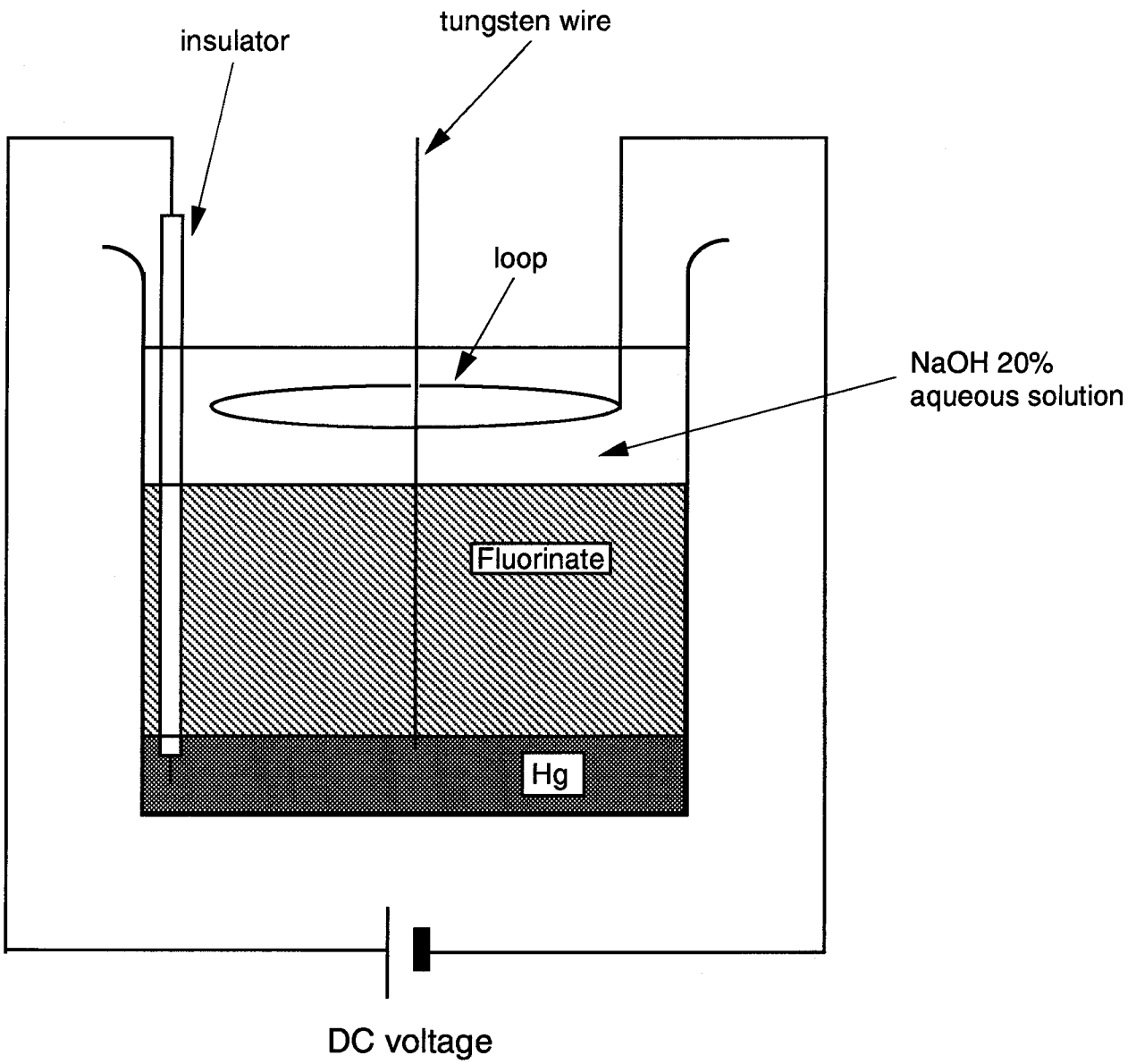

Fig. 2-12. Electrochemical etching of a tungsten wire for tip-fabrication.

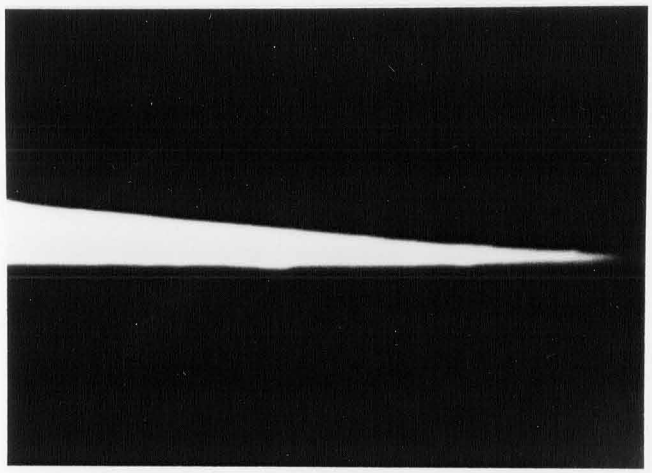

1 μm

(a)

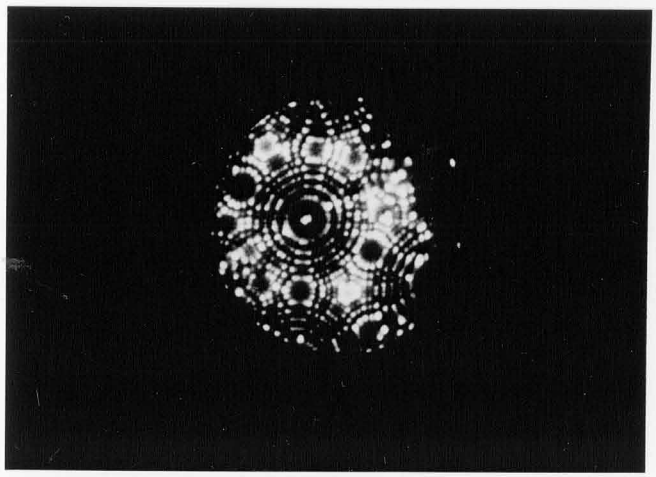

(b)

Fig. 2-13. (a) Scanning electron microscope image of a tungsten tip fabricated by electrochemical etching;
(b) Field ion microscope image of the tungsten tip.

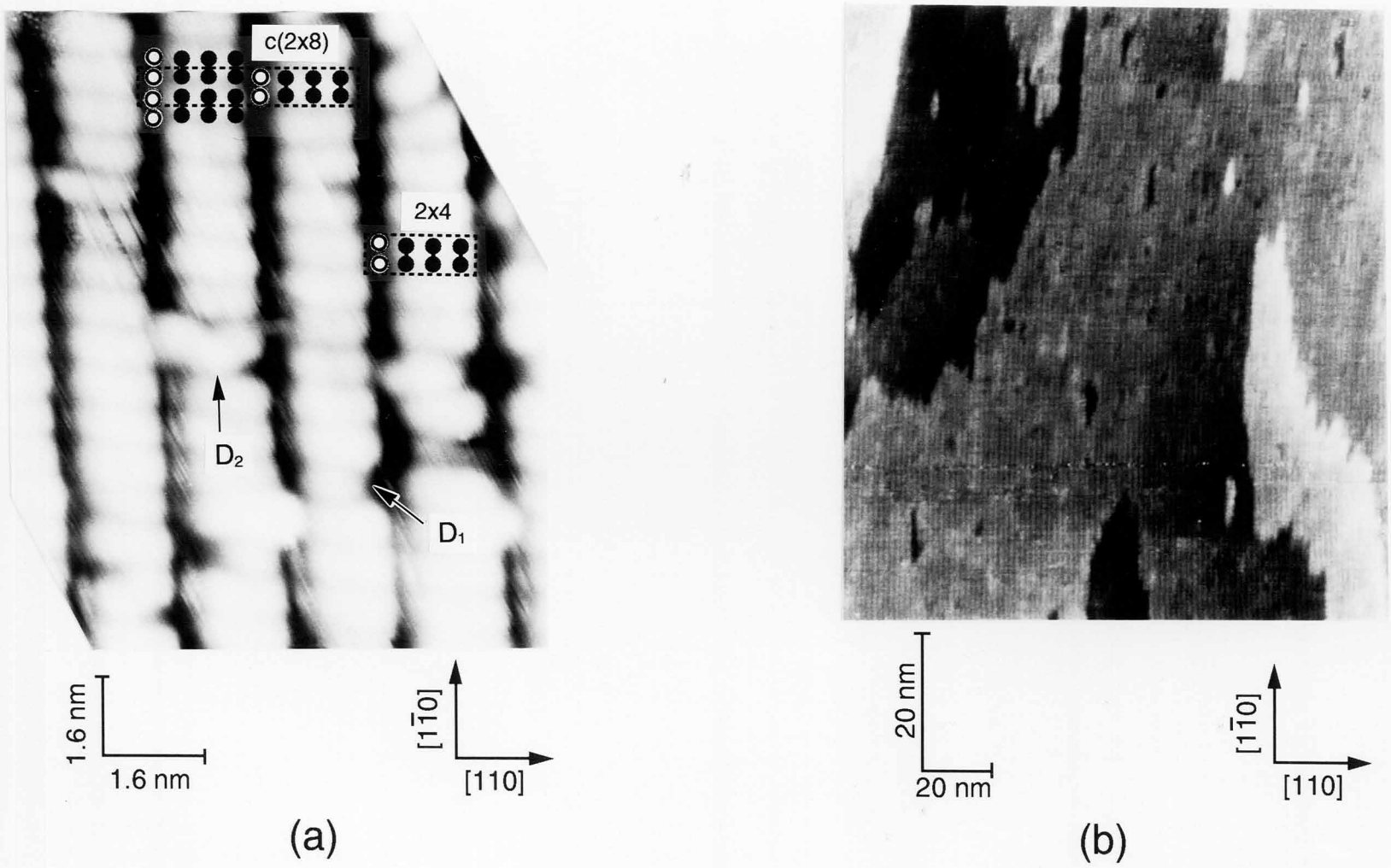

Fig. 2-14. (a) STM image of an MBE-grown GaAs (001) surface;
(b) lower-magnification image.

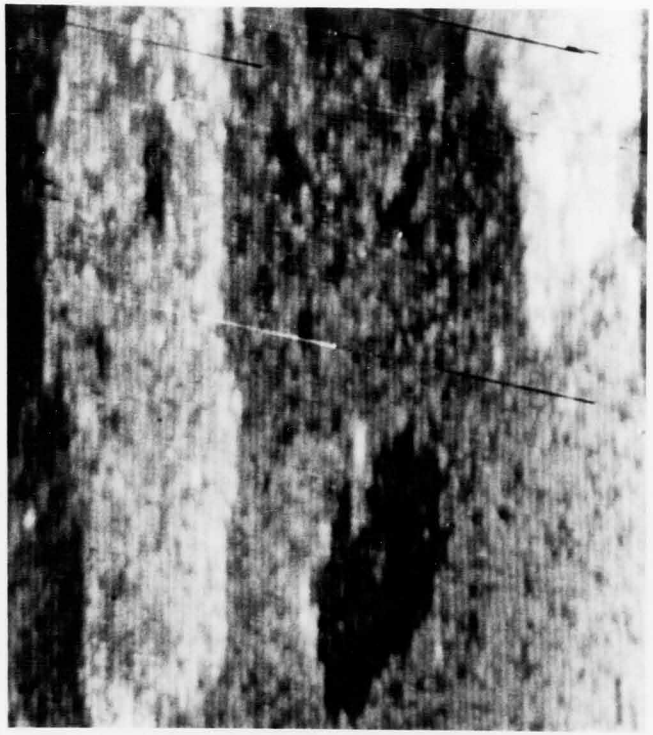

(a)

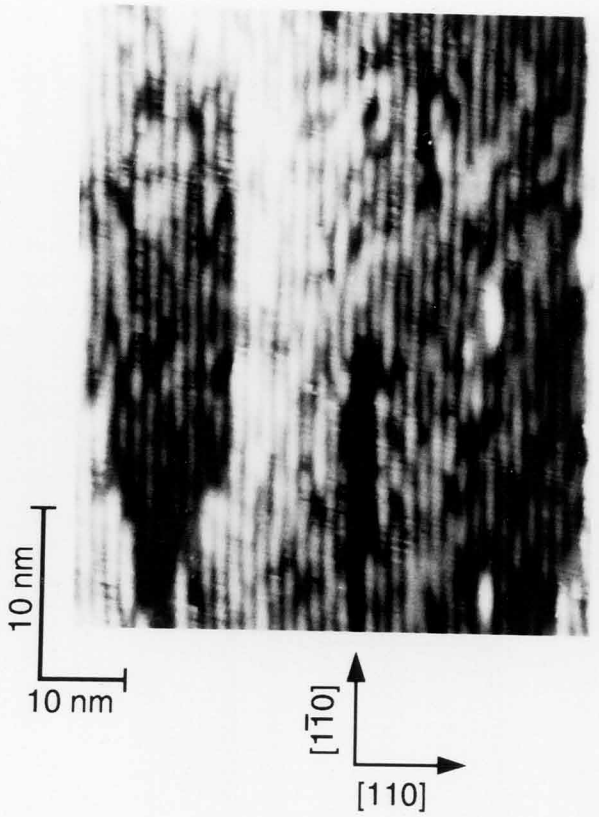

(b)

Fig. 2-15. (a) STM image of an argon-ion-bombarded GaAs (001) surface;. (b) higher-magnification image.

3. Surface Reconstructed Structure of Molecular Beam Epitaxially Grown GaAs Layers [21]

3-1. Introduction

The GaAs (001) surface is of considerable interest because it is the most widely used type in various processes, such as epitaxial growth and etching. It is considered that a more detailed understanding of materials and processes on the atomic scale is required for the development of more sophisticated technologies which will realize future electronic and optoelectronic devices.[2] In particular, the atomic-scale structure of this surface is attracting much attention to reveal the mechanism of important processes like atomic layer epitaxy.

Recently, the reconstructed dimer structures of MBE-grown arsenic-stabilized GaAs (001) surfaces have been observed by STM, and atomic-scale surface morphologies which correspond to 2×4 and c(4×4) electron diffraction patterns of the surface have been reported.[7,10,22]

In this chapter we present STM images of reconstructed MBE-grown GaAs surfaces which have not only 2×4 and c(4×4) symmetries, but also other symmetries, such as c(4×2). The results are discussed in comparison with RHEED data and the process conditions.

3-2. Experiment

GaAs(001) samples were prepared from nominally on-axis wafers by a sequence of cleaning steps which are described in the previous chapter, and soldered onto a molybdenum block of 23 mm diameter with indium. After entry into the exchange chamber, the doped GaAs(10^{18} cm^{-3} Si) samples were prebaked at 370 °C for three hours. After being transferred to the MBE chamber, surface oxides were sublimed off at 590 °C in an As_4 flux. The substrate temperature was

measured with an infrared radiation thermometer. The sublimation of the surface oxides was confirmed through the appearance of the 2×4 RHEED pattern. The experimental procedures are shown in Fig.3-1. The growth of a 600 nm doped (10^{18} cm^{-3} Si) GaAs epitaxial layer proceeded at 600 nm/hr in an As stabilized regime at 600 °C. After growth the sample was cooled to a certain temperature in an As_4 flux. It was transferred into a UHV of the sample exchange chamber as soon as the arsenic flux is shut off. Then it was again transferred to the STM chamber for observations.

STM measurements were performed in the constant current mode. In this study, the STM images were taken at sample voltages of -2 V relative to the tip and a constant tunneling current of 200 pA.

3-3. RHEED Observations

First, we monitored the symmetry of surface reconstruction at various temperatures by RHEED. A 2×4 pattern was observed when the sample was kept in an As_4 flux at temperatures ranging from the growth temperature (600 °C) to about 530 °C. A 4-fold pattern for the incident electron beam in the [1$\bar{1}$0] azimuth at 570 °C is shown in Fig.3-2 (a). The 4-fold pattern changed to a 1-fold pattern over a narrow temperature range between 530 and 520 °C. At the temperature lower than 520 °C a 2-fold pattern appeared for the [1$\bar{1}$0] azimuth; the 2-fold pattern at 515 °C is shown in Fig.3-2 (b). It became clear at about 500 °C. On the other hand, a 4-fold pattern for the beam in the [010] azimuth corresponding to the c(4×4) structure was clearly observed at temperatures lower than 510 °C (Fig.3-2 (c)). With an increase of the temperature, this 4-fold pattern became indistinct at about 520 °C. We therefore found that 520 °C is about the temperature at which the

transition from the 2×4 structure to the c(4×4) structure takes place in our particular As_4 flux.

When a sample with the c(4×4) surface was heated in a UHV, the transition from the c(4×4) to 2×4 was observed at about 460 °C as shown in Fig.3-3 (a) to (c). The 4-fold pattern for the [010] azimuth observed clearly at 330 °C became weak at 460 °C, and a clear 4-fold pattern was observed for the $[1\bar{1}0]$ azimuth at 470 °C. It is thus concluded that the c(4×4) structure is unstable in a UHV at temperatures higher than 460 °C.

3-4. STM Observations

We next performed STM observations of the MBE-grown GaAs surfaces. Three samples were examined. One of them was cooled to 330 °C in the As_4 flux after the growth. It was then transferred to the STM chamber through the exchange chamber and cooled in a UHV. The others were cooled to 470 and 570 °C in the As_4 flux, respectively, before being transferred.

A clear c(4×4) RHEED pattern was observed on the surface of the sample cooled to 330 °C in the As_4 flux and transferred into a UHV. Figure 3-4 (a) is an STM image of this surface. Rectangles of about 0.8 nm×1.2 nm size, which are considered to be made up of three arsenic dimers, are arranged so as to have the c(4×4) symmetry as Biegelsen et al. reported.[9] The ball-and-stick model for this reconstruction is shown in Fig.3-4 (b). The large, medium, and small closed circles represent the top, second, and fourth As-layers, respectively; the medium and small open circles correspond to the third and fifth Ga-layers, respectively in the model.

The c(4×4) symmetry is most clear in the lower-left region and the upper-right region of the image. There are two white defects which

appear as some type of contamination in this image. One is in the upper middle region and the other at the lower side of the image. More disordered structures, namely, smaller and larger blocks, can be seen around these defects. This type disorder might thus be caused by these defects.

An anti-phase boundary, indicated by an arrow, appears in the image. The upper sides of the units of three dimers on the left side of the boundary are lined up with the lower sides of the units on the right side of the boundary.

Also, the center of each rectangle appears to be lower than both sides. Although the tip artificial effect cannot be ruled out, the center dimer could be lower than the other dimers.

The STM image of the GaAs epilayer surface cooled to 570 °C in the As_4 flux and quenched in a UHV is shown in Fig.3-5 (a). (This surface showed the 2×4 RHEED pattern.) Ordered structures with a 1.6 nm periodicity along the [110] direction and a 0.8 nm periodicity along the $[1\bar{1}0]$ direction appear in the upper-right and lower regions. This type structure is similar to that previously reported by Pashley et al. and Biegelsen et al.[7],[9],[22] The ball-and-stick model for this reconstruction is shown in Fig.3-5 (b). Disordered regions appear in the upper-left and the middle parts of the image. Other parts of the surface also show a partially disordered 2×4 structure similar to this image.

When the sample was cooled to 470 °C in the As_4 flux, the 4-fold and 2-fold RHEED patterns were observed for beams in the [100] and $[1\bar{1}0]$ azimuths, respectively. The surface reconstruction thus changed to the c(4x4) structure in the arsenic flux. After being transferred into a UHV and cooled, less distinct 2-fold RHEED streaks were observed for the $[1\bar{1}0]$ azimuth and an incomplete 4-fold RHEED pattern comprising relatively strong 1-fold streaks and very weak higher-order diffraction

lines was observed for the [100] azimuth. An incomplete c(4×4) structure was therefore expected from the RHEED patterns for this surface.

The STM image of this sample often showed a c(4×2) structure, and sometimes a mixture of c(4×2) and 2×2 structures as shown in Fig.3-6 (a). This result and the fact that the c(4×4) structure is not stable at 470 °C in a UHV suggest that the c(4×2) and 2×2 structures were formed by desorption of As atoms from the c(4×4) structure in a UHV. Although an incomplete c(4×4) RHEED pattern was observed, no c(4×4) region was observed on this surface by STM. It is therefore considered that most of the c(4×4) reconstructed region was changed to the c(4×2) or the 2×2 structure at 470 °C in a UHV, and only a small region of c(4×4) remained. It is thus possible to explain the RHEED pattern by the co-existence of intense 1-fold streaks from the large c(4×2) region and weak higher order diffraction lines from the small c(4×4) region.

A proposed ball-and-stick model for the c(4×2) and the 2×2 structure is shown in Fig.3-6 (b). In this model As dimers bonded to As atoms are arranged so as to have c(4×2) or 2×2 symmetry; that is, one third of the surface As atoms of the c(4×4) structure desorbed and c(4×2) or 2×2 structure was formed. Because the 2×4 RHEED pattern was observed in a UHV and c(4×4) in the As_4 flux around 470 °C, it is considered that the As dimer coverage on the surface of this sample is between those of these two reconstructions. If the As dimers of the c(4×2) and the 2×2 reconstructions are bonded to Ga atoms, the As dimer coverage of the c(4×2) and 2×2 reconstruction is 0.5, which is smaller than that of the 2×4 reconstruction. Thus, the As dimers of the c(4×2) and 2×2 structure are probably on As atoms.

An STM image of the surface which was cooled to 470 °C in a three times denser As_4 flux than that of the above-mentioned experiments is

shown in Fig.3-7 (a). A reconstructed structure which has 2.8 nm periods along both the [110] and [1$\bar{1}$0] directions appears in the left region. The upper-right region of the image, which does not have any periodic structure, is probably contaminated, and a disordered structure exists near the contamination.

The proposed ball-and-stick model for this reconstruction is given in Fig.3-7 (b). Sets of three arsenic dimers are positioned along the [210] direction. The basis vectors A_1=(2,1) and A_2=(1,4) define the smallest unit cell of this structure. Compared with the c(4×4) structure, the arsenic dimer density of this structure is calculated to be 2.68×14cm^{-2}, which is 14% larger than that of the c(4×4) structure. This is therefore a new reconstructed phase with a larger arsenic dimer density. The calculated low-energy electron diffraction pattern for this structure is shown in Fig.3-8. From this figure it can be seen that for an incident beam in the [110] or [1$\bar{1}$0] azimuth the RHEED pattern should show only 1-fold spots, and for an electron beam whose azimuth has 27 degrees with the [110] direction the RHEED pattern should show 7-fold spots. However, we observed 2-fold patterns for both the [110] and [1$\bar{1}$0] azimuths and no 7-fold pattern for various azimuths. The structure shown in Fig.3-7 (a) thus seems to be a local type within a small area, and most parts of the surface could be a c(4×2) and/or c(4×4) structure.

3-5. Conclusions

We have observed the surfaces of MBE-grown GaAs epitaxial layers using a multi-chamber UHV-STM system. The observed structure changed from c(4×4) to 2×4 through c(4×2) and 2×2 structures with an increase of the temperature to which the sample was cooled in an As_4 flux. This result suggests that the c(4×2) and 2×2 structures are formed by desorption of As atoms from the c(4×4) structure. Also, a new

reconstruction phase of a larger arsenic dimer density than that of the c(4×4) structure was observed.

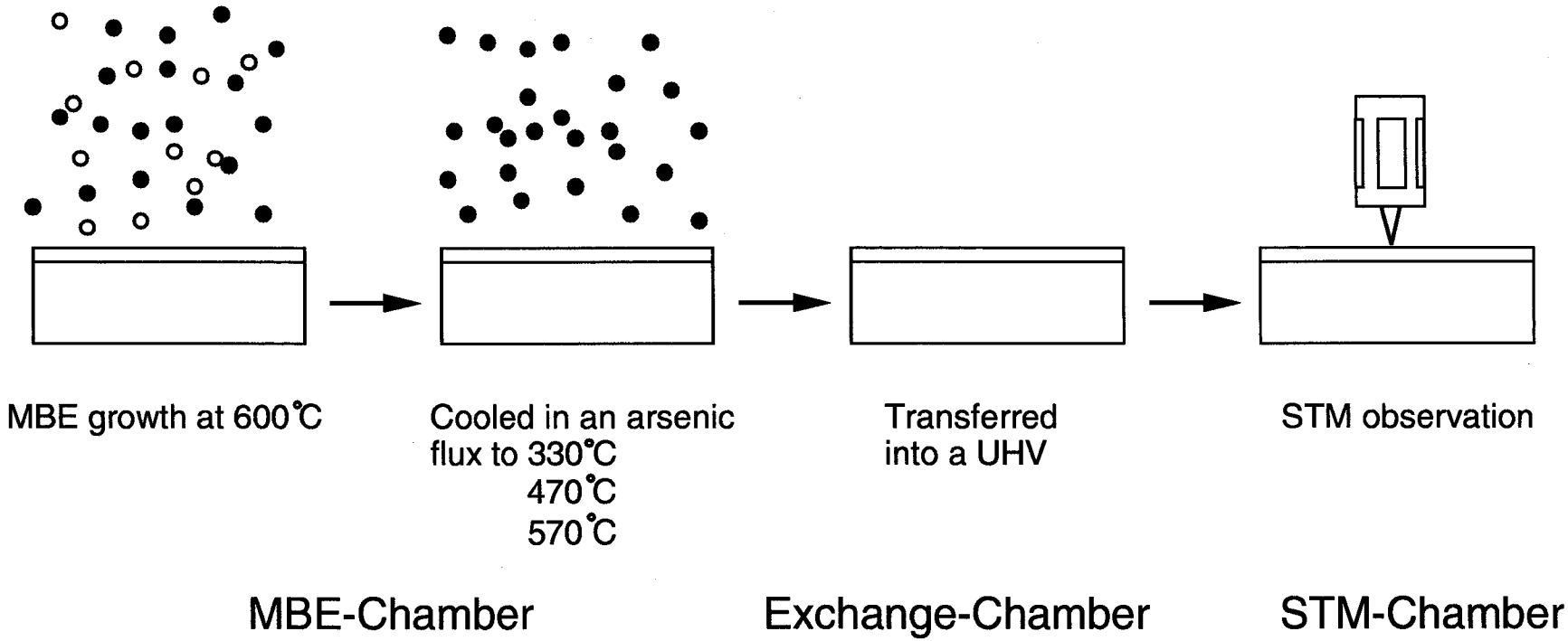

Fig. 3-1. The experimental procedures for STM observation of MBE-grown GaAs layers.

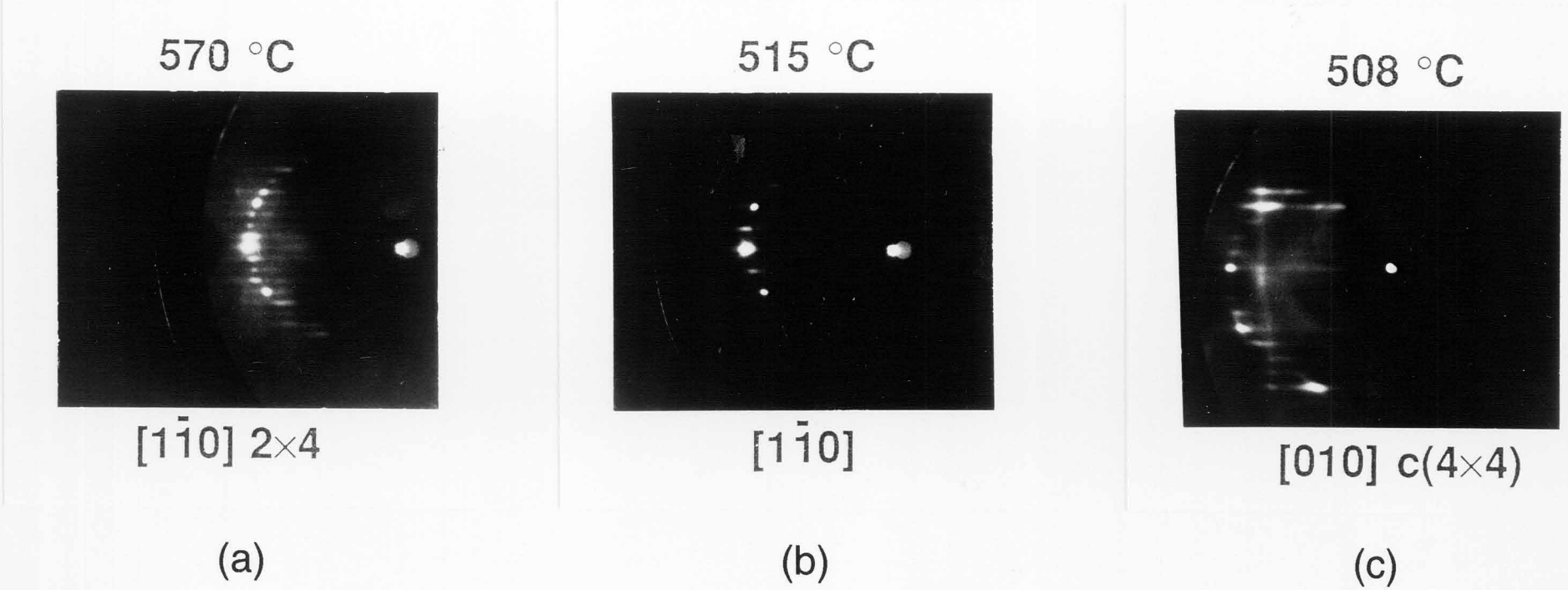

Fig. 3-2. Change of RHEED patterns of MBE-grown GaAs surface with lowering the substrate temperature in the arsenic flux; (a) at 570℃ for the electron beam in the [1$\bar{1}$0] azimuth; (b) at 515℃ in the [1$\bar{1}$0] azimuth; (c) at 508℃ in the [010] azimuth.

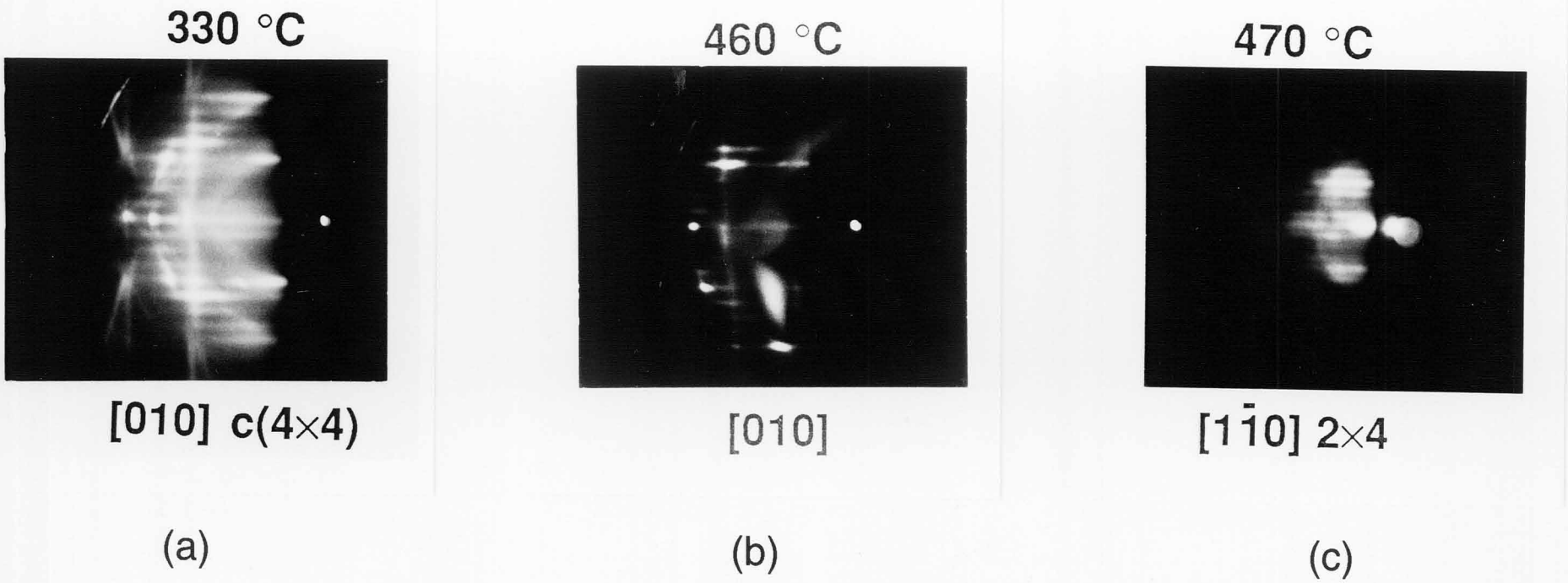

Fig. 3-3. Change of RHEED patterns of MBE-grown GaAs surfaces with raising the substrate temperature in a UHV; (a) at 330℃ for the electron beam in the [010] azimuth; (b) at 460℃ in the [010] azimuth; (c) at 470℃ in the [1$\bar{1}$0] azimuth.

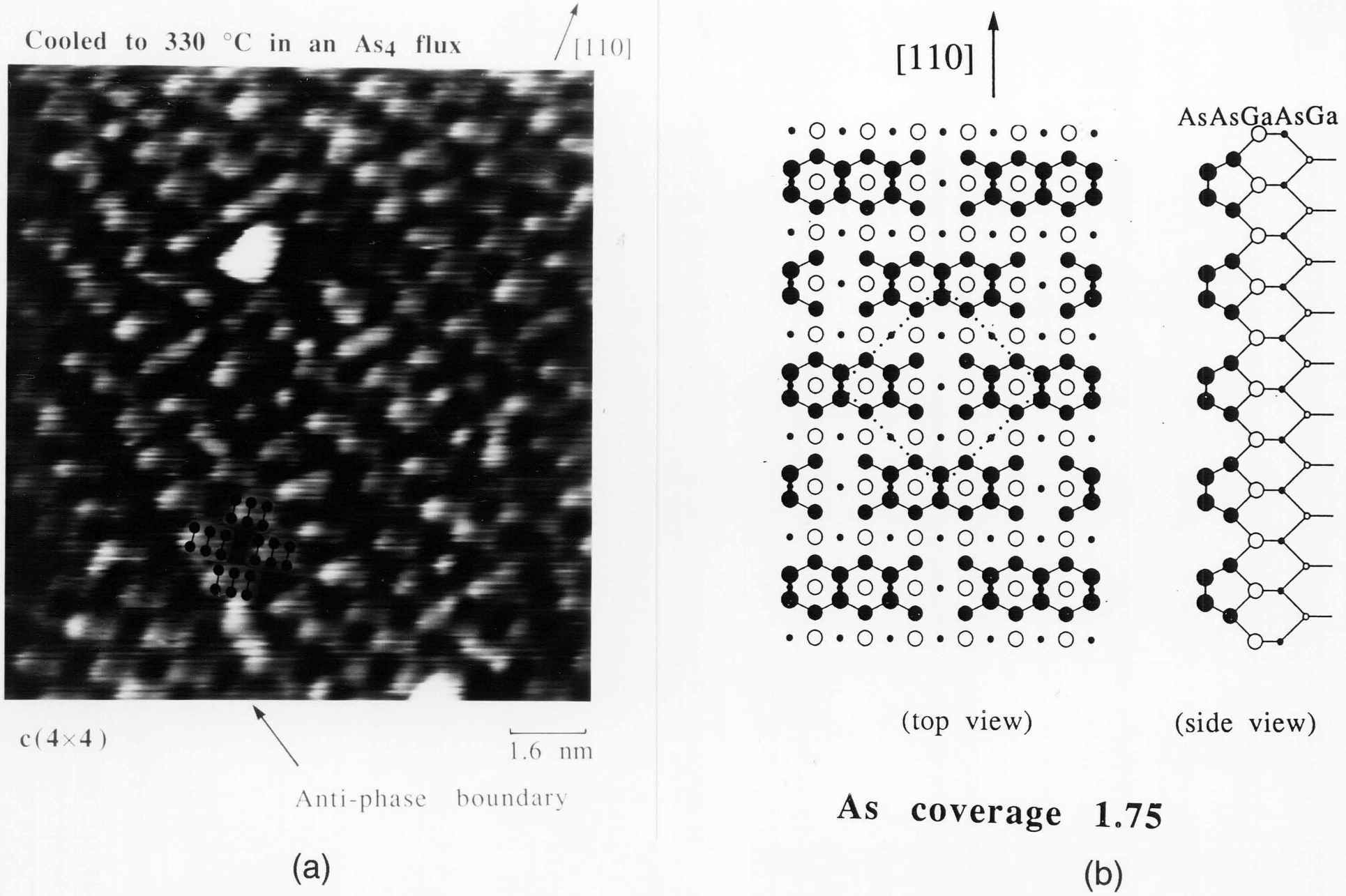

Fig. 3-4. (a) STM image and (b) ball-and-stick model of the MBE-grown GaAs (001) surface which was cooled to 330℃ in the arsenic flux having c(4x4) symmetry. This STM image is distorted by thermal drift.

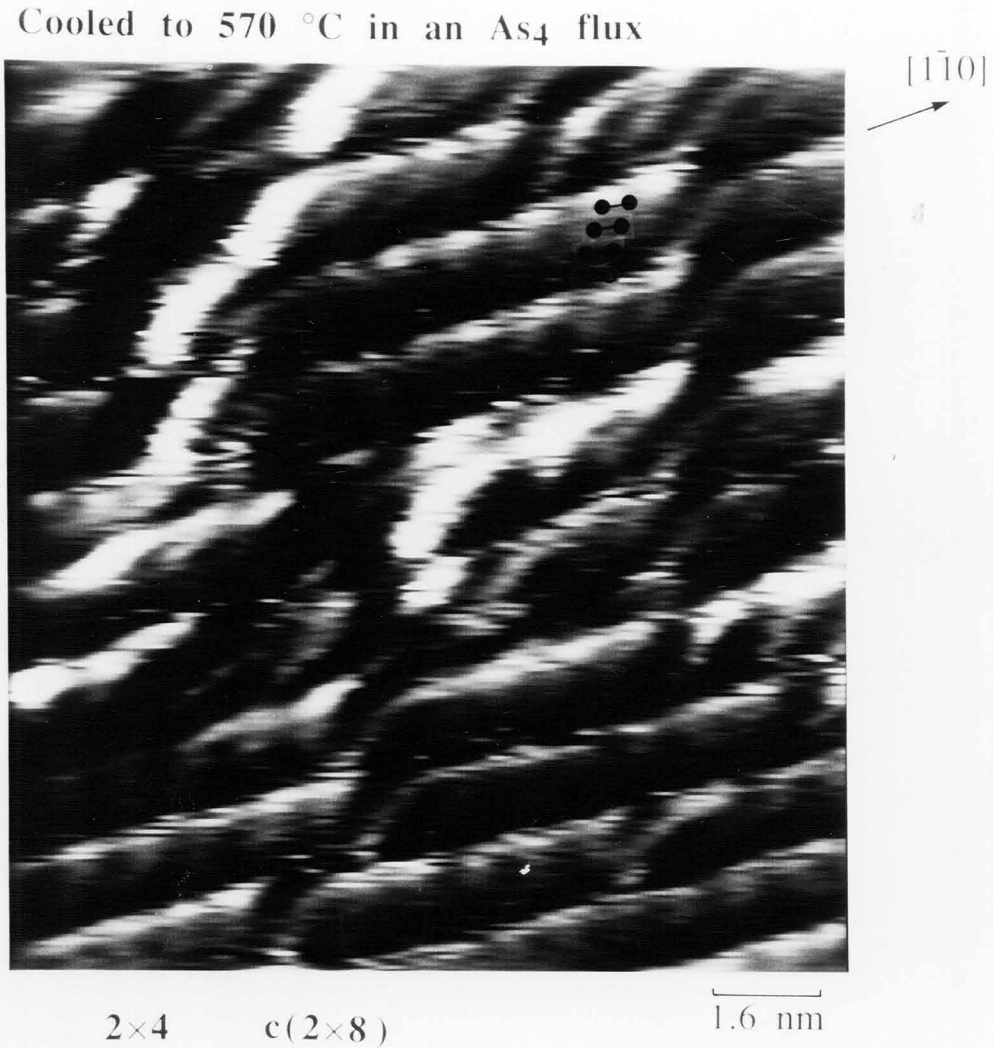

Fig. 3-5. (a) STM image and (b) ball-and-stick model of the MBE-grown GaAs (001) surface which was cooled to 570°C in the arsenic flux having 2x4 symmetry. This STM image is distorted by thermal drift.

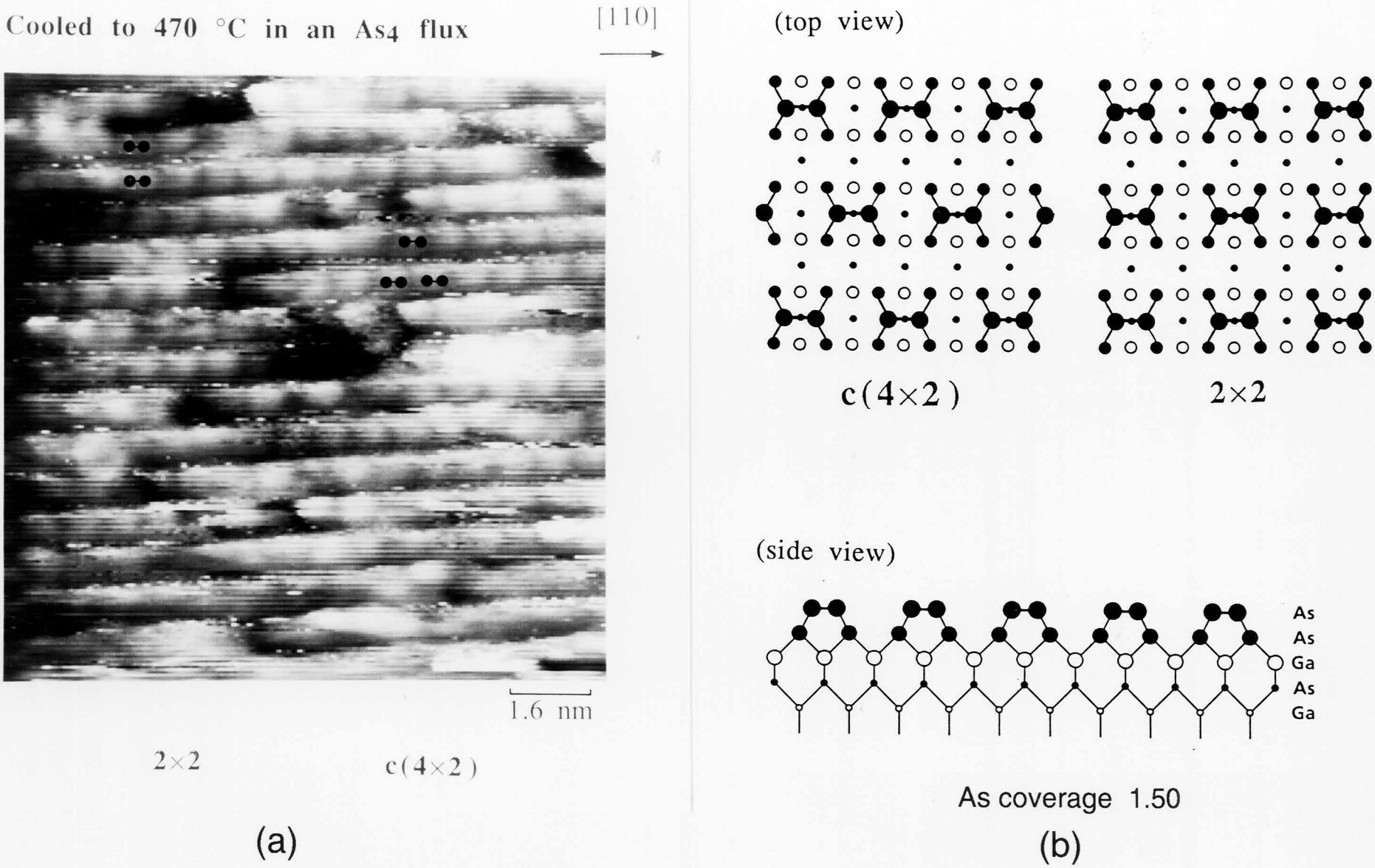

Fig. 3-6. (a) STM image and (b) ball-and-stick model of the MBE-grown GaAs (001) surface which was cooled to 470℃ in the arsenic flux having c(4x2) and 2x2 symmetry.

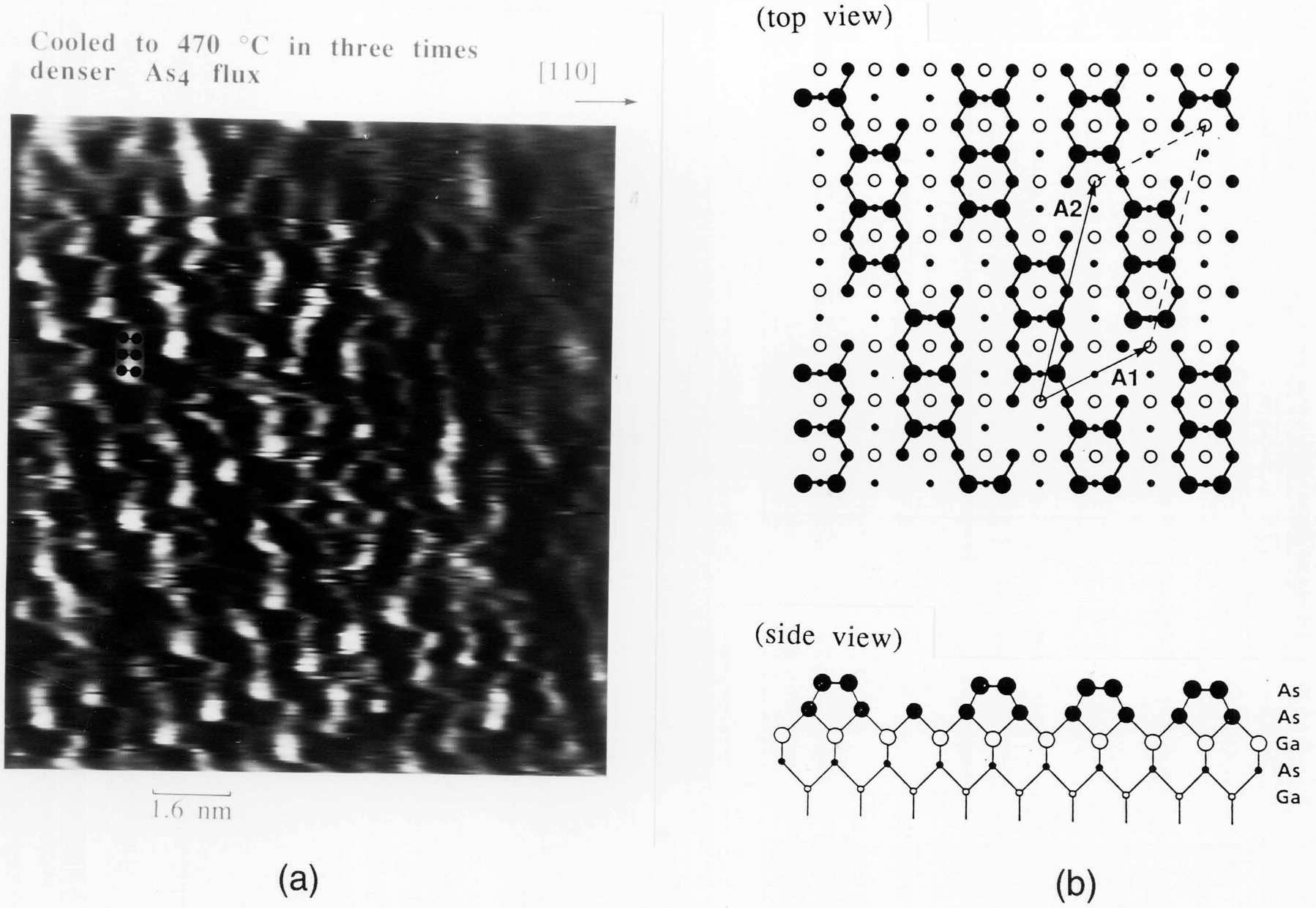

Fig. 3-7. (a) STM image and (b) ball-and-stick model of the MBE-grown GaAs (001) surface which was cooled to 470℃ in three times denser arsenic flux than the other experiments.

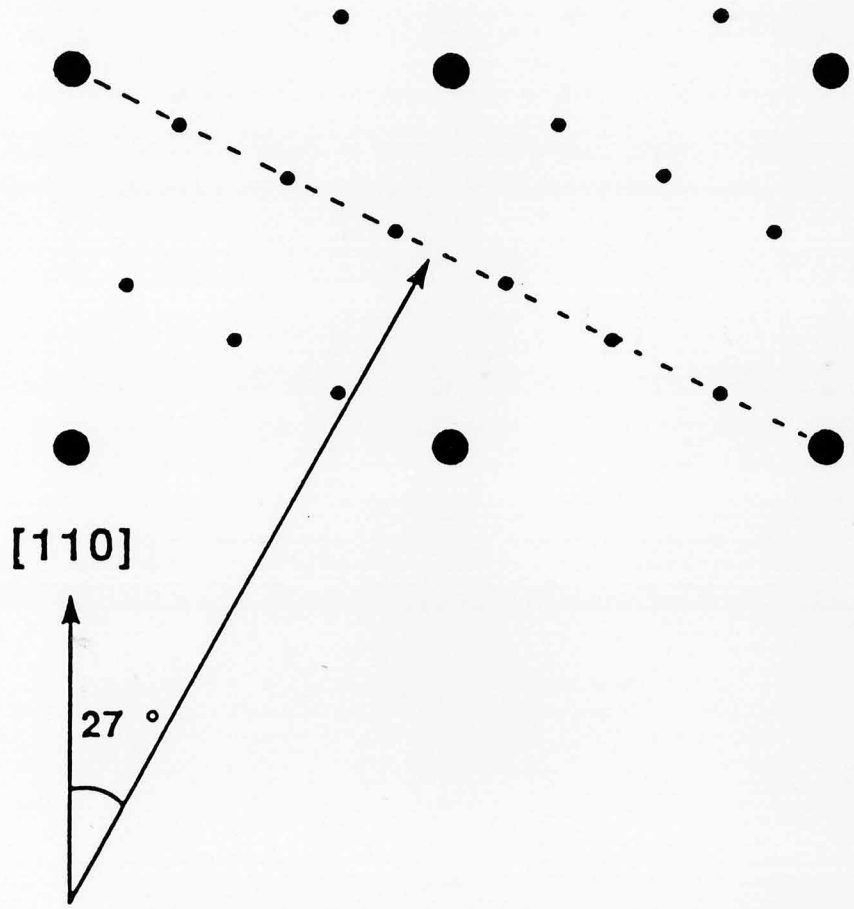

Fig. 3-8. Calculated low energy electron diffraction pattern for the reconstruction structure model shown in Fig. 3-7(b).

4. Step Structures of Molecular Beam Epitaxially Grown GaAs (001) Vicinal Surfaces [23,24]

4-1. Introduction

The tilted superlattice has been proposed as a candidate for nanometer structures.[25] It has a periodic structure perpendicular to the growth direction on a vicinal surface fabricated without lithography processes. The starting vicinal surface must have regular, straight step edges for the purpose of a uniform tilted superlattice structure. The step structure of MBE grown vicinal GaAs (001) surfaces, observed by STM, however, did not seem to be of sufficiently high regularity for use as the starting surface.[10] To our knowledge it is not clear how much we can improve the regularity by controlling the growth conditions. We therefore consider that it is important to understand the growth mechanism of GaAs on vicinal surfaces and that the surfaces should be observed both before and after growth in order to investigate the mechanism.

In this chapter we report on the surface structure of MBE-grown GaAs surfaces and its change with growth. We used substrates with vicinal (001) surfaces cut 2 degrees toward [111]A (A-surface) and toward [111]B (B-surface). We first compared their surface structures after the MBE growth of 30-monolayer (ML) GaAs. They showed characteristic structures which seemed to be formed by such wafer preparation processes as chemical polishing. We then observed how the structure evolved with MBE growth. Though no significant change of the structure was observed on the A-surface under the growth conditions, the B-surface structure became more uniform with growth.

4-2. Experiment

Two kinds of commercially available etched GaAs wafers with dimensions of 11 mm × 9 mm were used in this study. One kind of wafer had A-surfaces and the other had B-surfaces. Both kinds of wafers were already mechanically and chemically polished by the supplier in the same way.

One of the wafers was soldered onto a molybdenum block without any treatment, and then loaded into the multi-chamber UHV-STM system.

The loaded wafer was thermally cleaned in the MBE chamber under an arsenic flux with a pressure of 3.6×10^{-3} Pa. The substrate temperature was measured with an infrared radiation thermometer. After thermal cleaning, a 30-ML GaAs layer was grown at about 590 °C at a growth rate of 0.5 ML/s. The sample was kept at the growth temperature for a few minutes in order to recover the surface after growth. The substrate temperature was then lowered. As soon as the temperature reached 550 °C, the arsenic flux was shut off and the sample was transferred to the STM chamber for STM observations.

STM images were taken in the constant-current mode with a tunneling current of 200 pA and a sample bias voltage of -2 V to the tungsten tip.

After the STM observation, the sample was again transferred to the MBE chamber for further MBE growth under a step-flow condition in which no RHEED oscillation was observed. These procedures were repeated several times in order to observe changes in the surface structure with growth.

During thermal cleaning of the substrate, the process was monitored by RHEED. Only dim fundamental streaks were observed for the

incident electron beam in the [1$\bar{1}$0] azimuth until the temperature reached 590 °C. At that temperature, a diffused fourfold pattern appeared for the beam in the [1$\bar{1}$0] azimuth. It changed to a clear fourfold streak pattern after 30 MLs of GaAs was grown on the surface. At the same time, a twofold streak pattern was observed for the beam in the [110] azimuth. This result shows that the surface of the 30-ML GaAs was reconstructed to an arsenic-stabilized 2×4 structure; 30 ML is the minimum thickness necessary to obtain clear RHEED patterns. When the sample was transferred to the MBE chamber again for further growth after an STM observation, a RHEED observation was performed to confirm the 2×4 structure.

4-3. Step Structure of GaAs (001) Vicinal Surfaces

Figures 4-1 and 4-2 show STM images of 30-ML GaAs grown on the A- and B-surfaces, respectively. The scanning area is 290 nm × 290 nm. The dark lines running in the [1$\bar{1}$0] direction correspond to the missing dimer rows of the 2×4 reconstructed structure.

It is shown that the A-surface comprises only terraces parallel to the [1$\bar{1}$0] direction and relatively straight A-type step edges. The average misorientation angle is measured to be 2.0 ± 0.1 degrees from the image, which agrees with the specification of 2 ± 0.5 degrees. The terrace width, however, varies by a few nanometers to a few tens of nanometers; the surface is undulated according to the nonuniformity of the terrace width. A high step density region raises from left to right, and a low step density region is down-sloping from left to right. In the image, the former region is relatively bright, and the latter region is relatively dark. The reason is as follows: the electric signal needed to construct an STM image is weakly high-pass-filtered in order to

eliminate the effect of a slight tilt of the sample. Due to the high-pass-filter, the STM signal is weakly differentiated. Increasing signals are differentiated as being positive and decreasing signals negative; that is, up-sloping regions are brighter than down-sloping regions. In addition, the scanning direction is from left to right. Hence, from left to right, the up-slope seems to be whiter and the down-slope darker. (This is the same for all of the images discussed in this chapter.) In the upward-slope region the step density is higher than that in the downward-slope region.

On the other hand, both A-type and B-type step edges exist on a B-surface as shown in Fig.4-2. There are wide, flat terraces which have B-steps as well as narrow, long terraces which have long A-steps and short B-steps. The height of the narrow terrace region is typically 3-4 nm from the surface of the wide terraces. The misorientation by 2 degrees toward [111]B seems to be formed by the combination of the wide terraces and the narrow ones. In addition, several holes of about 50 nm $\times$ 100 nm size are observed. They are 7-8 nm deep, as measured from the wide terrace surface.

It is considered that the observed surface structure is nearly the same as that of the substrate, since only 30-ML GaAs was grown. The difference between the structure of the A-surface and that of the B-surface, therefore, reflects a difference in the surface structure of the wafers. The surface structure of a wafer is considered to be strongly related to the preparation process, such as mechanical and chemical polishing. The observed structure difference between the two kinds of wafers results from a difference in the misorientation directions, since they were prepared according to the same process. Thus, not a physical effect but a chemical effect seems to be responsible for the observed

difference of the surface structures. In fact, we have observed different surface structures for other wafers which were not chemically polished as much as the wafers used in this experiment. This result will be reported elsewhere.

4-4. Step Structure Changes with MBE Growth

It was reported that the surface structure changed, becoming more uniform with epitaxial growth.[26] We performed further MBE growth on the B-surface after the STM observation; 150-ML, 0.17-μm, and 1.5-μm-thick GaAs layers were successively grown in the step-flow mode on the same B-surface and observed with the STM after each growth.

Figure 4-3 shows the surface structure of the 150-ML MBE grown GaAs on the B-surface. The holes shown in Fig.4-2 cannot be seen in Fig.4-3. They may be filled with the MBE-grown layer under the step-flow condition. Although the terrace width distribution has become more uniform in the $[1\bar{1}0]$ direction, nonuniformity is still clearly observed. The left-hand area consists of narrower terraces, and the right-hand area consists of wider terraces; undulation in the [110] direction remains. It seems that the height difference between the two domains of the B-surface shown in Fig.4-3 is less than that in Fig.4-2. Because of the undulation in the [110] direction, the A-steps are still observed in the transition region from the narrow-terrace area to the wide-terrace area.

Figure 4-4 shows the surface of the 0.17-μm-thick GaAs layer. The nonuniformity still remains; the left-hand area also has narrower terraces, and the right-hand area wider terraces. A-type step edges are observed in the left region, which is the result of a slight undulation in the [110] direction.

Figure 4-5 shows the surface of the 1.5-μm-thick GaAs layer. The structure has become uniform, and the undulation in the [110] direction has disappeared. The average terrace width is observed to be uniform, with the B-type step edges corresponding to the misorientation direction. However, the misorientation angle measured from this image is 1.3 ± 0.1 degrees, smaller than the specification of 2 ± 0.5 degrees. It is considered that the surface structure is uniform over a submicron-size region, but may not be completely uniform all over the surface. The step edges are rugged and the terrace width is scattered from a few tens of nanometers to a few nanometers.

We also performed 1.5-μm-thick MBE growth on the A surface under the same growth conditions for the growth on the B-surface, and then performed STM observation. However, there was no observed significant structure change, and the terrace width uniformity was not improved; that is, the up- and down-slope regions still exist. This result shows that step-flow growth occurred only in the $[1\bar{1}0]$ direction under the conditions used in this study.

Islands can be seen on the terraces of the A-surface shown in Fig.4-1. Most of them are only 1.6 nm long in the [110] direction and more than 10 nm long in the $[1\bar{1}0]$ direction. (A typical island is indicated by an arrow.) It should be noted that the average terrace width of 80 nm, calculated from the misorientation angle, is larger than the island length along the [110] direction, and that the average terrace width is shorter than the island length along the $[1\bar{1}0]$ direction. It is considered that a transition from two-dimensional nucleus growth to step-flow growth occurs when the terrace width and maximum size of two-dimensional nuclei become equal. The anisotropy of the observed island shape therefore seems to be the cause of that of the step-flow growth

condition. However, the reason for the anisotropy of the island shape has not yet been clarified. The anisotropy of the diffusion constant [27] and/or the difference in the sticking coefficient to the A- and B-step edges [28] may be the reason.

As for the terrace width ordering mechanism, it has been observed that steps grow faster in a region of high step density than in a region of low step density, as shown in Fig.4-2 to Fig.4-5. A simulation of the terrace width ordering process was performed by Tokura et al.[29] It was, however, impossible to judge its reasonability, since the structure of the starting surface was not known. We consider that a quantitative analysis of the STM images of MBE-grown surfaces is necessary in order to check such calculations. In addition, further quasi-in-situ STM observations of MBE-grown surfaces under different growth conditions, such as those involving wafers of different misorientation angles, are required for a more detailed study of the MBE growth mechanism.

4-5. Summary

The surface of MBE-grown GaAs layers on vicinal (001) wafers cut toward the [111]A and [111]B directions were observed with a multi-chamber UHV-STM. STM images of the 30-ML grown surfaces showed that the A-surfaces comprised terraces with only A-type steps; the step density was not uniform on the surface.

On the other hand, the B-surfaces comprised wide terraces with B-steps and narrow terraces with A-steps. The surface structure was, thus, much less uniform than that of the A-surface.

It was observed that MBE growth under the step-flow condition on the B-surface made the surface structure more uniform. No terrace

width ordering was observed on A-surfaces under the same growth condition.

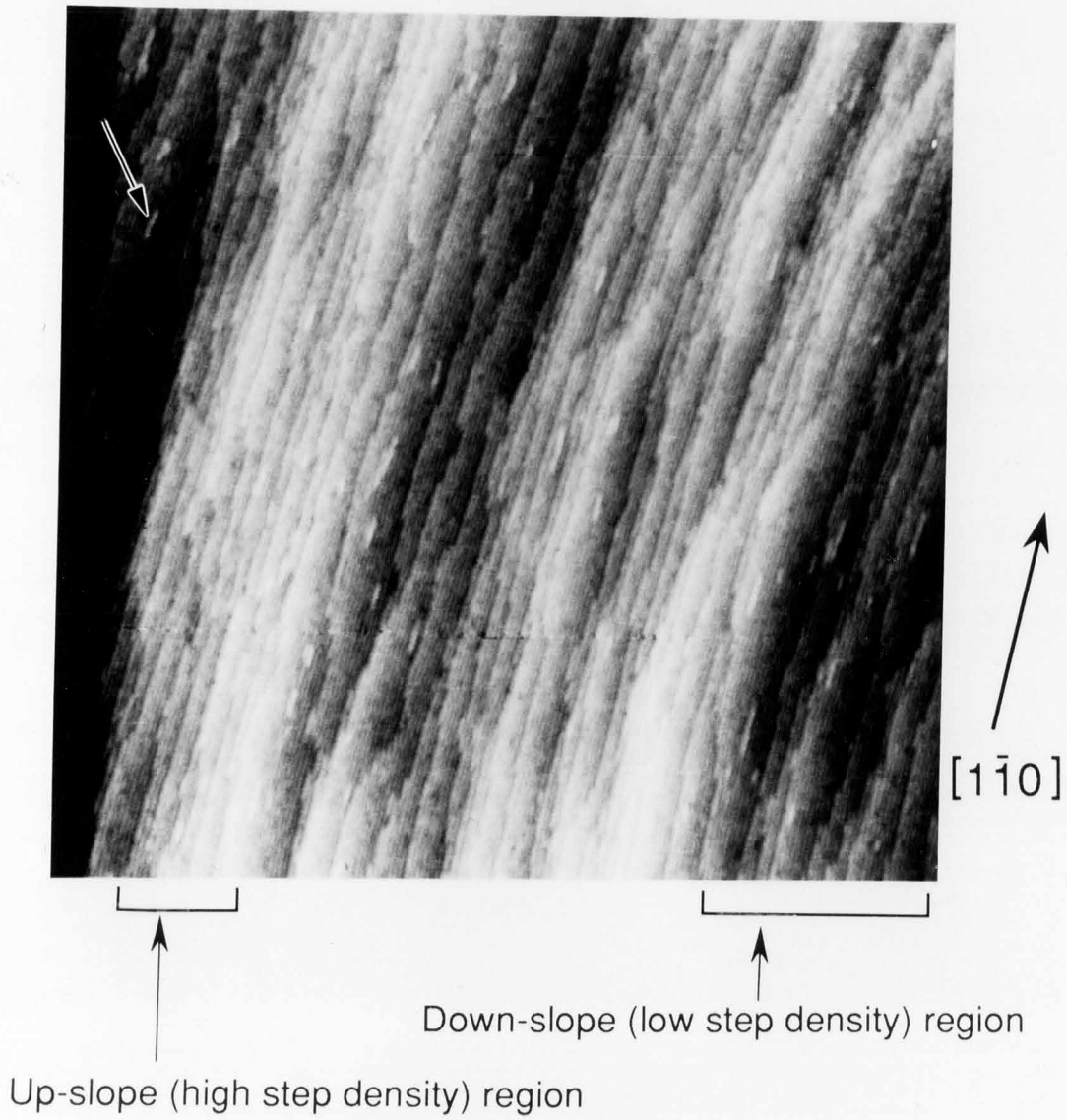

Fig. 4-1. STM images of 30-ML GaAs grown by MBE on vicinal (001) surfaces cut 2 degrees toward [111]A.

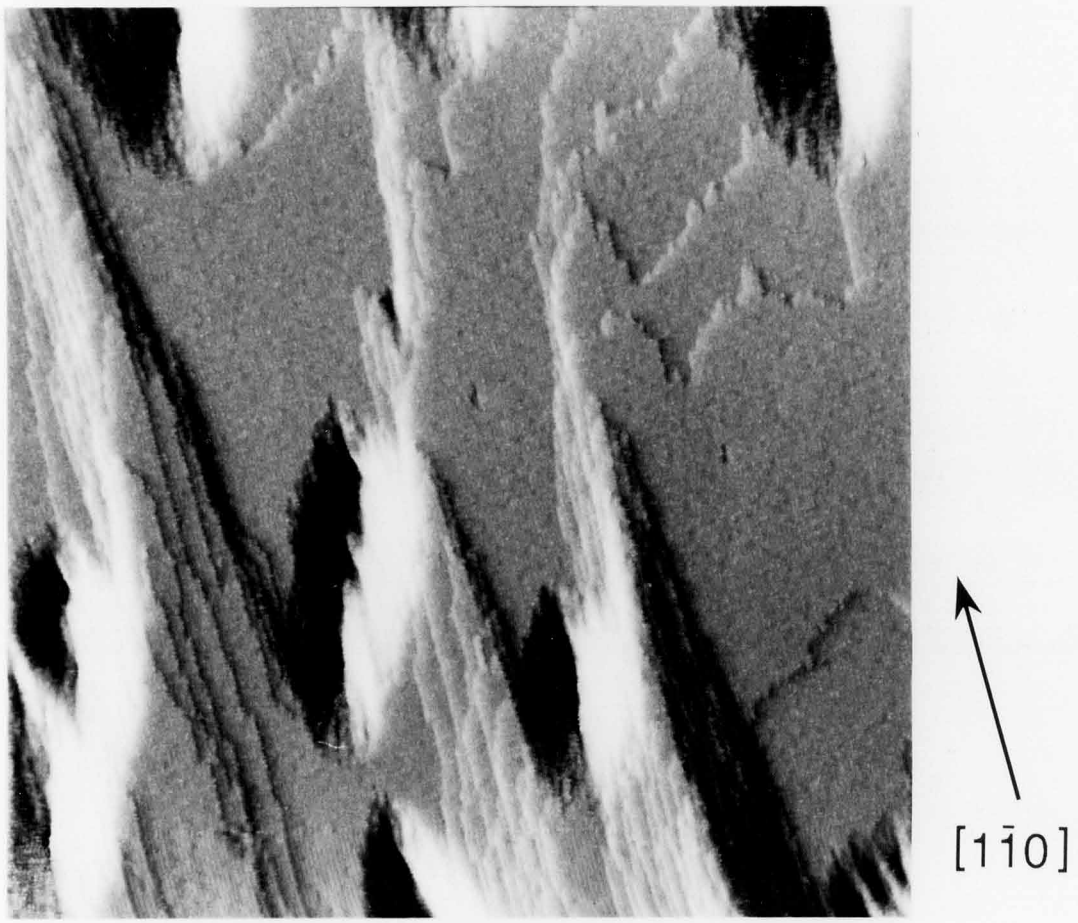

Fig. 4-2. STM images of 30-ML GaAs grown by MBE on vicinal (001) surfaces cut 2 degrees toward [111]B.

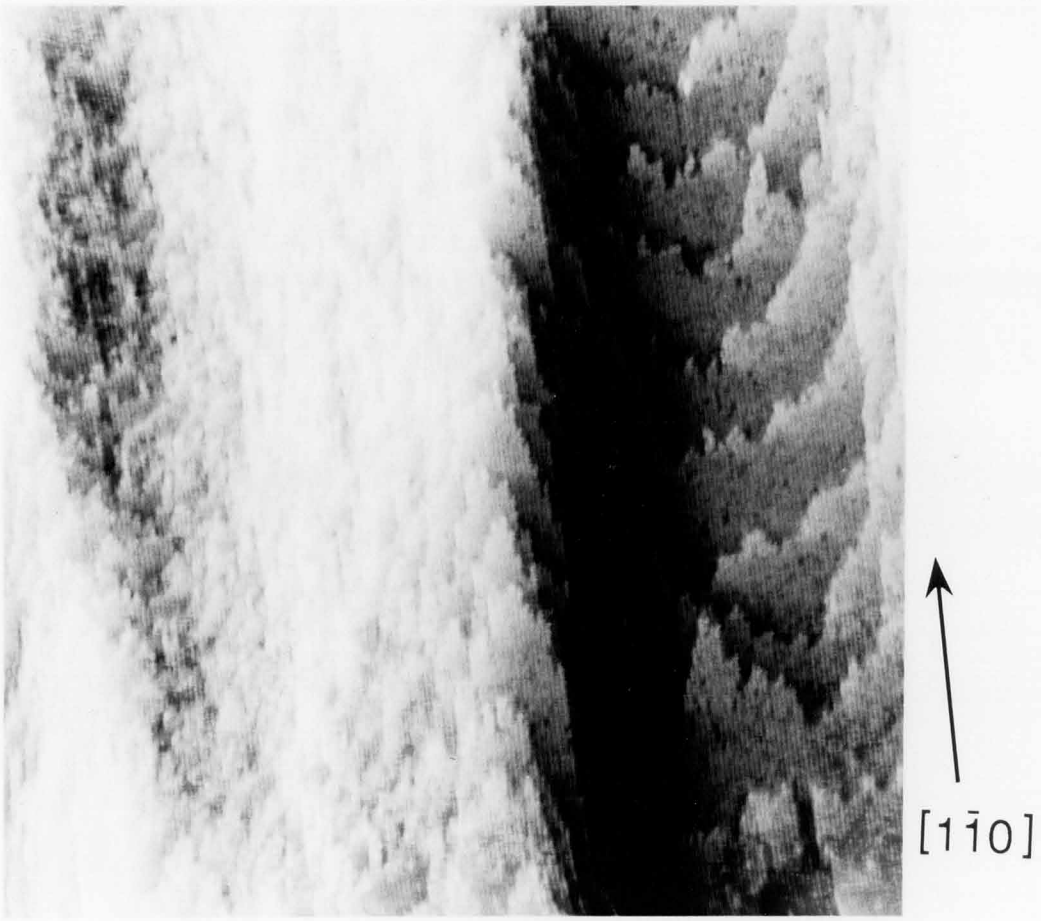

Fig. 4-3. STM images of 150-ML GaAs grown by MBE on vicinal (001) surfaces cut 2 degrees towards [111]B.

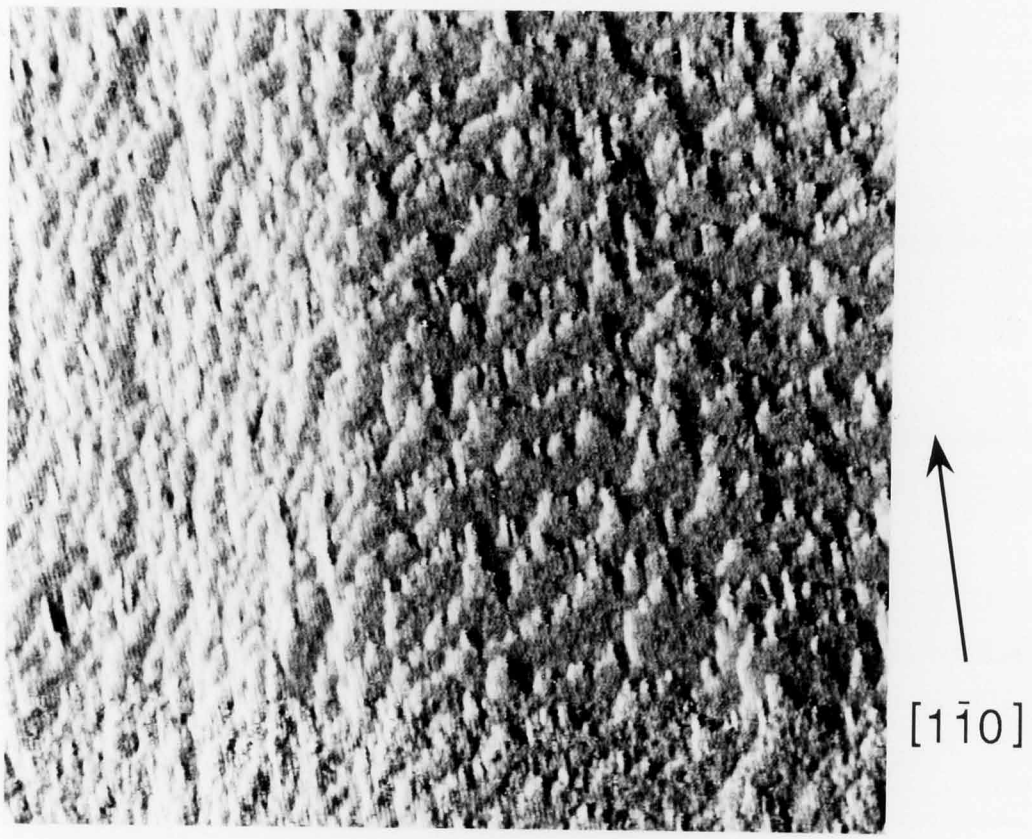

Fig. 4-4. STM images of a 0.17-μm-thick MBE-grown GaAs layer on a vicinal (001) surface cut 2 degrees towards [111]B.

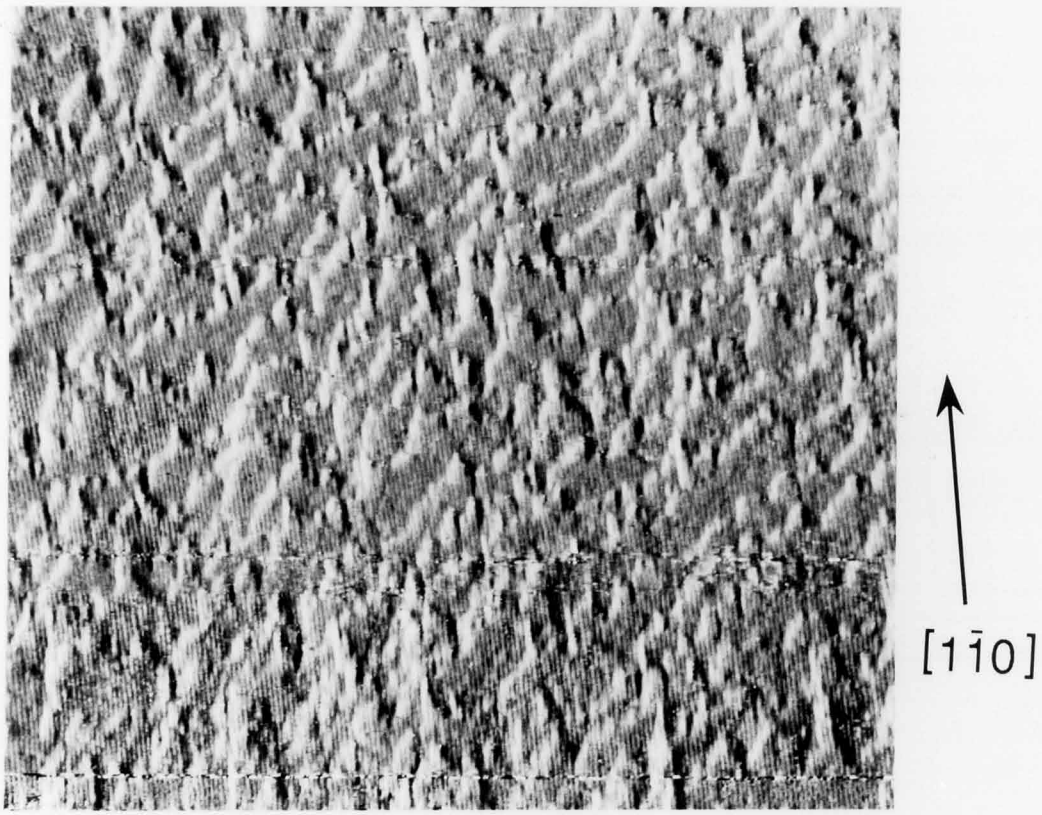

Fig. 4-5. STM images of a 1.5-μm-thick MBE-grown GaAs layer on a vicinal (001) surface cut 2 degrees towards [111]B.

5. Heteroepitaxy of GaAs on InP (001) Substrates.

5-1. Introduction

The heteroepitaxy technology of a lattice mismatched system has been attracting much attention since it can provide an additional degree of freedom for the material design of novel devices.[30-32] For example, MBE grown GaAs-on-InP optoelectronics integrated circuits (OEIC's) which combine InP long-wave optical devices and high-speed GaAs electric devices have been demonstrated and have exhibited promising performances.[33,34] Although various heteroepitaxy system such as GaAs-on-Si have been studied, the large defect density seems to put a limitation on further development. we consider that it is necessary to understand the mechanism of heteroepitaxial growth in more detail in order to reduce the defect density. In particular, the atomic-scale structure of the hetero-interface seems to be important to understand the growth process.

In this chapter, we describe observations of GaAs-on-InP growth processes using our multi-chamber UHV-STM system. Before the MBE growth of a GaAs layer on an InP (001) substrate, the surface of the InP substrate is thermally cleaned in an arsenic flux. The thermally cleaned InP (001) surfaces were, therefore, firstly observed, and two types of reconstruction of the In-stabilized surface were found for different cleaning conditions; 0.8 nm wide lines running along the [110] direction were positioned with 1.6 nm period in the [1$\bar{1}$0] direction in one type of reconstruction and 0.4 nm wide lines were observed in the other type of reconstruction. We have proposed ball-and-stick models comprising In-In dimers and missing dimers per 4×2 cell for these types of reconstruction.[35,36]

Secondly we observed the surface of the heteroepitaxially grown GaAs layers for different amount of deposited GaAs at the same substrate temperature. When either 1 monolayer (ML) or 1.5 ML GaAs was deposited on an InP (001) substrate, the growth seemed to be two-dimentional. On the other hand, dramatic island formation was observed for 2.5 ML GaAs deposition.[37,38]

5-2. Observation of InP (001) Surfaces Thermally Cleaned in an Arsenic Flux

Thermally cleaned InP(001) surfaces were observed before heteroepitaxial growth of GaAs because it is important to know about the structure of the starting surface for investigation of the growth mechanism.

An InP substrate was first entered into the multi-chamber UHV-STM system and then transferred into the MBE chamber. The sample was heated up to about 460 °C in order to remove the surface arsenic oxide in an arsenic flux, with an arsenic partial pressure of 3×10^{-3} Pa. The temperature was measured using an infrared radiation thermometer. Sublimation of the surface oxide was confirmed through the appearance of a RHEED pattern. After keeping the substrate temperature at 460 °C for ten minutes, the temperature was gradually raised to about 510 °C in order to remove the surface indium oxide and to make the surface In-stabilized. After the surface was In-stabilized, the arsenic flux was shut off and the substrate temperature was lowered to 480 °C. The sample was then transferred to the STM chamber for an STM study.

STM measurements were performed in the constant-current mode. In this study, STM images were taken at a sample voltage of -2 V relative to the tungsten tip and a constant tunneling current of 200 pA.

After the STM measurements, the sample was transferred to the MBE chamber again and the surface reconstruction symmetry was reconfirmed by RHEED.

The cleaning process was monitored by RHEED in the MBE chamber. A two-fold RHEED pattern was observed when the sample was heated to 460 °C in the arsenic flux for the incident electron beam in the direction of the [110] azimuth. When the substrate temperature was gradually raised, the two-fold pattern changed to a four-fold one of the In-stabilized surface at about 510 °C. On the other hand, the RHEED pattern for the beam in the [1$\bar{1}$0] azimuth showed a two-fold symmetry at this temperature. Figures 5-1 (a) and (b) show the RHEED patterns for the beam in the [110] azimuth and in the [1-10] azimuth, respectively. This result means that the surface is reconstructed to be either a 4×2 and/or a c(8×2) structure. The four-fold pattern consisted of strong fundamental streaks and relatively weak higher order streaks when they appeared. The fundamental streaks then became weaker, and a more uniform four-fold pattern was observed within one minute. This intensity change of the RHEED streaks may be related to a change in the surface structure.[39] When the arsenic flux was shut off and the substrate temperature was lowered to 480 °C, the four-fold RHEED pattern remained.

STM measurements were performed for the samples prepared under three different conditions. Fig.5-2 (a) shows an STM image of a sample which was heated at 510 °C for about one minute in the arsenic flux. It shows 1.6 nm periodic lines of about 0.8 nm width running in the [110] direction. Each line comprises two rows. It is, thus, obvious that the four-fold RHEED pattern is due to these lines. We consider that these lines represent In-In dimers parallel to the [110] direction, since

the surface is In-stabilized. According to our STM image, a set of two In-In dimers are positioned every 1.6 nm in the [1$\bar{1}$0] direction. Namely, two of every four In-In dimers are missing and the dimer coverage is estimated to be 0.5 for this type surface. A proposed ball-and-stick model for this surface is shown in Fig.5-2 (b). In this model the In-stabilized surface comprises 4×2 cells made of two In-In dimers and two missing dimers. Since it is reported that the P atoms of the InP surface are replaced by As atoms during the cleaning, we consider that the In dimers to be bonded to As atoms on InP bulk.[40] The arrangement of the 4×2 cells is not unique, both 4×2 and c(8×2) structures are considered to be possible since individual In-In dimers are not resolved in the STM image. The reason seems to be as follows. The electron density is so uniform along the [110] direction that our STM was not able to resolve individual dimers along this direction. There is another possibility that an asymmetric tip structure effect could have caused this STM image. This, however, does not seem to be the reason, since similar STM images of 1.6 nm periodic lines were observed when another tip was used, with which a well-resolved STM image of As-stabilized GaAs 2×4 structure was obtained.

The STM image of a sample which was heated at 512 °C for three minutes in the As flux is shown in Fig.5-3 (a). Although 1.6 nm periodic lines are also seen in the image, each line is about 0.4 nm wide and comprises a single raw. It is therefore considered that the 4×2 cells comprise one In-In dimer and three missing dimers for this type surface. This result suggests that a larger number of surface In atoms are evaporated during cleaning, since the second sample was heated at a higher temperature for a longer time than was the first one. The In-In dimer coverage is estimated to be 0.25 for this surface.

Two weak lines can also be seen between the 1.6 nm periodic lines in Fig.5-3 (a). They are 0.2 nm lower than the top In surface. We consider that these lines represent a reconstructed structure of a lower layer. Since these weak lines are parallel to the top In-In dimers, they probably comprise In-In dimers of the third layer. The As atoms of the second layer thus seem to be evaporated from the surface. The proposed ball-and-stick model for this surface is shown in Fig.5-3 (b). Figure 5-4 is a lower-magnification image of this surface. The 1.6 nm periodic lines of 0.4 nm width running in the [110] are observed in the wide area, which suggests that the reconstruction structure is uniform all over the surface. Also there are various surface structures such as terraces, steps, islands, and holes.

Fig.5-5 shows an STM image of a sample which was kept at 480 °C for about ten minutes in a vacuum of 10^{-5} Pa after being cleaned and the arsenic flux was shut off. This image shows two domains : one comprising 1.6 nm periodic lines in the [110] direction and the other comprising 2×4 cells. The first domain seems to consist of 4×2 cells which have one In-In dimer and three missing dimers, just like the second sample. The second domain comprises 2×4 cells which seem to have three As-As dimers and one missing dimer. This sample showed four-fold RHEED patterns for the beams in both [110] and [1$\bar{1}$0] azimuths. The RHEED patterns can be explained in terms of this two-domain structure. This type surface therefore was formed by a desorption of the upper layer atoms when the sample was annealed at 480 °C in a vacuum.

5-3. GaAs Heteroepitaxial Growth on InP (001) Substrates

The surface structures of heteroepitaxially grown GaAs were observed for different amount of GaAs deposited on the thermally cleaned InP (001) substrates.

An InP (001) substrate was cleaned in the arsenic flux as described in the previous section. The substrate temperature was kept at 510 °C for three minutes in order to sublime the native indium oxide off and to make the surface indium-stabilized. A certain amount of Ga was then deposited onto the sample for growing the GaAs layer. The growth rate was 0.12 ML/s for all experiments. After growth, the sample was transferred to the STM chamber for STM study. The surface temperature was measured with an infrared radiation thermometer, and the surface reconstruction symmetry was observed by RHEED.

STM measurements were performed in the constant-current mode. The tunneling current was 200 pA and the sample bias voltage was -2 V for all STM measurements mentioned in this section.

A fourfold streak RHEED pattern was observed for the incident electron beam in the direction of the [110] azimuth and a twofold streak pattern for the [1$\bar{1}$0] azimuth when the sample was cleaned in an arsenic flux at about 510 °C. This result shows that the surface was In-stabilized. After 1 ML GaAs was grown on the sample surface, the fourfold and twofold RHEED streak patterns changed to twofold and fourfold streak patterns, respectively. This change in the RHEED pattern means that the surface became As-stabilized after the growth of 1 ML GaAs. Furthermore, the growth seems to be two-dimensional with a scale of a few tens of nm, since the streak pattern was maintained.

Figure 5-6 shows a typical STM image of the surface of the 1 ML GaAs on the InP substrate. Although it is not possible to resolve each

individual unit cell in this large-area image, the observed dark lines running in the [1$\bar{1}$0] direction correspond to the missing dimer rows and the white lines to the arsenic dimer rows. These lines are not so straight as those of the homoepitaxial GaAs surface but are ragged. These ragged lines are probably due to the larger number of kinks on this surface. Steps can be seen in the upper middle and lower left regions of the image. The height of these steps is about 0.57 nm which is close to the two atomic height of GaAs. We took twenty-one STM images of a 40 nm × 36 nm area at various points on this surface. Although steps were observed, no island was found on the surface. It is therefore considered that the 1 ML GaAs growth on the InP substrate was two-dimensional.

For 1.5 ML GaAs deposition, the streak RHEED pattern was also maintained. Although more steps were observed in the STM images than in those of 1ML GaAs, the growth still seemed to be two-dimensional.

When Ga atoms for 2.5 ML GaAs growth were supplied on an InP substrate, the fourfold RHEED pattern became spotty and the fundamental streaks became extended, as shown in Fig.5-7. The extended angles were measured to be about ±20 degrees, corresponding to the [114] and [11$\bar{4}$] directions. This result suggests that the (114) and (11$\bar{4}$) facets were formed on the surface.[41]

A typical STM image of this surface is shown in Fig.5-8 (a). It is clear that the growth had already changed to three-dimensional. In Fig.5-8 (a), one island of about ten nm by a few tens of nm size, and two parts of other islands appear in a 67 nm × 60 nm area. They are typical-size islands observed on this surface. We took twelve images of this surface; every image showed at least one island. The average island density was calculated to be 7×10^{10} cm^{-2}. Figure 5-8 (b) shows a larger-

magnification image of another island surface. The surface layer also shows 1.6 nm periodic missing dimer rows. It is thus concluded that these islands are not made of contamination such as carbon, but of GaAs. It should be noted that these islands are longer in the [1$\bar{1}$0] direction in which the diffusion length of Ga atoms is larger than in the [110] direction.[42]

The cross section of an island parallel to the [110] direction is nearly trapezoid. The facets of the islands along the [1$\bar{1}$0] direction form certain angles with the surface. We measured this angle at 32 points for 16 islands (2 points per each island). The average of the measured angles was 22 $\pm$ 3 degrees, coinciding with the extension angle of the RHEED streaks. The extension of the fundamental RHEED streaks in Fig.5-7 can therefore be explained by these faceted islands.

The height of a typical island is about 3 nm, which is more than four times larger than that of the average overlayer thickness if it were uniformly deposited. The number of GaAs atoms which form one island in Fig.5-8 (a) is roughly estimated to be 10^4, and the density of GaAs atoms of 1 ML is 5×10^{14} cm^{-2}. If the island density (7×10^{10} cm^{-2}) is taken into account, the number of GaAs atoms which form the islands on this surface is nearly same as the number of GaAs atoms of 1.5 ML. The excess GaAs atoms on the first GaAs layer, therefore, probably formed these islands. In Fig.5-8 (a), surfaces other than those of the islands appear, which are rather rough and have steps. These results suggest that the three-dimensional island growth process involves an incorporation of previously deposited GaAs atoms. Figure 5-9 explains our model for the heteroepitaxial growth of GaAs on an InP (001) surface. Two-dimensional growth proceeds for 1 ML and 1.5 ML GaAs. Because the streak RHEED pattern is maintained, the two-dimensional

growth continues until 2 ML GaAs is grown. When the supplied amount of Ga atoms becomes lager than that for 2 ML GaAs, the growth mode changes to three-dimensional one, which incorporates previously deposited GaAs layer, and islands are formed on the first GaAs layer. The islands have (114) and (11$\bar{4}$) surfaces which makes 20° with the (001) surface.

To date, various models for the growth mechanism of strained layers have been proposed. The Stranski-Krastanov model is representative, in which a few ML's of a crystal layer grow two-dimensionally, and then change to the three-dimensional growth mode. Biegelsen et al. have observed the early stages of GaAs-on-Si heteroepitaxy and have reported that a three-dimensional nucleation of GaAs may have occurred when 0.6 ML of GaAs was deposited. In their case, the Stranski-Krastanov model is not suitable because the three-dimensional growth mode seems to have begun before the first GaAs layer was completed.[43] On the other hand, our situation is closer to that of the Stranski-Krastanov model, since two-dimensional growth was observed for more than 1 ML deposition of GaAs. However, there is a possibility in our case that the two-dimensionally grown layer might not completely cover the surface in a more microscopic range. Recently, Snyder et al. reported on GaInAs-on-GaAs heteroepitaxy and observed two-dimensional growth of GaInAs layers for several-ML deposition. They proposed the nucleation and growth of two-dimensional islands and a coarsening process in which three-dimensional islands grow. They suggested a rapid and dramatic microstructural change when sufficient kinetics are given.[44] Although it is difficult to determine whether two-dimensional island growth occurred or not in our case, the transition seems to be dramatic.

5-4. Conclusions

We have observed thermally cleaned InP surfaces in an arsenic flux. The STM image of the In-stabilized surface shows 1.6 nm periodic lines in the [110] direction. This result suggests that the reconstructed surface comprises 4×2 cells which seem to have either one In-In dimer and three missing dimers or two In-In dimers and two missing dimers which depend on the cleaning conditions. The co-existance of In-stabilized 4×2 domains and As-stabilized 2×4 domains is also observed on a sample annealed at 480 °C in a vacuum of 10^{-5} Pa. This structure seems to have been formed by a desorption of surface atoms.

GaAs heteroepitaxial growth process on thermally cleaned InP (001) surfaces has been investigated. Island formation of GaAs is observed when 2.5 ML GaAs is deposited, while the growth of GaAs seems to be two-dimensional when either 1 ML or 1.5 ML GaAs is deposited. The island formation seems to involve previously deposited Ga atoms when a critical thickness of GaAs layer is grown.

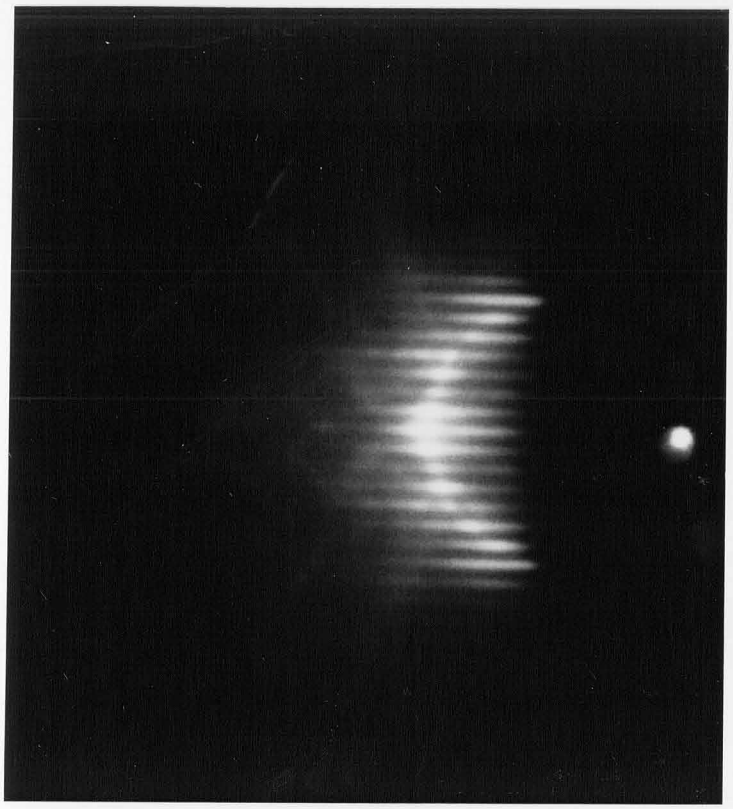

(a)

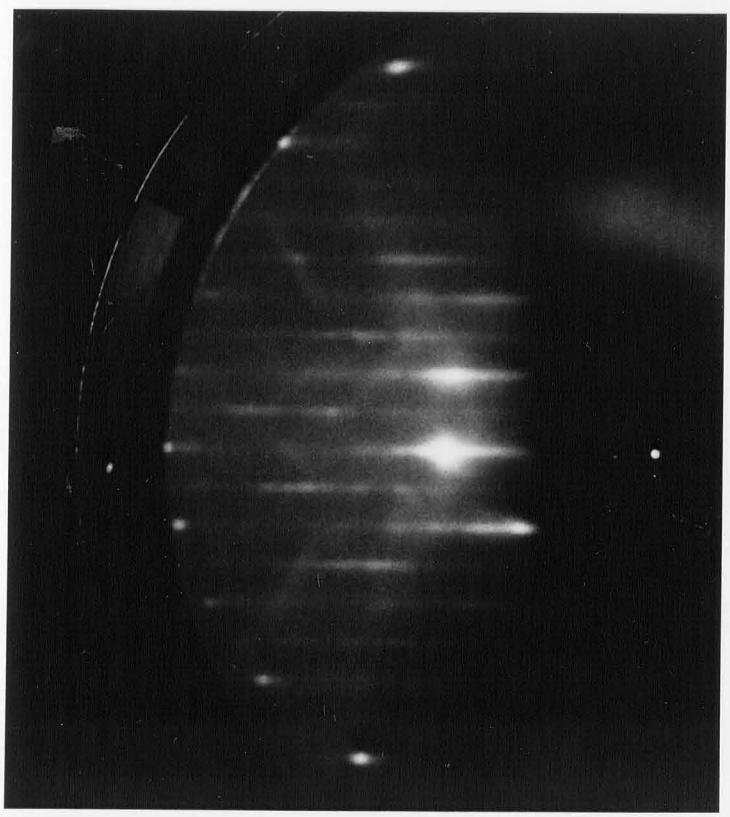

(b)

Fig. 5-1. RHEED patterns of the thermally cleaned InP (001) surface in an arsenic flux at 510°C for the electron beam (a) in the [110] azimuth and (b) in the [1$\bar{1}$0] azimuth.

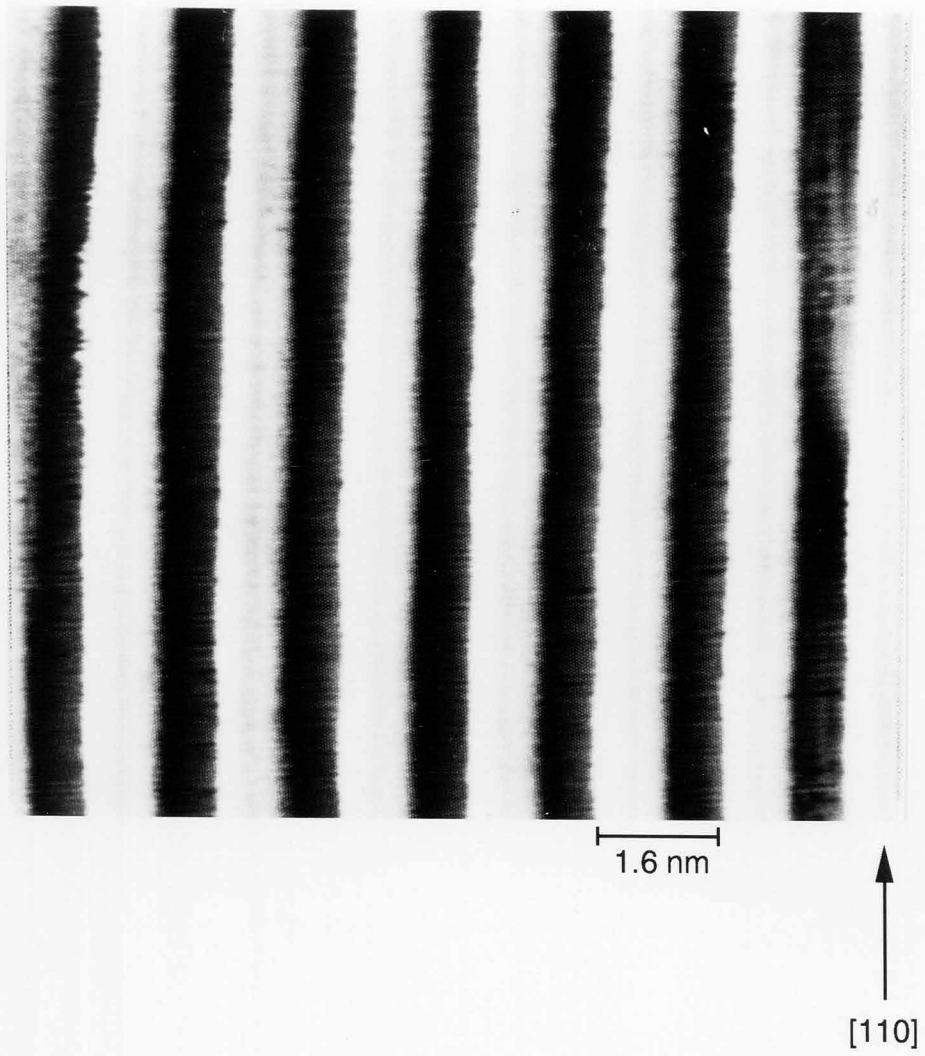

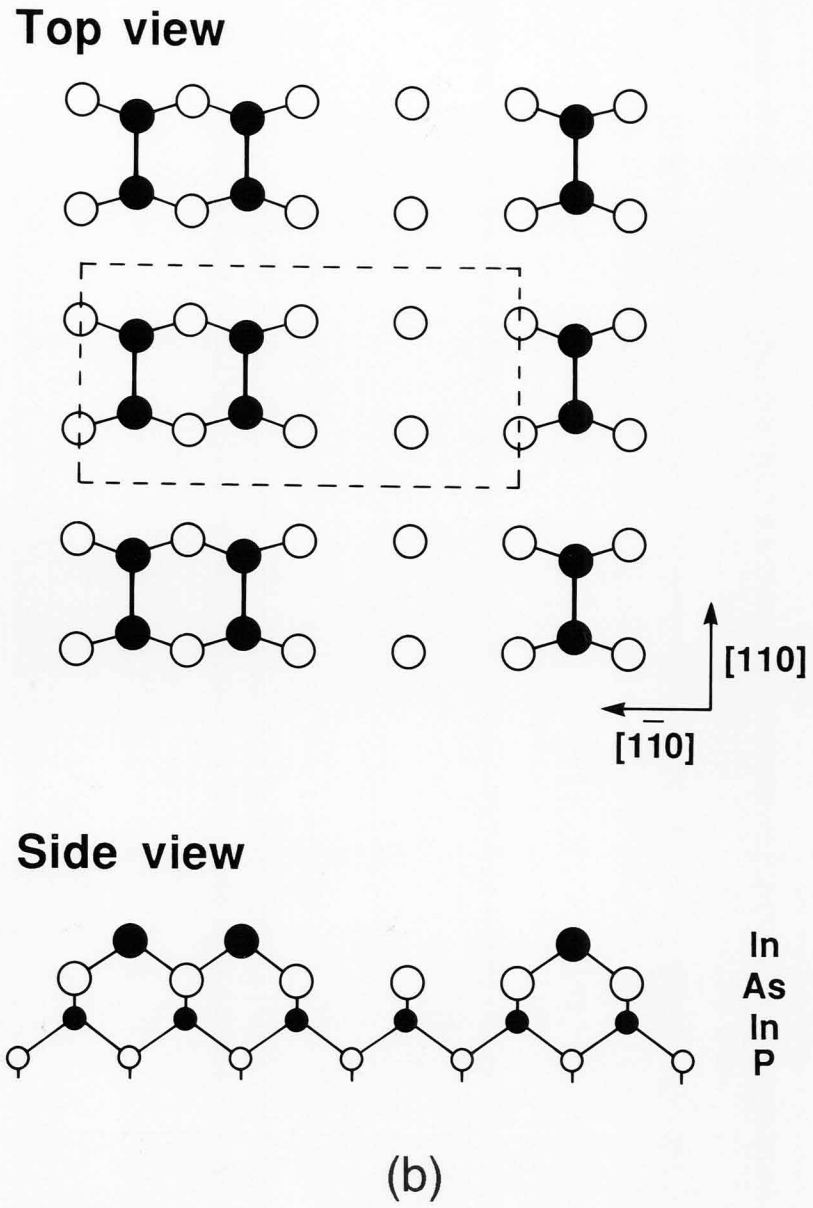

Fig. 5-2. (a) STM image and (b) ball-and-stick model of the InP (001) surface thermally cleaned in the arsenic flux at 510℃ for 1 min.

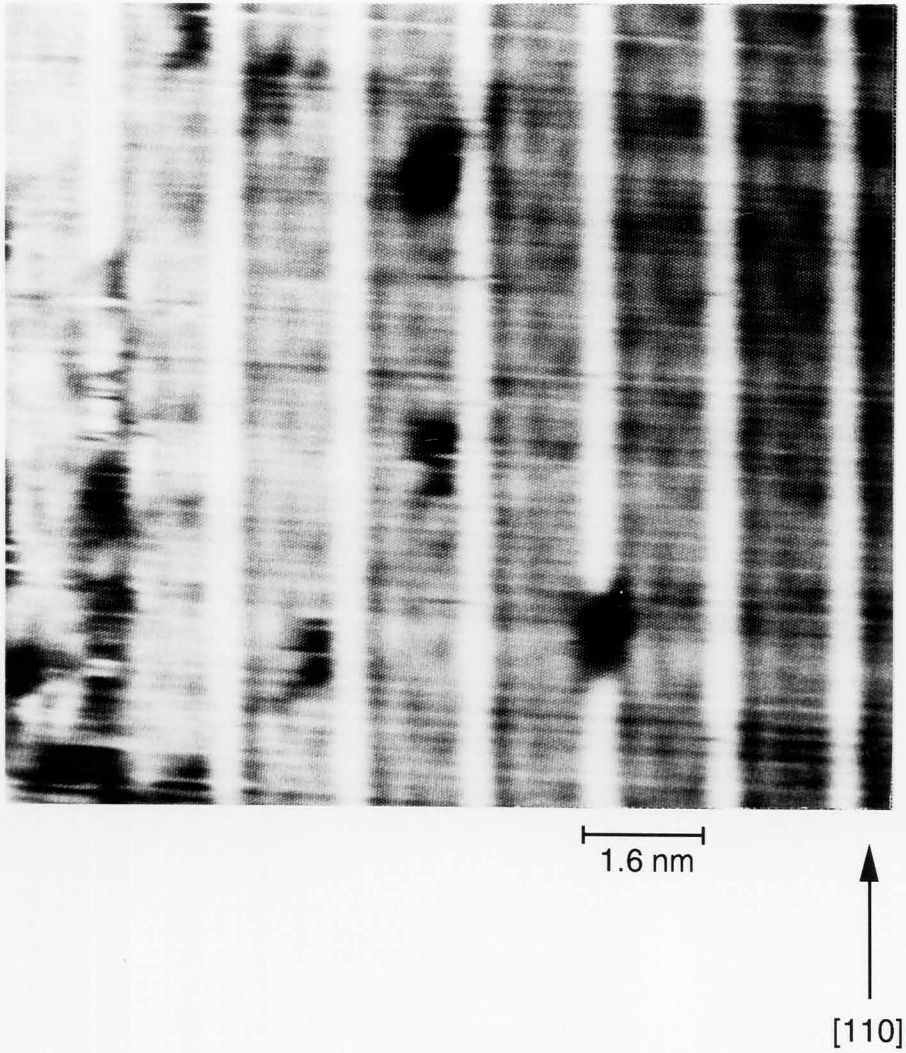

(a)

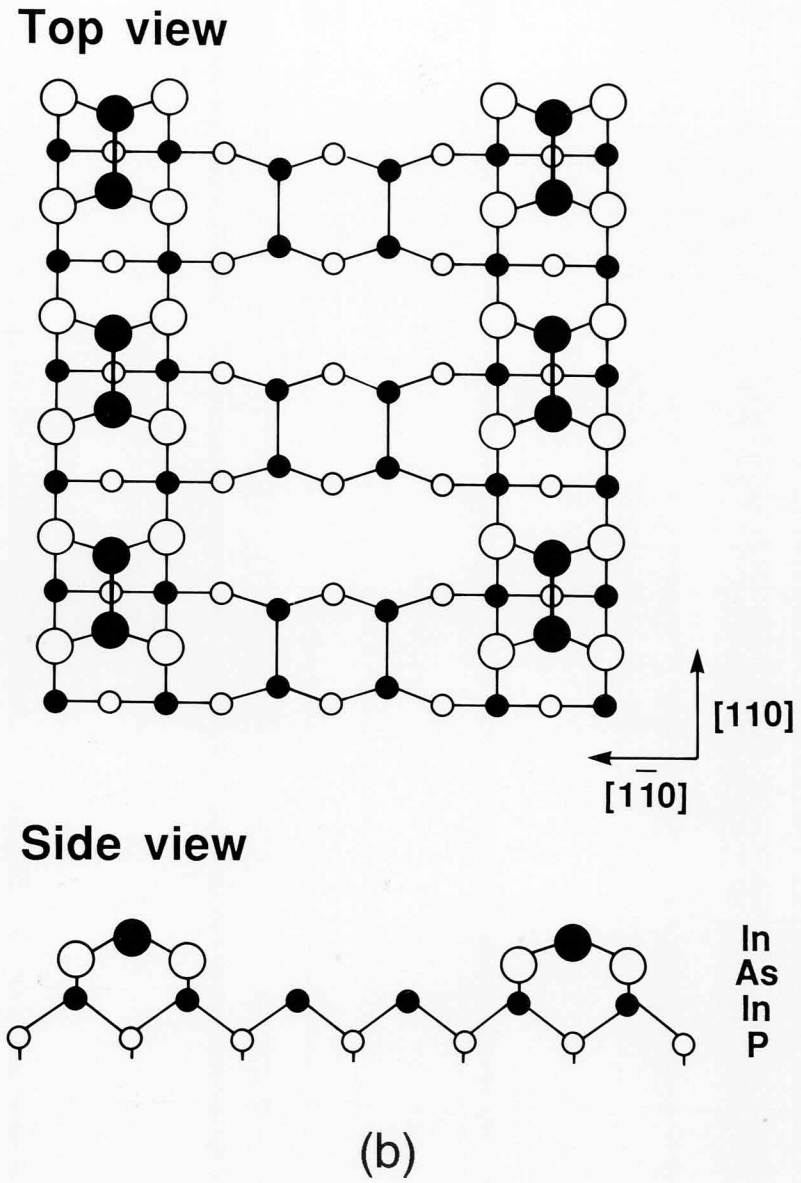

(b)

Fig. 5-3. (a) STM image and (b) ball-and-stick model of the InP (001) surface thermally cleaned in the arsenic flux at 512℃ for 3 minutes.

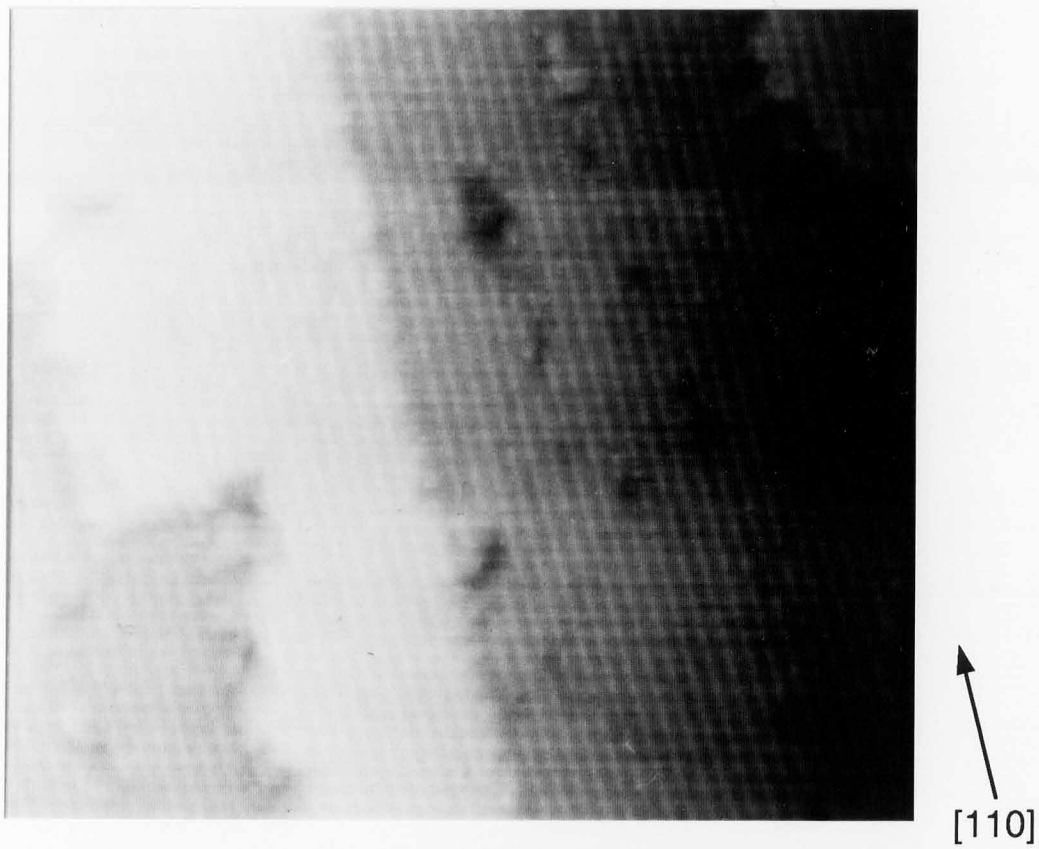

Fig. 5-4. Lower-magnification STM image of an InP (001) surface thermally cleaned under the same conditions as those in Fig. 5-3. The scanning area is 74 nm x 66 nm.

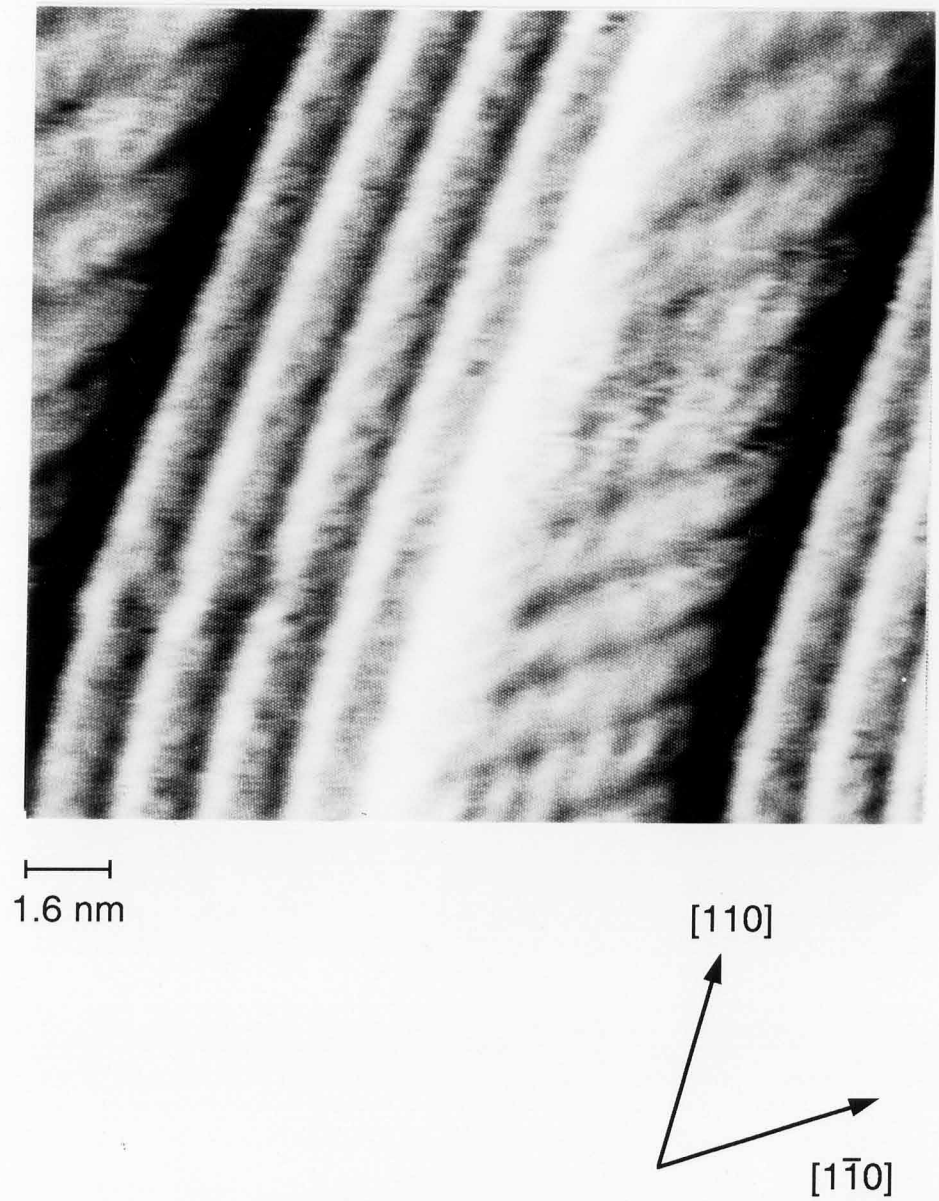

Fig. 5-5. STM image of an InP (001) surface kept at 480℃ for about 10 minutes in a vacuum of 10^{-5} Pa after the thermal cleaning.

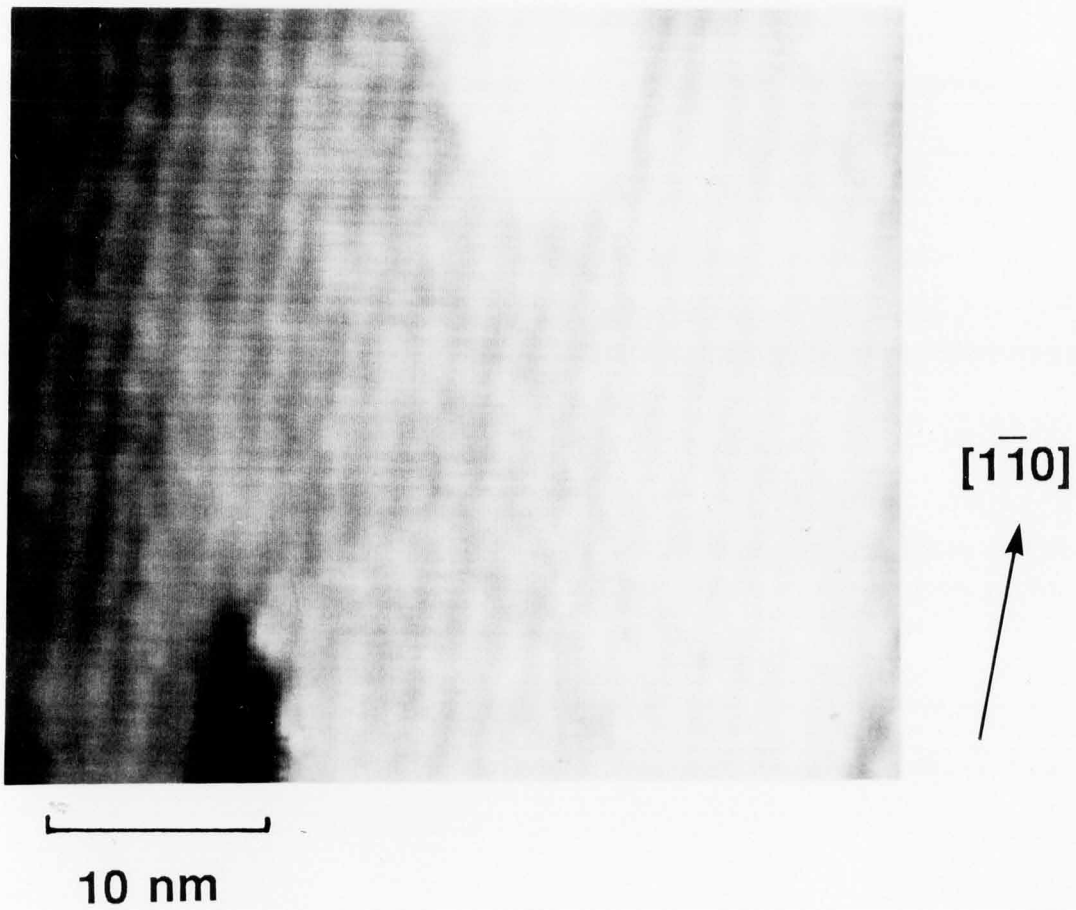

Fig. 5-6. STM image of the surface of 1-ML GaAs on a InP (001) substrate by MBE.

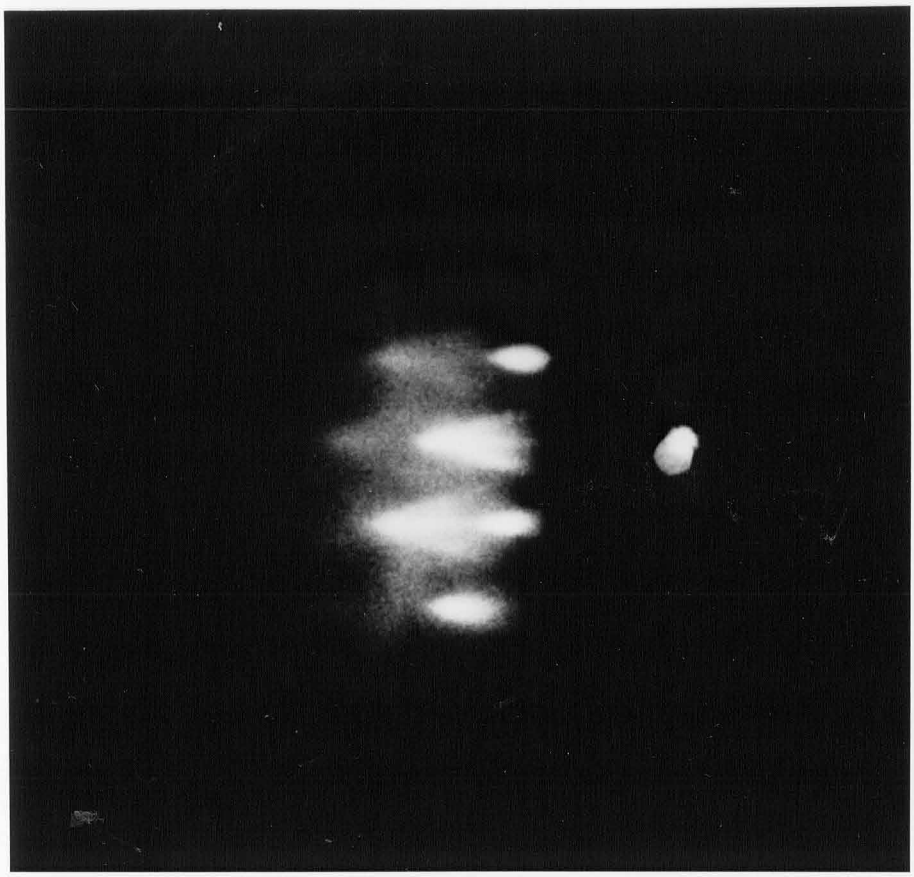

Fig. 5-7. RHEED pattern of an InP (001) surface for the electron beam in the [1-10] azimuth when Ga atoms for 2.5-ML GaAs-growth was supplied on the surface.

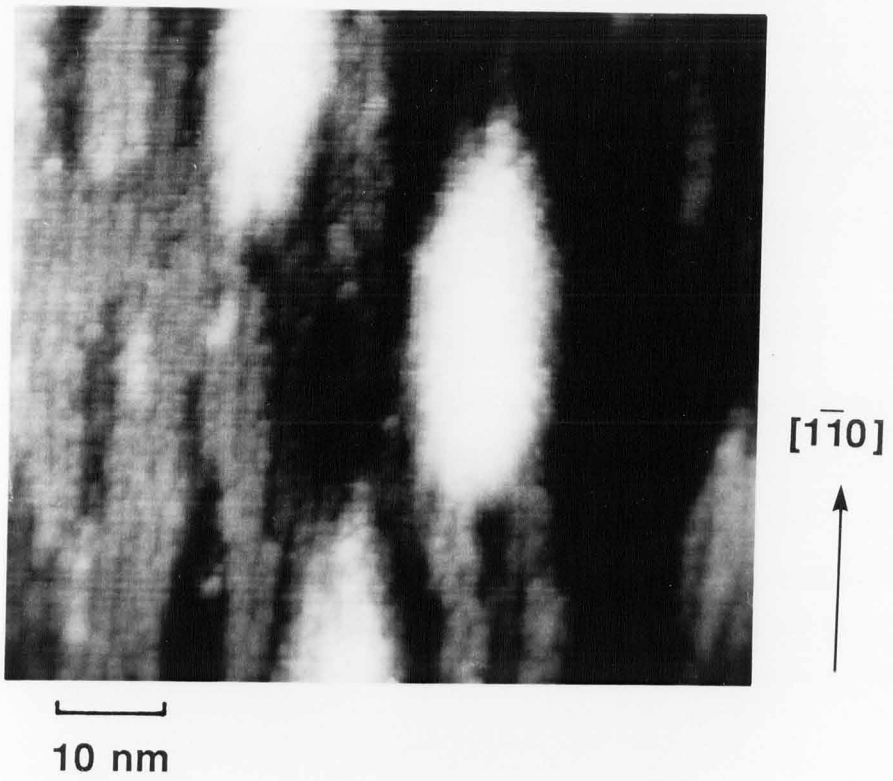

(a)

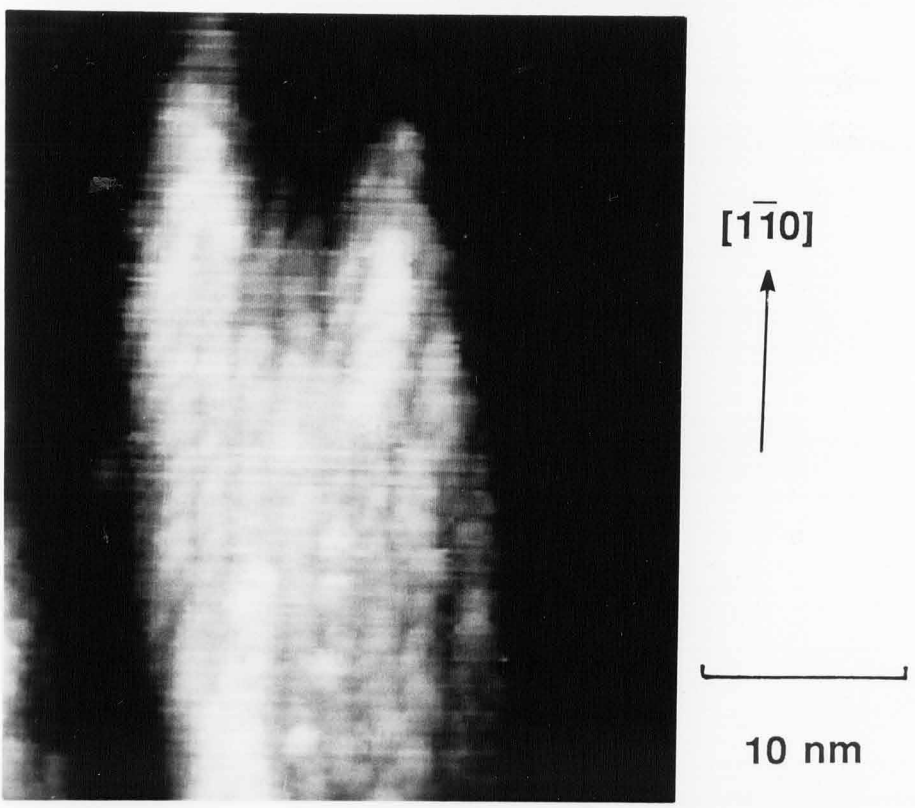

(b)

Fig. 5-8. (a) Low and (b) high magnification STM images of the surface of an InP (001) substrate when Ga atoms for 2.5-ML GaAs-growth were deposited.

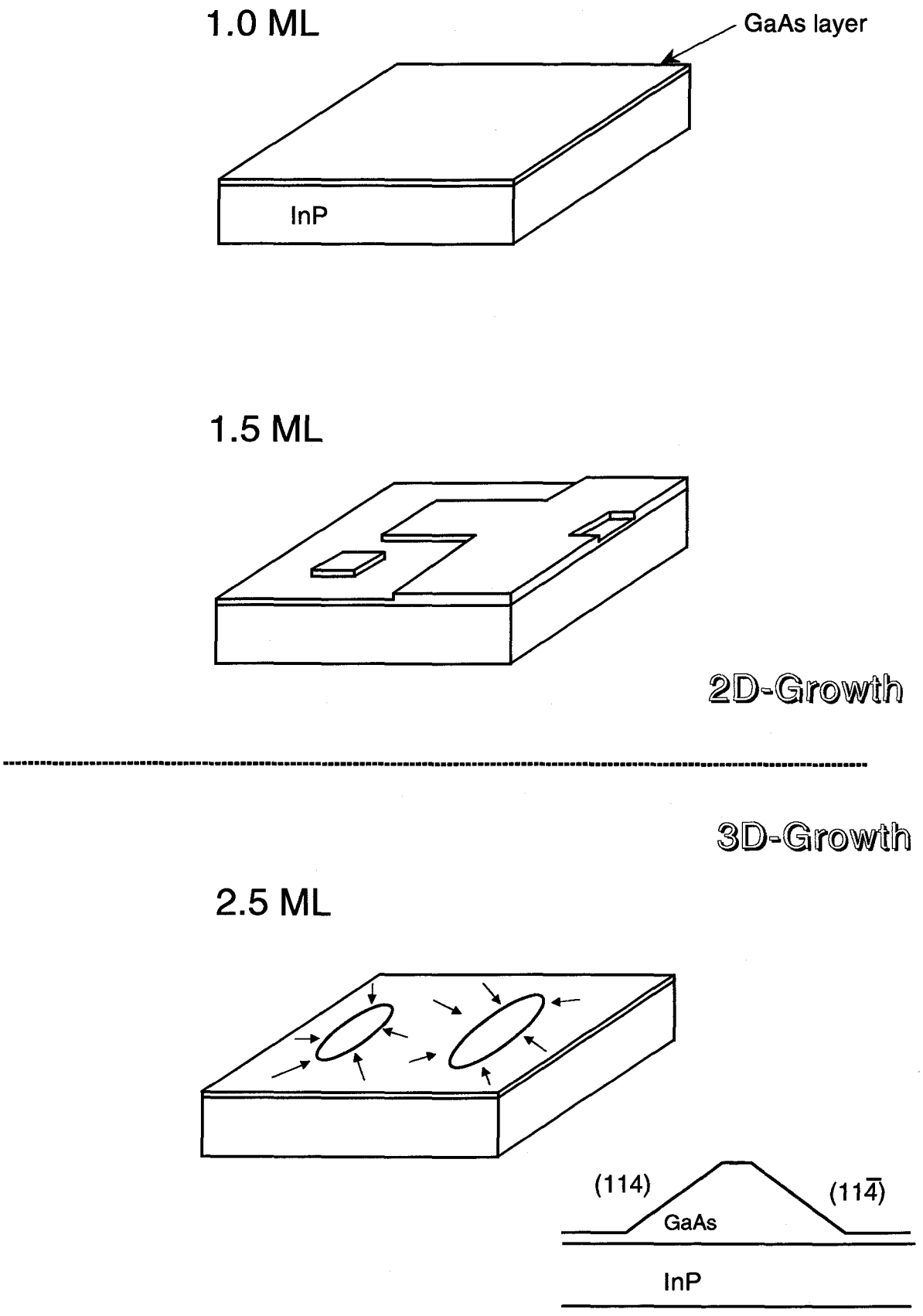

Fig. 5-9. Schematic illustration of the heteroepitaxial growth process of GaAs on an InP (001) surface.

6. Conclusions

A multi-chamber UHV-STM system, which comprises STM chamber, MBE chamber, process chamber, sample-exchange chamber and load-lock chamber, has been constructed for investigating processed compound semiconductor surfaces.

MBE-grown GaAs surfaces have been investigated; surface reconstruction of arsenic dimers are observed, and various types of reconstructions are found for different process conditions. Step-structure of vicinal (001) surfaces are also studied; different types of the structures are found in nanometer-scale corresponding to different misorientation directions. The changes of the step-structures with epitaxial growth are observed, and the uniformity of the structure is considerably improved in the case of the surfaces misorientated toward the [111]B direction while significant change is not observed on the surfaces misorientated toward [111]A direction under the same growth conditions.

In-stabilized surfaces of InP (001) substrates are observed by UHV-STM after cleaned in an arsenic flux in the MBE chamber. The 4×2 structures are investigated, and two types of surface reconstruction are found for different cleaning conditions. In-In dimer models for these structures have been proposed.

Furthermore, hetero-epitaxial growth process of GaAs on InP (001) substrates is investigated. Two-dimensional growth is observed for 1ML and 1.5 ML GaAs deposition, and island formation for 2.5ML GaAs deposition. A dramatic growth-mode transition from two-dimensional to three-dimensional which involves previously deposited GaAs has been suggested from the observations.

It has been demonstrated through this study that the UHV-STM system combined with MBE and process chambers is useful for

observation of processed semiconductor surfaces as well as investigation of the processes on the atomic level.

References

[1] H.Sakaki, Jpn. J. Appl. Phys., **19**, L735 (1980).

[2] I.Hayashi, Extended Abstracts of the 1992 International Conference on Solid State Devices and Materials (August 1992, Tsukuba, Japan).

[3] G.Binning, H.Rohrer, Ch.Gerber, and E.Weibel, Phys. Rev. Lett., **50**, 120 (1983).

[4] K.Takayanagi, Y.Tanishiro, M.Takahashi, and S.Takahashi, J. Vac. Sci. Technol., **A3**, 1502 (1985); Surf. Sci. 164, 367 (1985).

[5] R.M.Tromp, R.J.Hamers, and J.E.Demuth, Phys. Rev. Lett., **55**, 1303 (1985).

[6] R.M.Feenstra, W.A.Thompson, and A.P.Fein, Phys. Rev. Lett., **56**, 608 (1986).

[7] M.D.Pashley, K.W.Haberern, W.Friday, J.M.Woodall, and P.D.Kirchner, Phys. Rev. Lett., **60**, 2176 (1988)

[8] D.J.Chadi, J. Vac. Sci. Technol., **A5**, 834 (1987).

[9] D.K.Biegelsen, R.D.Bringans, J.E.Northrup, and L.-E.Swartz, Phys. Rev., **B41**, 5701 (1990).

[10] M.D.Pashley, K.W.Harberern, and J.M.Gaines, Appl. Phys. Lett., **58**, 406 (1991).

[11] I.Tanaka and S.Ohkouchi, to be published in Jpn. J. Appl. Phys.,**32**, No.5 (1993).

[12] D.K.Biegelsen, L.E.Swantz, and R.D.Bringans, J. Vac. Sci. Technol., **A8**, 280 (1990).

[13] M.D.Pashley, K.W.Harbern, and J.M.Gaines, J. Vac. Sci. Technol., **B9**, 938 (1991).

[14] B.G.Orr, C.W.Snyder, and M.Johnson, Rev. Sci. Instrum.,**62**, 1400 (1991).

[15] T.Kato and I.Tanaka, Rev. Sci. Instrum., **61**, 1664 (1990).

[16] R.Harmers, R.M.Tromp, and J.E.Demuth, Phys. Rev. Lett., **56**, 1972 (1986).

[17] P.H.Schroer and J.Beckoer, IBM J. Res. Develop., **30**, 543 (1986).

[18] A.P.Fein, J.R.Kirtley, and R.M.Feenstra, Rev. Sci. Instrum., **58**, 1806 (1987).

[19] E.W.Muller and T.T.Tsong, "Field Ion Microscopy, Principles and Applications", Elsevier Publ. (1969).

[20] S.Ohkouchi and I.Tanaka, submitted to Jan. J. Appl. Phys.

[21] I.Tanaka, S.Ohkouchi, T.Kato, and F.Osaka, J. Vac. Sci. Technol., **B9**, 2277 (1991).

[22] D.K.Biegelsen, L.-E.Swantz, and R.D.Bringans, J. Vac. Sci. Technol., **A8**, 280 (1990).

[23] I.Tanaka, S.Oukouchi, and A.Hashimoto, Jpn. J. Appl. Phys., **31**, 2216 (1992).

[24] S.Ohkouchi and I.Tanaka, Jpn. J. Appl. Phys., **30**, L1826 (1991).

[25] P.M.Petroff, A.C.Gossard, and W.Wiegman, Appl. Phys. Lett., **45**, 620 (1984).

[26] J.M.Van Hove and P.I.Cohen, J. Vac. Sci. Technol., **20**, 726 (1982).

[27] M.Kawabe and T.Sugaya, Jpn. J. Appl. Phys., **28**, L1077 (1989).

[28] Y.Horikoshi, Oyo Buturi, **59**, 27 (1990) [in Japanese].

[29] Y.Tokura, H.Saito, and T.Fukui, J. Crystal. Growth, **94**, 46 (1989).

[30] M.Akiyama, Y.Kawarada, and K.Kaminishi, J. Cryst. Growth, **68**, 21 (1984).

[31] C.J.Keavney, S.M.Vernon, V.E.Haven, and S.J.Wojtczuk, Appl. Phys. Lett., **54**, 1139 (1989).

[32] M.K.Lee, D.S.Wuu, and H.H.Tang, J. Appl. PHys., **62**, 3209 (1987).

[33] K.Asano, K.Kasahara, and T.Itoh, IEEE Electron Device Lett., EDL-8, 289 (1987).

[34] A.Suzuki, T.Itoh, T.Terakado, K.Kasahara, K.Asano, Y.Inomoto, H.Ishihara, T.Torikai, and S.Fujita, Electronics Lett., **23**, 954 (1987).

[35] S.Ohkouchi and I.Tanaka, Appl. Phys. Lett., **59**, 1588 (1991).

[36] I.Tanaka, S.Ohkouchi, F.Osaka, and T.Kato, Surf. Sci., **267**, 191 (1992).

[37] I.Tanaka and S.Okouchi, Jpn. J. Appl. Phys., **30**, L1662 (1991).

[38] S.Okouchi and I.Tanaka, Ultramicroscopy, **42-44**, 771 (1992).

[39] H.H.Farrell and C.J.Palmstrom, J. Vac. Sci. Technol., **B8**, 903 (1990).

[40] K.Y.Cheng, A.Y.Cho, W.R.Wanger, and W.A.Bonner, J. Appl. Phys., **52**, 1015 (1981).

[41] N.Ohshima, Y.Koide, K.Itoh, and Y.Yasuda, Appl. Phys. Lett., **57**, 2434 (1990).

[42] M.Hata, T.Isu, A.Watanabe, and Y.Katayama, J. Vac. Sci. Technol., **B8**, 692 (1990).

[43] D.K.Biegelsen, R.D.Bringans, J.E.Northryr, and L.E.Swarts, Appl. Phys. Lett., **57**, 2419 (1990).

[44] C.W.Snyder, B.G.Orr, D.Kessler, and L.M.Sander, Phys. Rev. Lett., **66**, 3032 (1991).

Acknowledgments

The author would like to thank Mr. S. Ohkouchi, Dr. F. Osaka, and Mr. T. Kato for their collaboration in the STM research at Optoelectronics Technology Research Laboratory (OTL), and Dr. I. Hayashi and Dr. Y. Katayama for their advice, discussions and encouragement for the this study. He is grateful to Professor T. Kushida of OSAKA University (Department of Physics) for his advice and lead for the construction of this thesis. He is also grateful to Professor K. Murase (Department of Physics), Professor M. Ikeya (Department of Physics), Professor T. Ohyama (Department of Physics), and Associate Professor S. Kinoshita (Department of Physics) of OSAKA University for their fruitful discussions. Furthermore, he would like to thank Professor S. Morita of HIROSHIMA University for his introduction, advice and discussions on STM measurements, Professor T. Sakurai and Associate Professor T. Hashizume of TOHOKU University for their advice on FIM observation of tungsten tips, Professor K. Kuriyama of HOSEI University for his instruction concerning direct-current electrochemical etching of tungsten tips.